Grand Canyon provenance for orthoquartzite clasts in the lower Miocene of coastal southern California

Leah Sabbeth, Brian P. Wernicke, Timothy D. Raub, Jeffrey A. Grover, E. Bruce Lander, Joseph L. Kirschvink; Grand Canyon provenance for orthoquartzite clasts in the lower Miocene of coastal southern California. Geosphere: 15 (6): 1973–1998. doi: https://doi.org/10.1130/GES02111.1

ABSTRACT

Orthoquartzite detrital source regions in the Cordilleran interior yield clast populations with distinct spectra of paleomagnetic inclinations and detrital zircon ages that can be used to trace the provenance of gravels deposited along the western margin of the Cordilleran orogen. An inventory of characteristic remnant magnetizations (CRMs) from >700 sample cores from orthoquartzite source regions defines a low-inclination population of Neoproterozoic-Paleozoic age in the Mojave Desert-Death Valley region (and in correlative strata in Sonora, Mexico), and a moderate- to high-inclination population in the 1.1 Ga Shinumo Formation in eastern Grand Canyon. Detrital zircon ages can be used to distinguish Paleoproterozoic to mid-Mesoproterozoic (1.84 to 1.20 Ga) clasts derived from the central Arizona highlands region from clasts derived from younger sources that contain late Mesoproterozoic zircons (1.20 to 1.00 Ga). Characteristic paleomagnetic magnetizations were measured in 44 densely cemented orthoquartzite clasts, sampled from lower Miocene portions of the Sespe Formation in the Santa Monica and Santa Ana mountains, and from a middle Eocene section in Simi Valley. Miocene Sespe clast inclinations define a bimodal population with modes near 15° and 45°. Eight samples from the steeper Miocene mode for which detrital zircon spectra were obtained all have spectra with peaks at 1.2, 1.4, and 1.7 Ga. One contains Paleozoic and Mesozoic peaks and is probably Jurassic. The remaining seven define a

population of clasts with the distinctive combination of moderate to high inclination and a cosmopolitan age spectrum with abundant grains younger than 1.2 Ga. The moderate to high inclinations rule out a Mojave Desert-Death Valley or Sonoran region source population, and the cosmopolitan detrital zircon spectra rule out a central Arizona highlands source population. The Shinumo Formation, presently exposed only within a few hundred meters elevation of the bottom of eastern Grand Canyon, thus remains the only plausible, known source for the moderate- to high-inclination clast population. If so, then the Upper Granite Gorge of the eastern Grand Canyon had been eroded to within a few hundred meters of its current depth by early Miocene time (c. 20 Ma). Suh an unroofing event in the eastern Grand Canyon region is independently confirmed by (U-Th)/He thermochronology. Inclusion of the eastern Grand Canyon region in the Sespe drainage system is also independently supported by detrital zircon age spectra of Sespe sandstones. Collectively, these data define a mid-Tertiary, SW-flowing "Arizona River" drainage system between the rapidly eroding eastern Grand Canyon region and coastal California.

INTRODUCTION

Among the most difficult problems in geology is constraining the kilometer-scale erosion kinematics of mountain belts (e.g. Stüwe et al., 1994, House et al., 1998). A celebrated example of the problem, and the subject of vigorous contemporary debate, is the post-100 Ma erosion kinematics of the Colorado Plateau of western North America (e.g. Pederson et al., 2002), and especially of the Grand Canyon region (e.g. Polyak et al., 2008; Karlstrom et al., 2008, 2014, Flowers et al., 2008, Wernicke, 2011, Beard et al., 2011; Flowers and Farley, 2012, 2015; Lucchitta, 2013; Hill and Polyak, 2014; Darling and Whipple, 2015; Fox et al., 2017; Winn et al., 2017). The erosion problem of the plateaus is particularly well-posed. It was a broad cratonic region that lay near sea level for most of Paleozoic and Mesozoic time (e.g. Burchfiel et al., 1992).

During the Late Cretaceous-Paleogene Laramide orogeny, the Cordilleran orogen roughly doubled in width. The Colorado Plateau and southern Rocky Mountains thus underwent a transition from residing near sea level, as a retroarc Cordilleran foreland basin during the Late Cretaceous, to a mountain belt residing at elevations of 1 to 2 km during Paleogene and younger time (e.g., Elston and Young, 1991, Flowers et al., 2008, Hill et al., 2016, Huntington et al., 2010, Karlstrom et al., 2014, Winn et al., 2017). The key challenge posed by this framework lies in using thermochronological information on the unroofing history, and the distribution of sedimentary source regions and corresponding depocenters, to constrain erosion kinematics.

Existing models of erosion kinematics of the region differ mainly in the role they assign to the modern Colorado River (c. 6 Ma and younger), versus more ancient drainage systems dating back to Laramide time. Despite the lack of consensus, a significant and recent point of agreement, based primarily on thermochronological data, is that a kilometer-scale erosional unroofing event occurred in mid-Tertiary time (c. 28-18 Ma) in the eastern Grand Canyon region (Figure 1; Flowers et al., 2008; Lee et al., 2013; Karlstrom et al. 2014; Winn et al., 2017). This unroofing event (described in more detail in the next section) is relatively localized compared with erosion histories of adjacent regions across orogenic strike to the SW and NE, also defined by thermochronological data. To the SE in the Arizona Transition Zone and Mojave-Sonora Desert region, unroofing to near-present levels occurred in Laramide time (c. 80-40 Ma), with the exception of rocks tectonically exhumed by Tertiary extension (Bryant et al., 1991; Foster et al., 1992; Spotila et al., 1998; Blythe et al., 2000; Mahan et al., 2009; Fitzgerald et al., 1991, 2009). To the NE, in the Colorado Plateau interior, erosional unroofing occurred mainly after 10 Ma, presumably as a result of integration of the Colorado River drainage system at 6 Ma (e.g., Pederson et al., 2002; Flowers et al., 2008; Wernicke, 2011; Hoffman et al., 2011; Winn et al., 2017; Karlstrom et al., 2017).

Independent of thermochronological data, constraints on erosion kinematics are imposed by the arrival of specific clast types within basins along the flanks, placing a minimum age on the time at which any particular clast type was exposed to erosion. The overall pattern of unroofing thus motivates examination of depocenters along the margins of the Cordillera for evidence of unroofing in the Cordilleran interior, such as migration of drainage divides toward the interior (e.g. Ingersoll et al., 2018). In particular, the mid-Tertiary unroofing event predicts the appearance of eroded detritus from the eastern Grand Canyon region in mid-Oligocene to early Miocene depocenters.

We investigate this hypothesis by applying a new technique that combines paleomagnetic inclination spectra and detrital zircon age spectra of conglomerate clast populations to the gravel fraction of the Sespe Formation, a mid-Tertiary conglomeratic sandstone interval that is broadly distributed throughout coastal southern California (Figure 2) (Howard, 2000, 2006; Ingersoll et al., 2013, 2018). We focus on the orthoquartzite clast population (as opposed to volcanic, metavolcanic, and metaquartzite clasts also abundant in the Sespe Formation), because it is both ultradurable and its potential sources are widely exposed in the headwater regions of all proposed major paleodrainages tributary to the Sespe basin (Figure 1). The scope of our study includes characteristic remnant magnetizations (CRMs) from 44 samples from the Sespe orthoquartzite clast population, collected from three well-dated Sespe exposure areas. We compare these data with CRMs of some 700 samples from potential source regions in the Death Valley-Mojave region, the central Arizona highlands, Grand Canyon, and Sonora, Mexico. Our study also includes 936 detrital zircon ages from 12 Sespe orthoquartzite clasts, which we compare to 1,870 detrital zircon ages from 23 samples of potential sources.

GEOLOGIC BACKGROUND

Sespe Formation

The modern outcrop distribution of the Sespe Formation (Figure 2) has been substantially modified by right-lateral shear on the San Andreas fault system and transrotation of the Western Transverse Ranges (e.g. Howard, 1996; Atwater and Stock, 1998). The mid-Tertiary configuration of the Sespe basin can be determined with a high degree of confidence on the basis of palinspastic reconstructions (e.g. Atwater and Stock, 1998; McQuarrie and Wernicke, 2005; Jacobson et al., 2011; Ingersoll et al., 2018), all of which restore the most proximal Sespe depocenters (Santa Monica and Santa Ana mountains) to a position near the modern Colorado River delta (Figure 1).

The middle Eocene to lower Miocene Sespe Formation consists predominantly of fluvial to deltaic sandstone and conglomerate, ranging from a few hundred up to 1,000 meters thick (e.g. Howard, 1989, 2000; Schoellhamer et al., 1981). Although much of the Sespe Formation appears to be Eocene, it also contains an Oligocene to early Miocene component that includes tongues of marine strata. The younger strata have locally been defined as the ca. 27-20 Ma Piuma Member, the upper part of which is paleontologically dated as Hemingfordian in the Santa Monica and Santa Ana mountains (e.g. Lander, 2011, 2013). Compositionally, Sespe sandstones are lithic-poor arkoses derived predominantly from granitic source rocks, with 50% to 95% of detrital zircon ages indicating provenance within the Mesozoic Cordilleran arc, and the remainder derived from various primary and recycled sources of pre-300 Ma grains (Ingersoll et al., 2013, 2018).

Sespe Formation conglomerates are dominated by populations of highly survivable volcanic, metavolcanic, and quartzitic clasts, with smaller populations of less durable rock types (Woodford et al., 1968; Abbott and Peterson, 1978; Howard, 1989; Belyea and Minch, 1989; Minch et al., 1989). The quartzite clast population can be subdivided into orthoquartzites and metaquartzites.

Orthoquartzite is defined as an unmetamorphosed quartz arenite with a densely cemented silica matrix (Howard, 2005) and is distinguished from metaquartzite petrographically, due to the destruction of detrital grain boundaries beginning under sub-greenschist to lower greenschist facies conditions (Wilson, 1973; Howard, 2005). Our focus on orthoquartzite is motivated by two key considerations.

First, crystalline sources tend to be proximal to the coast, and consist mainly of feldspathic rock types that are only moderately durable, with the exception of ultradurable metarhyolite, chert, and metaquartzite clasts (e.g., Abbott and Peterson, 1978). It has long been established that orthoquartzite clasts in the Sespe Formation are derived from relatively distant sources within the Cordilleran interior (Howard, 1996, 2000), generally well NE of source regions for clasts of metaquartzites and most crystalline rocks (Figure 1). Crystalline source regions also occur in the Cordilleran interior, but, given the moderate durability of crystalline clasts (owing to both the mechanical weakness of cleavage and solubility of feldspar), they tend to be eliminated from the gravel fraction during long transport, especially in the presence of ultradurable quartzitic clasts (e.g., Abbott and Peterson, 1978). Fingerprinting of orthoquartzite clasts in the basins thus affords a broad aperture for the observation of erosion kinematics using this approach (Howard, 1989, 2000). Second, one potential Sespe orthoquartzite source, the 1.1 Ga Shinumo Formation, is at present only exposed within a few hundred meters elevation of the bottom of eastern Grand Canyon, in the Upper Granite Gorge area (Figure 3). Its appearance in the Sespe Formation would therefore constrain the time by which eastern Grand Canyon was in existence, more-or-less as it is today, greatly limiting the extant range of erosion models.

Orthoquartzite Source Regions

Eastern Grand Canyon is, however, only one of four potential source regions in the Cordilleran interior for orthoquartzite clasts (Figure 1). The other three include (1) the Death Valley-Mojave region, which contains Neoproterozoic-Cambrian orthoquartzites (e.g. Stewart et al, 2001; Shoenborn et al., 2012), (2) the central Arizona highlands, which contain late Paleoproterozoic to mid-Mesoproterozoic orthoquartzites (e.g. Mulder et al., 2017; Doe et al, 2012), and (3) the Caborca area of NW Sonora, Mexico, which contains Neoproterozic-Cambrian orthoquartzites in strata correlative with the Death Valley-Mojave strata (Gehrels and Stewart, 1998; Stewart et al., 2001). In the broader Sonoran region (mainly south of the area shown in Figure 1), widespread exposures of Jurassic conglomerates (Coyotes Formation and equivalents) contain orthoquartzite clasts of presumed Proterozoic-early Paleozoic age (Stewart and Roldán-Quintana, 1991). In NW Sonora, the only known Mesoproterozoic quartzites, which may or may not be orthoquartzite, occur in a small exposure (6.5 km^2) at Sierra Prieta (Figure 1), where they are intruded by ca. 1.08 Ga anorthosite sills (Izaguirre and Iriondo, 2007; Molina-Garza and Izaguirre, 2008).

Various Tertiary paleodrainages have been proposed to connect these potential source regions with mid-Tertiary coastal basins in southern California (Howard, 2000, 2006; Ingersoll et al., 2018). These include the Poway (Abbot and Smith, 1989), Amargosa (Howard, 2000), Gila (Howard, 2000), Arizona (Wernicke, 2011), and Tejon (Lechler and Niemi, 2011) paleodrainage systems (Figure 1).

To distinguish among these source regions, we augment previous studies of orthoquartzite clasts and sources (Howard, 1989, 1996, 2000, 2006) with a novel method, using the combination of paleomagnetic inclination and detrital zircon spectra of orthoquartzite clast populations, to trace

provenance (Wernicke et al., 2010, 2012; Wernicke, 2011; Raub et al., 2013). A key finding from the earlier conglomerate studies was that lowest Sespe sources appear to be dominated by a Gila paleodrainage system, which included (1) Paleoproterozoic orthoquartzites from the central Arizona highlands, and (2) metarhyolite clasts derived from southeastern Arizona. The system appears to have evolved by Oligocene time into a more latitudinally extensive system to include a component of metavolcanic and orthoquartzite clasts from the Death Valley-Mojave region (Howard, 2000, 2006).

An important distinction between the Sespe Formation and its Eocene equivalent in the San Diego area, the Poway Group, is the percentage and petrology of quartz porphyry metarhyolite clasts (Belyea and Minch, 1989; Woodford et al., 1968, 1972). In the Poway Group, quartzites constitute up to 24% of the clast population, which averages 73% quartz porphyry metarhyolite clasts (Bellemin and Merriam, 1958). These "Poway-type" metarhyolite clasts have been texturally and geochemically traced to bedrock sources in the Caborca region of Sonora, Mexico (Figure 1) (Abbott and Smith, 1989). The Sespe Formation, in contrast, contains a much smaller percentage (<10%) of metarhyolite clasts, which are petrographically and geochemically dissimilar to Poway-type clasts and Sonora metarhyolites, but are similar to Jurassic metarhyolites from the Mt. Wrightson Formation of southeastern Arizona (Abbott et al., 1991). These relations are generally interpreted to indicate that the Poway Group and Sespe Formation represent distinct drainage basins in Eocene time (Woodford et al., 1968, 1972; Kies and Abbott, 1983; Belyea and Minch, 1989; Abbott et al., 1991; Howard, 2000, 2006). Although there may be some overlap of the two source areas (e.g., Ingersoll et al., 2018), transport of significant quantities of Caborca-area orthoquartzites (either Mesoproterozoic Sierra Prieta or Neoproterozoic-Cambrian strata, Figure 1) in a regional drainage system of any age would also result in a preponderance (≥3:1) of Poway-

type clasts relative to the orthoquartzite component, as suggested by the clast composition of the Poway group. The lack of Sonora-derived metarhyolite clasts in the Sespe drainage basin thus strongly suggests the absence of any significant drainage connection between NW Sonora and the Sespe basin.

Two key attributes have the potential to distinguish between a population of clasts with Shinumo provenance from populations derived from Death Valley-Mojave or central Arizona highlands sources: (1) moderate to high paleomagnetic inclination, and (2) the presence of late Mesoproterozoic (1.3-1.0 Ga) or "Grenville-age" detrital zircon. Whereas orthoquartzite populations from the Death Valley-Mojave region generally contain abundant 1.3-1.0 Ga detrital zircons, their CRMs are of low inclination (0-30°), contrasting them with the Shinumo population. Whereas orthoquartzite populations from the central Arizona highlands may have moderate to high inclinations, they are mostly too old to contain 1.3-1.0 Ga detrital zircons, distinguishing them from the Shinumo population. Therefore, identification of these attributes within a population of Sespe orthoquartzite clasts has the potential to distinguish a Shinumo source from the other sources. If the Shinumo Formation is a Sespe gravel source, it would strengthen the "Arizona River" hypothesis (Wernicke, 2011), independent of low-temperature thermochronometry studies on which it is based (e.g. Flowers et al., 2008, 2015; Wernicke, 2011 Flowers and Farley, 2012; 2013). According to this hypothesis, the mid-Tertiary drainage configuration of the Cordillera included a paleoriver system with headwaters cut near the modern level of erosion of the Upper Granite Gorge area in the eastern Grand Canyon region.

Below, we present paleomagnetic and detrital zircon data from three Sespe clast populations and one potential source rock from the Shinumo Formation, as well as a compilation of existing paleomagnetic and detrital zircon data from the literature. We then compare data from

the various source populations with data from Sespe clast populations, focused on the issue of which, if any, of the Sespe clast populations indicate a Shinumo provenance.

Mid-Tertiary (28 to 18 Ma) Unroofing of the Southwestern Colorado Plateau

As noted above, the primary erosional event in the Cordilleran interior during upper Sespe (Piuma) time occurred within a NW-trending zone, running from the eastern Grand Canyon region through east-central Arizona (Figure 1), contrasting it with predominantly Laramide unroofing to the SW in the Mojave-Sonoran region and post-10 Ma unroofing to the NE on the Colorado Plateau. In addition to thermochronological data, this event is recorded by kilometer-scale erosion between aggradation of the Eocene to lower Oligocene Chuska Formation and aggradation of the Miocene Bidahochi Formation, whose ages bracket the unroofing event between 26 and 16 Ma (Cather et al., 2008). Numerous thermochronological cooling models indicate approximately 30 °C of cooling at that time, from about 60 °C prior to 28 Ma (with some interpretations of the data suggesting temperatures as high as 80-90 °C in the Upper Granite Gorge prior to 28 Ma) to <30 °C after 18 Ma (Flowers et al., 2008; Flowers and Farley, 2012; Lee et al., 2013; Karlstrom et al., 2014; Winn et al., 2017).

In the Upper Granite Gorge of eastern Grand Canyon, where the Shinumo Formation is exposed (Figure 3), the 30 °C (or less) temperatures at the end of the 28-18 Ma erosion event were probably very close to surface temperatures in the SW US, indicating very little post-18 Ma erosion (Flowers et al., 2008; Flowers and Farley, 2012, 2014; Wernicke, 2011; Karlstrom et al., 2014; Winn et al., 2017). Modern surface temperatures measured throughout the interior of the SW US (Sass et al., 1994) vary according to

$$T_s(h) = (29 \pm 2)°C + (-8 \pm 1°C/km)h,$$

where T_s is surface temperature, and h is elevation above sea level (Equation 7 in Wernicke, 2011). Early Miocene surface temperatures were at least 3°C, and perhaps as much as 8°C, warmer than today (e.g. Huntington et al., 2010). Hence, assuming no erosion, rocks now exposed at a modern elevation of 600 m at the bottom of eastern Grand Canyon, would have T_s in the range of 27°C to 32°C, depending on the degree of atmospheric cooling since 20 Ma. However, some additional erosion must have occurred after the 28-18 Ma unroofing event. Given a very conservative upper temperature limit for river-level samples of 40°C after mid-Tertiary erosion ended (see discussion of error sources for these estimates in Wernicke, 2011, p. 1303-1305) and an early Miocene upper crustal geothermal gradient of 25°C/km (based on thermochronometric profiles through tilted fault blocks in the eastern Lake Mead region; e.g. Quigley et al., 2010, and discussion on p. 1295 in Wernicke, 2011), net erosion since 18 Ma would lie in the range

(8 to 13°C)/(25 °C/km)/(1000 m/km) = 320 to 520 m,

which corresponds to a maximum average regional erosion rate of 18 to 29 m/Myr.

This erosion rate for the bottom of eastern Grand Canyon is in good agreement with the late Tertiary erosional history of the surrounding plateau region based on stratigraphic constraints. Just south of eastern Grand Canyon, the basalt at Red Butte, which lies on an erosion surface 220 m above the surrounding Coconino Plateau, is 9 Ma (Reynolds et al., 1986), indicating an average erosion rate of 24 m/Myr since then (Figure 3). East of Grand Canyon, average regional erosion since 16 Ma (i.e., regional unroofing below the basal Bidahochi unconformity) is at most 300 to 400 m (e.g. Fig. 15 in Cather et al., 2008), suggesting rates of 19-25 m/Myr, albeit much of the erosion may have been concentrated in the last 6 Myr at higher rates (Karlstrom et al., 2017).

In the Upper Granite Gorge area, the Shinumo Formation is the most erosionally resistant unit within the gently north-tilted Grand Canyon Supergroup. It is the only stratified unit in eastern

Grand Canyon that contains abundant ultradurable orthoquartzite. It eroded into steep, south-facing cuestiform ridges, during both Cenozoic erosion and erosion prior to the Cambrian Sauk transgression, when it formed a series of paleoislands (Figure 3). The Cambrian paleoislands rose 100 to 200 m above the coastal plain, around which Tonto Group strata, including sandstones of the Tapeats Formation, were deposited in buttress unconformity (Figure 3; Noble, 1910, 1914; Sharp, 1940; McKee and Resser, 1945; Billingsley et al., 1996; Karlstrom and Timmons, 2012). At present, the Shinumo Formation crops out in a 70 km-long, quasi-linear array of seven exposure areas, with each area 2 to 5 km long, as measured parallel to the array, mostly on the north side of the modern Colorado River (e.g. Figure 3.1 in Hendricks and Stevenson, 2003). The Shinumo Formation is now preserved at elevations as much as 600 m above the modern river level (Billingsley et al., 1996). If our estimate of 300-500 m of post-18 Ma erosion is correct, the Shinumo Formation would have been a highly proximal source of ultradurable, gravel-sized clasts in the high-relief headwaters of a mid-Tertiary Arizona River (Figure 3).

A second significant source of orthoquartzite in the Grand Canyon region is the Tapeats Formation, but only in the Lower Granite Gorge area of western Grand Canyon (Figure 1) where it is the oldest exposed stratified unit. In eastern Grand Canyon, exposures of the Tapeats Formation, in contrast to much of the Shinumo Formation, are not densely cemented orthoquartzites (Billingsley et al., 1996). In the Lower Granite Gorge area, however, a large fraction of the Tapeats Formation is "quartzitic and very hard," in contrast to relatively weak sandstones in the remainder (p. 16 in McKee and Resser, 1945).

SAMPLING AND METHODS

We sampled Sespe gravel clasts from the Santa Ana and Santa Monica mountains and from Simi Valley (Figure 2). We also collected several samples of potential source rocks, in order to

reproduce results from extensive existing paleomagnetic and detrital zircon data (Elston and Grommé, written commun., 1994; Bloch et al., 2006; Mulder et al., 2017), including one sample of the Shinumo Formation, and one sample each of the Shinumo and Tapeats formations from the Caltech sample archive (Table 1).

Because dated Sespe sections range broadly in age, from middle Eocene to early Miocene (c. 48 to 20 Ma), sample locations (Figure 2) were restricted to three sections with local paleontological, radiometric, and magnetostratigraphic control of depositional age. They included (1) a middle Eocene section in Simi Valley (exposed along View Lane Drive at the terminus of exit 22A of California Highway 118; Kelly and Whistler, 1994; Kelly et al., 1991; Lander, 2013), (2) the lower Miocene Piuma Member in the Saddle Peak area of the western Santa Monica Mountains (exposed along upper Piuma Road and upper Schueren Road, along and near the range crest) (Lander, 2011, 2013), and (3) correlative lower Miocene strata in the Limestone Canyon Park area of the Santa Ana Mountains (Red Rock Canyon Trail and a nearby roadcut through the "marker conglomerate" horizon (Belyea and Minch, 1989) on Santiago Canyon Road (Figure 2).

In these areas of exposure, in situ paleomagnetic sampling of orthoquartzite clasts in quantity proved to be unfeasible, precluding a conglomerate test. Steep badlands topography along ridgecrest exposures of the Sespe Formation results in a scarcity of exposed orthoquartzite clasts in outcrops that are both sufficiently indurated and accessible for in-situ drilling. Orthoquartzite clasts were mainly sampled from thin, proximal colluvial deposits within a few meters of their Sespe bedrock sources. As discussed further below, the results of Hillhouse (2010) and this study indicate that the CRMs of Sespe orthoquartzite clasts predate weathering, transport, and deposition of the clasts, and diagenesis of their sandstone matrix.

A total of 92 Sespe clasts were collected, including 71 from the Miocene sections (30 from Piuma Road, 19 from Schueren Road, and 22 from the Santa Ana Mountains), and 21 from the Eocene section (Table 2). Following petrographic screening (mainly to distinguish orthoquartzites from metaquartzites and other rock types), and assessment of the quality of preserved stratification (often best observed on cut or drilled surfaces; Figure S1 shows representative examples), 49 samples were selected for paleomagnetic analysis. These included 34 samples from Miocene Sespe sections (17 from Piuma Road, 13 from Schueren Road, 4 from the Santa Ana Mountains), and 15 samples from the Eocene Sespe section. All 34 samples from the Miocene Sespe Formation yielded interpretable paleomagnetic data, but only 10 of the 15 samples from the Eocene section yielded interpretable data. We therefore report paleomagnetic data for a total of 44 Sespe orthoquartzite clasts (Tables 3 and 4; Table S1).

Our general approach is to compare the distribution of inclinations within clast populations with those of potential source regions, which requires comparison of inclination-only data from the clast populations with three-dimensional paleomagnetic vectors of the source populations. Whereas the latter can be expressed using Fisher statistics, the former cannot, and at present there is no parametric test of statistical distributions applicable to such comparisons (p. 135 in Fisher et al., 1987; McFadden and Reid, 1982). Further, we cannot rigorously define any sort of mean for our clast populations, because as shown below, the clast populations are not normally distributed.

Following paleomagnetic analysis, detrital zircon spectra were determined for a subset of 12 of the 44 Sespe clast samples. This subset was selected based on quality of paleomagnetic data (good orientation statistics and demagnetization temperatures suggestive, in most cases, of hematite as the carrier phase), and included 2 samples with low inclination, and 10 samples with moderate to high inclination. Of the 10 with moderate to high inclination, 8 were from the Miocene

Sespe, and 2 were from the Eocene. The two samples with low inclination were both from the Miocene Sespe, from the roadcut on Santiago Canyon Road (Table 4).

Paleomagnetic Analysis

All selected Sespe orthoquartzite clasts and the Shinumo sample were cut along their bedding planes with a non-magnetic brass blade, and then cored in-lab using an electric drill with a nonmagnetic bit. Sample cores were soaked in dilute HCl for up to 36 hours to remove any possible fluid-related magnetic signatures, and then stored in a magnetically-shielded room.

Demagnetization and paleomagnetic measurements were carried out at the California Institute of Technology Paleomagnetics Laboratory using 2G^{TM} Enterprises rock magnetometers with three-axis DC SQuID sensors with sensitivities of 2 x 10^{-13} Am^2 per axis, using a RAPID automatic sample changer. Details of the equipment and demagnetization procedures are described in Kirschvink et al. (2008). After measuring the natural remnant magnetization (NRM), we used five alternating field (AF) steps of 2 to 10 mT to remove viscous components of multi-domain magnetite and other soft magnetic components. To thermally demagnetize our samples, we heated them in a magnetically-shielded ASC furnace in steps of 5 – 50 °C, from 0 °C up to a maximum of 710 °C to constrain the CRM. Magnetization components were defined by least squares using the principal component analysis technique of Kirschvink (1980) and software of Jones (2002).

Detrital Zircon Analysis

Mineral separations and U-Pb isotopic analyses were performed for a total of 13 samples, 12 from Sespe clasts and one from the Shinumo Formation. Six of these samples, including 4 samples from the Santa Ana Mountains, 1 sample from the Santa Monica Mountains, and 1 sample of Shinumo Formation (Tables 1 and 2) were separated and analyzed by Apatite to Zircon, Inc., using standard separation techniques and Laser Ablation-Inductively Coupled Plasma-Mass

Spectrometry. Analysis and preparation of zircon age data followed procedures described in Moore et al. (2015). For the 7 additional samples, including 5 from the Santa Monica Mountains and 2 from the Simi Valley area, zircon extractions, using standard techniques, were performed at the California Institute of Technology and the University of Arizona. U-Pb analyses were performed at the University of Arizona Laserchron Center. Zircon grains were mounted in epoxy with Sri Lanka, FC-1, and R33 primary standards. The epoxy mount was sanded down to 20 μm, polished, and imaged with a Hitachi 3400N scanning electron microscope (SEM). Laboratory procedures for U-Pb isotopic analyses and screening for discordant grains follow methods described in Gehrels et al. (2006, 2008) and Gehrels and Pecha (2014).

RESULTS

Paleomagnetic Data

Demagnetization data for all samples are summarized in Table 4 and presented in complete form in Table S1. Demagnetization plots for all samples are shown in Figure S2. Representative demagnetizations of Sespe cobbles, including two from Miocene (Figure 5a, b) and two from Eocene (Figure 5c, d) sections, show well-preserved, high-temperature CRMs of moderate to high inclination. Measured remnant magnetizations of the sample suite have intensities ranging from 10^{-9} – 10^{-6} Am^2, well above instrument sensitivity of 10^{-13} Am^2. Up to five steps of alternating field (AF) demagnetization in 20 mT increments up to 100 mT generally had little effect on remanence, indicating magnetite is not a significant carrier. Characteristic directions in most samples are defined by multiple demagnetization steps ranging from 590 to 670° C, suggesting that hematite is the main carrier of magnetization in these samples. This observation is consistent with petrographic evidence that samples typically contain pigmentary hematite, which imparts their characteristic red and red-purple hues (Figure S1). However, in 15 of the 44 samples with interpretable data, the

carrier phases were magnetite or other lower temperature phases. Maximum angular deviations (MAD) calculated from principal component analysis average about 5° in our sample set (Table 4).

Distributions of paleomagnetic inclination from the Sespe clast populations, plotted in Figure 6 in 4° bins, show that both Miocene and Eocene populations exhibit bimodal distributions with maxima near 15° and 45°, and minima near 30° (Figure 6). The Miocene population, however, has a stronger peak near 45° and the Eocene population has a stronger peak near 15°, although the latter population includes only 10 samples. For the dataset as a whole, only 3 of 44 samples lie in the three bins between 24° and 36°. By comparison, the three bins between 12° and 24° contain 13 samples, and the three bins between 36° and 48° contain 11 samples.

In addition to the new data, we compiled existing paleomagnetic data from possible source regions (references provided in Table 5), which we present as (1) directions from individual, demagnetized sample cores, corrected for bedding tilt (Figure 7), and (2) histograms showing spectra of inclinations (Figures 7 and 9). The compilation is limited to Neoproterozoic-Cambrian strata from the Death Valley-Mojave region, the Caborca region, the Shinumo and Tapeats formations in Grand Canyon, and the Tapeats Formation and equivalents in the central Arizona highlands. The only published paleomagnetic study on Proterozoic strata in the central Arizona highlands were measurements of the NRM of Mesoproterozoic strata of the Apache Group (Pioneer Shale), which did not differ significantly from the modern field (Runcorn, 1964). Diabase sills that intruded the Apache Group at 1.1 Ga yield moderate inclinations (Harlan, 1993), as expected for late Mesoproterozoic time (e.g., Evans et al, 2016; Meert and Stuckey, 2002). Although we might expect moderate inclinations for central Arizona orthoquartzites, at present there is no basis to assume any particular distribution of inclinations from a population of Proterozoic clasts derived from the central Arizona highlands.

Because any given clast population represents a regional mixture of individual pebbles and cobbles from disparate sources, clast magnetizations are best compared with regional populations of magnetizations from individual paleomagnetic cores, as opposed to, for example, any particular site mean. In this form, a ready comparison can be made between a clast population and source populations according to some defined area. The Shinumo data (Figure 7a and 7b) show well-grouped, moderate to high inclination, with only a few measurements (3 of 95) below 30°. The Tapeats Formation cores in Grand Canyon (Figure 7c and 7d) are shallowly inclined and well-grouped into an east-west orientation. The Tapeats and related strata in the central Arizona highlands (Figure 7e and 7f) are also mostly of low inclination, but are far more scattered in declination, likely due in part to their more complex thermal and tectonic history. The Death Valley-Mojave region data (Figure 7g and 7h) are also generally of low inclination, and fairly diverse in declination. These data generally reflect a period of long residence of SW Laurentia at low paleolatitude in Neoproterozoic-Paleozoic time, not returning to higher paleolatitudes until the Jurassic. In sum, the extant data from potential source populations show broadly unimodal, shallow inclination spectra, except for the Shinumo Formation, which shows a moderate- to high-inclination spectrum.

Detrital Zircon Data

Detrital zircon age spectra of orthoquartzites from both potential sources and the Sespe Formation, including new data presented here and a compilation of published data (Table 5), are presented in Figure 8. Representative spectra from sources in Grand Canyon, including the Shinumo Formation and Tapeats Formation, are shown in the left-hand column (Figure 8a-8h), which includes sample IC-1-35 obtained for this study (Figure 8e). Representative spectra from potential sources in the Death Valley-Mojave region (Figure 8u and 8v) and central Arizona

highlands (Figure 8w-8aa) are shown in the right-hand column. Also shown in the right-hand column, for reasons discussed in detail below, are representative spectra from the Westwater Canyon Member of the Upper Jurassic Morrison Formation, which appears to be a source for one of the Sespe clasts. Representative spectra from the Death Valley region include the Zabriskie and upper Stirling Formations, and from the Arizona region include the Troy, Dripping Springs, Del Rio, Blackjack, Yankee Joe and White Ledges Formations. Samples in the center column include 10 clasts from the Miocene Sespe Formation and 2 clasts from the Eocene Sespe. As noted above, of the 10 Miocene Sespe samples, 8 have moderate to high paleomagnetic inclinations, and 2 have low paleomagnetic inclinations. As noted above, the low inclination samples (Figure 8q and 8r) were both collected from the same outcrop of "marker conglomerate" at the base of the Sespe along Santiago Canyon Road in the Santa Ana Mountains. The two clasts from Eocene Sespe both have moderate inclination. Analytical data for the 13 samples analyzed for this study are presented in Table S2.

The most prominent observation regarding the source spectra is that Grand Canyon and Death Valley sources both have multimodal ("cosmopolitan") spectra, with discernable peaks near 1.2, 1.4, and 1.7 Ga. In contrast, the central Arizona highlands sources tend to have unimodal or bimodal spectra, and include small numbers of pre-2.0 Ga grains. The only central Arizona highlands source with a Grenville-age peak is the Troy Quartzite, which features a strong peak at 1.26 Ga and a broad distribution of older ages, with a much weaker peak at 1.48 Ga (Figure 8w). The only other source with any Grenville component is the Dripping Springs Formation, which contains a few ages (<5%) younger than 1.3 Ga, associated with a broad peak at 1.4 Ga. The youngest zircons in the Dripping Springs and Troy formations are 1.23 and 1.20 Ga, respectively. Depositional ages of the other central Arizona orthoquartzite bodies are too old to contain

Grenville-aged zircons, and tend to be strongly unimodal at 1.7 Ga. Therefore, either (1) strong unimodality or (2) absence of pre-1.20 Ga Grenville-aged zircons, discriminate central Arizona sources from both Death Valley-Mojave region sources and Grand Canyon sources.

The data from the 12 Sespe clasts fall into two basic groups, which include 9 samples with cosmopolitan spectra (Figure 8i-q), and 3 with strongly unimodal spectra (Figure 8r-t). The cosmopolitan spectra tend to have 3 modes near 1.2 Ga, 1.4 Ga, and 1.7 Ga, and minor amounts of pre-2.0 Ga grains. Although the modes are variable in detail, they are mostly subequal, with the exception of sample BW4809, in which Grenville-age grains are much less abundant than in other cosmopolitan samples. The three samples with unimodal spectra all have peaks near 1.7 Ga, and each have a few pre-2.0 Ga grains.

Three of the nine cosmopolitan spectra also contain a small but significant fraction (ca. 5%) of Paleozoic and Mesozoic grains. The Paleozoic grains in sample LS1114 average 331 Ma, and a single Mesozoic age is 153.0 +/- 2.8 (1 sigma) Ma (Figure 8l). There are six Paleozoic grains in sample BW4809 that define a tightly clustered unimodal peak at 485 Ma, and no Mesozoic grains (Figure 8p). In sample BW1609, five Mesozoic grains cluster tightly near 168 Ma and a single Paleozoic grain is 510 +/- 10 Ma (Figure 8q).

We observe a general distinction in detrital zircon spectra between the Miocene and Eocene Sespe clast populations. In the Miocene population, 9 of 10 spectra contain abundant Grenville-aged zircons, with 8 of these 9 having a well-defined peak. All 9 samples contain grains younger than 1.20 Ga in their populations. The one remaining sample is unimodal with a 1.7 Ga peak. In contrast to the cosmopolitan spectra, the Eocene Sespe clasts are both unimodal with 1.7 Ga peaks.

DISCUSSION

Paleomagnetic inclination analysis

Comparison of Sespe Formation clasts and sandstone matrix

Paleomagnetic data from Piuma Member sandstones, collected in the same area that we collected orthoquartzite clasts along Piuma Road, have a tilt-corrected mean inclination of 39°+/- 6° (α_{95}) (Hillhouse, 2010). The CRM is carried by elongate, authigenic hematite that grew along cleavage planes within detrital biotite (Hillhouse, 2010). Because orthoquartzite clasts are generally devoid of detrital micas (Figure 4c, d) and other soluble phases, it is highly unlikely that the clasts carry this magnetization.

Further, in unmetamorphosed redbeds in general, the permeabilities of ultradurable clasts, such as orthoquartzite and metarhyolite ($<10^{-4}$ darcy), are at least 3 orders of magnitude lower than those of their porous sandstone matrix (0.1-1 darcy: e.g., Table 2.2 in Freeze and Cherry, 1979). This, in turn, suggests a strong contrast between clasts and matrix in exposure to diagenetic pore fluids. Thus, the elimination and replacement of the pre-depositional, CRM in orthoquartzite clasts with an early Miocene magnetization, similar to that of the Sespe sandstone matrix, is unlikely. We also note that, whereas the clast CRMs are of high coercivity and unblocking temperature, peak temperatures of the Sespe Formation are generally well below 150 °C, based on maximum burial depths of 5,000 m in the Saddle Peak area (e.g. Section D-D' of Dibblee, 1993) and 3,000 m in the northern Santa Ana Mountains (e.g. Section F-F' of Schoellhamer et al., 1981). These clasts, therefore, tend to retain their original CRMs during transport, deposition, and diagenesis in the shallow crust, especially if those magnetizations are of high coercivity and unblocking temperature (e.g., Hodych and Buchan, 1994; Pan and Symons, 1993).

Comparison of Sespe clasts to possible sources

Histograms of inclination data from each potential source formation are plotted at a uniform scale for comparison with histograms from clasts in the Sespe Formation at a suitably expanded vertical scale (Figure 9). An important assumption in any comparison of Sespe clasts to source data is that the latter are representative of the source region as a whole. In other words, we assume it is unlikely that the inclination distribution of 188 randomly sampled orthoquartzites in the Death Valley-Mojave region would differ significantly from the 188 samples shown in the left-hand column of Figure 9. The fact that distributions from individual samples and formations are, without exception, similar to the overall distribution, suggests that the extant dataset is representative of the region. There are probably sources where moderate to high inclinations are recorded by Death Valley-Mojave orthoquartzites, for example, by remagnetization in the contact aureoles of Mesozoic or Tertiary intrusions. But, such sources, if present, would occupy only a small fraction of the very extensive drainage area of Sespe gravels, and so they would be unlikely to influence the inclination distribution of the clast population as a whole.

With respect to sources in Figure 9, the low-inclination population of clasts from the Miocene and Eocene Sespe Formation could only have been derived from sources in the left-hand column, which includes Neoproterozoic/Cambrian formations in the Death Valley-Mojave region, the Tapeats Formation (both in the central Arizona highlands and in Grand Canyon), and Neoproterozoic-Cambrian strata of the Caborca region. The moderate- to high-inclination population of clasts, however, could not have been derived from the Neoproterozoic-Cambrian source populations, and require either a Shinumo Formation source, shown in the upper right-hand portion of Figure 9, or some other unidentified source with similar paleomagnetic characteristics. Such a source could plausibly be Mesoproterozoic or Paleoproterozoic orthoquartzites in the

central Arizona highlands, where as noted above, paleomagnetic data are lacking, or less plausibly from NW Sonora. Summations of the low-inclination distributions (from the Tapeats Formation and the Death Valley-Mojave region) and the moderate- to high-inclination distributions (Shinumo Formation) each define two unimodal distributions (Figure 10). A comparison of these distributions with the distribution of the Miocene Sespe clast population suggests that neither source alone could produce the bimodal clast distribution, but a combination of the two sources could.

Cumulative distribution functions (CDFs) from the Miocene and Eocene Sespe clast populations are compared to those from each of the three source regions in Figure 11. Distributions from the Death Valley-Mojave region, both as individual formations (including the Rainstorm Member of the Johnnie Formation, the Wood Canyon Formation, and the Zabriskie Formation), and as a whole, lie well to the left (low-inclination side) of the Miocene Sespe distribution, and somewhat to the left of the Eocene Sespe distribution (Figure 11a). Distributions from the Grand Canyon region lie either well to the left (Tapeats Formation) or well to the right (Shinumo Formation) of both Miocene and Eocene Sespe distributions (Figure 11b). A distribution from the central Arizona highlands region (Tapeats Formation) lies to the left of the Sespe distributions (Figure 11c).

The comparisons in Figure 11a-c appear to exclude the Death Valley-Mojave region as a sole source for the Miocene and Eocene Sespe distributions. However, because the central Arizona highlands region may contain sources with moderate to high inclinations, it cannot be ruled out as a source for either the Miocene or Eocene Sespe clast distributions. Linear combinations of the two Grand Canyon sources (Tapeats and Shinumo Formations as endmembers) compare well with the Miocene Sespe clast distribution for a broad range of mixtures (Figure 11d). For Shinumo fractions

ranging from about 30 to 60%, Kolmogorov-Smirnov tests yield p-values of 0.05 or greater (Figure 12), indicating that the derivation of Sespe clasts from this range of mixtures cannot be ruled out at 95% confidence. There is a strong maximum value of p for these mixtures of p = 0.34 for a Shinumo fraction of 35 to 40%. The same comparison of Grand Canyon sources and Eocene Sespe clasts is not as strong. For these mixtures, p-values of 0.05 or greater are restricted to Shinumo fractions of about 10 to 15%, with a maximum of only p = 0.07. These comparisons suggest that a sole Grand Canyon source comprising a mixture of Tapeats and Shinumo Formation clasts is a viable explanation of the inclination distributions the Sespe clast populations, and is particularly strong for the Miocene population. As noted earlier, ultradurable orthoquartzites in the Tapeats Formation are not exposed in eastern Grand Canyon, but are characteristic of western Grand Canyon exposures. Therefore, a roughly equal mixture of Tapeats and Shinumo clasts implies that the source areas included both the Upper Granite Gorge of eastern Grand Canyon and the Lower Granite Gorge of western Grand Canyon.

These comparisons, of course, may be equally well explained with mixtures that include components from both Death Valley-Mojave and central Arizona highlands sources, either with or without a very small contribution from Sonoran sources. Death Valley-Mojave sources cannot be distinguished from the Tapeats Formation in Grand Canyon, and Proterozoic sources from the central Arizona highlands may have moderate to high inclinations, and thus be indistinguishable from the Shinumo Formation. The key to distinguishing a Shinumo contribution to the Sespe clast population thus lies in a simple test that distinguishes the Shinumo Formation from orthoquartzites in the central Arizona highlands, using detrital zircon age spectra.

Detrital zircon analysis

Here, we apply the detrital zircon test to our analysis of populations of paleomagnetic inclinations, in order to discriminate source regions, both for individual clasts, and for the population of clasts as a whole in the Piuma Member and Eocene Sespe populations (Table 6).

In this analysis, it is important to first consider the three orthoquartzite clast samples containing small but significant populations of Paleozoic and Mesozoic grains (LS1114, BW4809, and BW1609; Figures 8l, 8p and 8q). These data raise the question of whether those grains are detrital components of the orthoquartzite, or whether they are "allochthonous" and incorporated upon or into the clast during weathering and transport.

Sample LS1114 (Figure 8l), from the Piuma Member, has a unique detrital zircon spectrum relative to all other samples, and its source is therefore quite uncertain. Based on comparison with the extensive detrital zircon dataset from Mesozoic sandstones on the Colorado Plateau (Dickinson and Gehrels, 2008), its most likely source is the Upper Jurassic Morrison Formation (Table 6). Similar to the Morrison, LS1114 has a moderate paleomagnetic inclination, scarcity of grains between 0.5 and 1 Ga in its detrital zircon spectrum, and is a well-indurated, light pinkish-gray, medium to coarse-grained orthoquartzite. Although the Mesozoic peak in the Sespe spectrum is not as prominent as in the two Morrison spectra, the ratio of Mesozoic to Proterozoic grains is more similar between LS1114 and CP21, from the Morrison, than it is between the two Morrison samples.

In contrast to LS1114, we interpret the Paleozoic grains in samples BW4809 and BW1609 (Figure 8p and q) to be allochthonous. Both samples were collected from the Miocene Sespe in the Santiago Canyon roadcut. Their detrital zircon spectra are a poor match for any known Paleozoic or Mesozoic sandstone in having a small, single Paleozoic mode. Further, clasts from this outcrop

exhibit petrographic evidence for the extensive development of silica glaze on the clast surface, beneath which thin films of allochthonous grains are adhered to the clast exterior, and narrow fractures in the clast interior that also locally contain allochthonous grains (Figure 13). Both of these clasts are densely-cemented, purple-hued orthoquartzites that are a poor lithologic match for even the most densely-cemented late Paleozoic or Mesozoic sandstones in the potential source regions. These samples both have low inclination but contrasting detrital zircon spectra (Figure 8q and 8r). The unimodal spectrum of BW1809 (Figure 8r) indicates that it was derived from the central Arizona highlands, suggesting that the inclination distribution of central Arizona orthoquartzites may include shallowly inclined samples. Sample BW1609 (Figure 8q), which has a strong Grenville-age peak, is probably derived from the Death Valley-Mojave region, based on its inclination, densely cemented grains, and purple hue (Table 6). This, of course, assumes that its small population of Mesozoic grains is allochthonous.

The two Eocene Sespe clasts with moderate inclinations both have unimodal peaks at 1.7 Ga and a smattering of Archaean grains, indicating derivation from the central Arizona highlands (Figure 8s, t, Table 6).

The remaining 7 samples were all collected from the Piuma Member (5 from the Piuma Road section, and 2 from the Red Rock Trail section), and have both moderate to high inclination and relatively broad Grenville-age zircon peaks. Among known potential sources, these characteristics restrict this population to a Shinumo Formation source, among known sources. As noted above, the Troy Quartzite at the top of the Apache Group is the only Proterozoic orthoquartzite in the central Arizona highlands to contain appreciable Grenville-age zircons (Figure 8w, versus Figures 8x-8ad), and therefore could be a potential source. However, the Troy data are dominated by an early Grenville peak near 1.26 Ga, with no grains younger than 1.20 Ga,

and very weak peaks near 1.4 and 1.7 Ga. In contrast, Miocene Sespe clasts and the Shinumo Formation are both characterized by broader Grenville peaks (including many grains between 1.0 and 1.20 Ga), and much stronger peaks at 1.4 and 1.7 Ga. A K-S test comparing the Troy data (Figure 8w) with Miocene Sespe clasts LS0814 and LS1214 (Figures 8j and 8m) yields p-values of 2.1×10^{-5} and 3.5×10^{-4}, respectively, ruling out derivation of sands in the Troy Formation and sands in the Miocene Sespe clasts from the same source. Therefore, extant data from the Apache Group do not provide a compelling match for orthoquartzite clasts in the Miocene Sespe Formation.

Interpretive complications

We consider here three important issues in interpreting the Shinumo Formation as the bedrock source for the moderately inclined mode of orthoquartzite clasts in the Miocene Sespe Formation. These include (1) primary structures within source formations, such as cross-stratification, and their influence on the inclination spectra of clast populations, (2) recycling of clasts from gravel sources that are intermediate in age between the Shinumo and Sespe Formations, which may compromise the interpretation of a Shinumo source for Miocene Sespe clasts, and (3) buried or now-eroded sources for the clasts outside of the eastern Grand Canyon region.

Primary structure

Orthoquartzites in the southwestern United States are substantially compacted after deposition, commonly cross-stratified, and locally contain paleoliquefaction structures. An analysis of the potential effects of primary structures on paleomagnetic inclination spectra is provided in Supplemental Text S1 and Figure S4. Our analysis suggests that primary structures, especially cross-stratification, may have a measurable effect on the distribution of paleomagnetic inclinations in any given sample population. Relationships between the measured orientations of foresets and

of paleomagnetic inclinations in potential source regions indicate that the difference between low inclination and moderate- to high-inclination populations would be augmented to some degree by this effect. Depending on the volume fraction of foreset laminations sampled by the clast population, such augmentation would be in the range of 0° to 15°, which serves to slightly enhance the distinction between the two populations, rather than obscure it.

Recycling of clasts

An additional complication in any provenance study is the possibility of recycling of clasts from secondary sources. It is possible that a significant fraction of Sespe gravel clasts are derived from conglomeratic strata that are intermediate in age between the time of exposure of their bedrock source and the time of Sespe deposition (e.g. Dickinson, 2008). As noted above, in the case of the Shinumo bedrock source region, extensive thermochronometric data demonstrate that unroofing of the Upper Granite Gorge in the eastern Grand Canyon region, which includes all known exposures of the Shinumo Formation, did not occur before c. 28-18 Ma (Flowers et al., 2008; Flowers and Farley, 2012; Lee et al., 2013; Karlstrom et al, 2014; Winn et al., 2017). Therefore, assuming lower Miocene Sespe orthoquartzites are indeed derived, in part, from the Shinumo Formation, the possibility of clast recycling does not alter the conclusion that sedimentary transport from Upper Granite Gorge bedrock sources to coastal California occurred between c. 28 and 20 Ma.

There is also the possibility that the clasts are recycled from conglomeratic strata that contain orthoquartzite detritus, either derived from the Shinumo Formation, or from an unknown source with similar paleomagnetic and detrital zircon characteristics. Because the Shinumo Formation was buried in Cambrian time, and remained so until the Oligocene, any pre-Oligocene recycling path must have begun prior to Cambrian burial. For example, Shinumo clasts could have been eroded into Neoproterozoic rift basins in the Death Valley region, and then supplied to the

Sespe Formation via an Amargosa paleoriver. Other potential recycled sources include the Jurassic cobble and boulder conglomerates of the Coyote Formation near Hermosillo, Mexico, and possible equivalents exposed as far north as the Caborca area, but these are unlikely as Sespe sources, as noted above. These and other recycling histories, although possible, thus require postulation of either distant or unknown reservoirs of orthoquartzite clasts that would somehow overwhelm extant, broadly exposed reservoirs in their contributions to the Miocene Sespe basin.

Buried or now-eroded sources

As in any provenance study, it is possible that an unknown source, either eroded away since 20 Ma or buried beneath the extensive alluvial deposits in the Basin and Range region, could have provided a clast population with any combination of the paleomagnetic and detrital zircon characteristics needed to explain the Sespe (clast) data. Nearly all of the moderate- to high-inclination clast population in the Piuma Road section has Shinumo characteristics (7 out of the 8 measured clasts, or 88%). Our results agree well with the observation (described above in Introduction and Geologic Setting) that the Shinumo Formation lies within the only known region in the Cordilleran interior that underwent kilometer-scale erosional denudation during Piuma time (c. 28-18 Ma). In other words, the Shinumo Formation is apparently the dominant source for the moderate- to high-inclination clast population. In contrast, the hypothesis that Piuma orthoquartzite clasts are substantially derived from the central Arizona highlands can be rejected at a high level of confidence, because eight out of eight clasts (Figure 14) failed the detrital zircon test. Deriving the Piuma orthoquartzite clast population from now-eroded or -buried sources in the Mojave region is clearly possible. However, it is inconsistent with the Laramide unroofing history of the region (80-40 Ma, versus the c. 20 Ma depositional age), which suggests a fairly stable landscape from 40 to c. 20 Ma (e.g. Spotila et al., 1998). In sum, we interpret our results to support the hypothesis stated

in the Introduction, that the mid-Tertiary, rapid unroofing event in the eastern Grand Canyon source region is reflected in an abundance of eastern Grand Canyon orthoquartzite clasts in coeval basins of coastal southern California.

Detrital zircon spectra in Sespe sandstone

In modern Colorado River sands, 20% of the detrital zircon population ranges in age from 300 to 900 Ma, reflecting the dominant contribution of Permian through Jurassic aeolianites widely exposed throughout the Colorado River drainage basin (Kimbrough et al., 2015). The Arizona River drainage proposed here (Figure 1) and in Wernicke (2011) includes part of the southwestern margin of the Colorado Plateau that, in turn, contains part of the region of 28-18 Ma erosion (stippled region in Figure 1). The area of the plateau included within the Arizona River drainage is nominally 30,000 km^2 (Figure 1), which is about 6% of the area of the modern Colorado River drainage basin that includes the Colorado Plateau and environs (about 500,000 km^2, Table 1 in Kimbrough et al., 2015). Thus, if the modern Colorado River drainage were limited to a Gila, Amargosa, and Colorado River with headwaters restricted to the eastern Grand Canyon region, the expected contribution of 300 to 900 Ma zircon grains would be (0.06) (0.20) = 0.012, or about 1% of the population. Detrital zircon age determinations from 22 samples of the Sespe Formation (including 1,378 total grains) yielded a contribution of 0.7% of 300 to 900 Ma detrital zircons (Table 1 in Ingersoll et al., 2013; Spafford, 2010), in reasonable agreement with the expected ratio. This 300 to 900 Ma population could be derived entirely from Mojave-Sonora region, entirely from the Grand Canyon region, or most likely from some combination of the two. In other words, the sandstone detrital zircon data are insufficient to discriminate between Mojave-Sonora and Grand Canyon sources for the 300 to 900 Ma detrital zircon component, contrary to the conclusion

of Ingersoll et al. (2013) that the data indicate no drainage link between southern California river deltas and the Grand Canyon region during Sespe time.

CONCLUSION

As summarized in Table 6 and Figure 14, our results show that combined intraclast paleomagnetic inclination and detrital zircon data provide significant new insights into the provenance of Sespe clast populations that cannot be derived from either dataset alone. The eight moderate- to high-inclination clasts from the Miocene Sespe for which we obtained detrital zircon spectra uniformly contain Grenville-age detrital zircon peaks (Figure 14), ruling out both the Death Valley-Mojave and central Arizona highlands regions as source populations. With the exception of LS1114, which appears to be Jurassic, we interpret them all as being derived from the Shinumo Formation (Figure 3, Figure 14). The two Miocene Sespe clasts that have low inclination were both collected from the Santiago Canyon Road locality, from the basal conglomerate of the lower Miocene Sespe Formation. Given that one yielded a unimodal detrital zircon peak at 1.7 Ga and the other a cosmopolitan spectrum, the central Arizona highlands and Death Valley-Mojave region both appear to be possible sources for the broader Miocene orthoquartzite population (Howard, 1996). The two Eocene Sespe clasts with moderate paleomagnetic inclinations yielded unimodal zircon age spectra with peaks at 1.7 Ga, indicating derivation from the central Arizona highlands. Clearly, more data will be required to further test the hypothesis that the Eocene Sespe is predominantly sourced from the central Arizona highlands (e.g. Howard, 2000, 2006). It is noteworthy, however, that the outcome of moderate inclination plus a unimodal 1.7 Ga peak observed in the Eocene Sespe was not observed in any of the ten Miocene Sespe samples. Therefore, regardless of how one interprets these data in terms of provenance, they have clear potential to identify and characterize contrasting clast populations (Figure 14).

Because all seven of the moderate- to high-inclination Miocene Sespe clasts of pre-Mesozoic age contain post-1.2 Ga zircons, it is likely that most or all of the total population of moderate- to high-inclination clasts (19 of 34 samples, or 56%) have similar characteristics. Therefore, if our interpretation is correct that these characteristics indicate a Shinumo source, it places an important constraint on the erosion kinematics of the Cordillera post-Laramide. Because the only known exposures of the Shinumo Formation lie within a few hundred meters elevation of the bottom of eastern Grand Canyon, our interpretation supports the existence of a mid-Tertiary drainage connection, or Arizona River, between high-relief, eroding uplands in the eastern Grand Canyon region and the coast. Further, it is highly unlikely that a SW-flowing Arizona River running near the bottom of eastern Grand Canyon would have "jumped" out of Grand Canyon before reaching the coast. Assuming it did not, the only plausible course would have run through an existing western Grand Canyon, as also implied by a roughly equal mixture of ultradurable Tapeats (exposed only in western Grand Canyon) and Shinumo clasts suggested by the simple linear mixing models of the Piuma inclination spectra. Our results thus provide independent support for models that suggest western Grand Canyon was carved to within a few hundred meters of its current depth no later than 20 Ma, and perhaps as early as Late Cretaceous/Paleocene time, based on thermochronological evidence (e.g., Flowers et al., 2008; Wernicke, 2011; Flowers and Farley, 2012).

ACKNOWLEDGMENTS

This research was supported by NSF grants EAR 10-19896 and EAR 14-51055 awarded to B. Wernicke, EAR 17-28690 awarded to J. Stock, and OPP 13-41729 awarded to J. Kirschvink. We also acknowledge NSF grant EAR 16-49254 awarded to G. Gehrels at the University of Arizona for support of the Arizona LaserChron Center. We thank Jonathan Hagstrum of the U.S.

Geological Survey for providing the unpublished paleomagnetic data of D. Elston and S. Grommé from the Shinumo Formation. Guidance from the Associate Editor and reviewers R. Molina-Garza and R. V. Ingersoll substantially improved the manuscript.

SUPPLEMENTAL MATERIAL

Table S1. Columns show sample number, measurement type (alternating field, AF, thermal, TT), field strength (mT) or temperature (T), declination and inclination, publicly available in MagIC Data Repository upon publication (https://earthref.org/MagIC/16652/0fc080bf-3661-45e4-bd5f-487142ef2f91).

Table S2. Sheets in Excel file include detrital zircon ages from LaserChron and Apatite to Zircon of Sespe orthoquartzite clasts and Shinumo Formation, publicly available in California Institute of Technology Research Data Repository (https://data.caltech.edu/records/1245).

Figure S1. Photos of 7 representative clasts showing stratification.

Figure S2. Zijderveld demagnetization plots for all paleomagnetic data.

Figure S3. Photomicrographs of selected samples.

Figure S4. Relationship between cross-stratification and paleomagnetic inclination in Neoproterozoic-Cambrian and Shinumo strata.

Text S1. Discussion of effect of primary structures on paleomagnetic inclination spectra.

REFERENCES CITED

Abbott, P. L., and Peterson, G.L., 1978, Effects of abrasion durability on conglomerate clast populations: examples from Cretaceous and Eocene conglomerates of the San Diego area, California: Journal of Sedimentary Research, v. 48, p. 31-42.

Abbott, P. L., Smith, T.E., 1989, Sonora, Mexico, source for the Eocene Poway conglomerate of southern-California: Geology, v. 17, p. 329-332.

Abbott, P. L., Smith, T. E., and Huang, C. H., 1991, On the origin of some rhyolitic clasts in the basal Sespe Formation, Los Angeles area, California: Society for Economic Paleontologists and Mineralogists, Pacific Section, Book 68, p. 93-98.

Atwater, T., and Stock, J., 1998, Pacific-North America plate tectonics of the Neogene southwestern United States: an update: International Geology Review, v. 40, p. 375-402.

Beard, L. S., Karlstrom, K. E., Young, R. A., and Billingsley, G.H., 2011, CRevolution 2 - Origin and Evolution of the Colorado River System, Workshop Abstracts: U.S. Geological Survey Open-File Report 2011–1210, 300 p.

Bellemin, G. J., and Merriam, R., 1958, Petrology and origin of the Poway Conglomerate, San Diego County, California: Geological Society of America Bulletin, v. 69, p. 199-220.

Belyea, R. R., and Minch, J. A., 1989, Stratigraphy and depositional environments of the Sespe Formation, northern Santa Ana Mountains, California, in Colburn, I. P. et al., eds., Conglomerates in Basin Analysis: a Symposium Dedicated to A. O. Woodford: Pacific Section, Society of Economic Paleontologists and Mineralogists, Bakersfield, p. 281-300.

Billingsley, G. H., and 12 others, 1996, Geologic map of the eastern part of the Grand Canyon National Park: Grand Canyon, Arizona, Grand Canyon Association, scale 1:65,500, 1 sheet.

Bloch, J. D., Timmons, J. M., Crossey, L. J., Gehrels, G. E. and Karlstrom, K. E., 2006, Mudstone petrology of the Mesoproterozoic Unkar Group, Grand Canyon, USA: Provenance, weathering, and sediment transport on intracratonic Rodinia: Journal of Sedimentary Research, v. 76, p. 1106-1119.

Blythe, A. E., Burbank, D. W., Farley, K. A., and Fielding, E. J., 2000, Structural and topographic evolution of the central Transverse Ranges, California, from apatite fission-track, (U-Th)/He and digital elevation model analyses: Basin Research, v. 12, p. 97–114.

Bryant, B., Naeser, C.W., and Fryxell, J.E., 1991, Implications of low-temperature cooling on a transect across the Colorado Plateau–Basin and Range boundary: Journal of Geophysical Research, v. 96, p. 12,375– 12,388, doi:10.1029/90JB02027.

Burchfiel, B. C., Davis, G. A., and Cowan, D. S., 1992, Tectonic overview of the Cordilleran orogen in the western United States, in Burchfiel, B. C., Lipman, P. W., and Zoback, M. L., eds. The Cordilleran Orogen: Conterminous U. S.: Boulder, Colorado, Geological Society of America, The Geology of North America, v. G3, p. 407-479.

Cather, S. M., Connell, S. D., Chamberlin, R. M., McIntosh, W. C., Jones, G. E., Potochnik, A. R., Lucas, S. G., and Johnson, P. S., 2008, The Chuska erg: Paleogeomorphic and paleoclimatic implications of an Oligocene sand sea on the Colorado Plateau: Geological Society of America Bulletin, v. 120, no. 1-2, p. 13-33.

Daneker, T. M., 1975, Sedimentology of the Precambrian Shinumo Sandstone, Grand Canyon, Arizona: M.S. thesis, Northern Arizona University, 195 p.

Darling, A., and Whipple, K., 2015, Geomorphic constraints on the age of the western Grand Canyon: Geosphere, v. 11, no. 4, doi:10.1130/GES01131.1.

Dibblee, T. W., Jr., 1993, Geologic map of the Malibu Beach quadrangle, Los Angeles County, California: Santa Barbara, California, Dibblee Geological Foundation, Map DF-47, scale 1:24,000.

Dickinson, W. R., 2008, Impact of differential zircon fertility of granitoid basement rocks in North America on age populations of detrital zircons and implications for granite petrogenesis: Earth and Planetary Science Letters, v. 275, p. 80–92.

Dickinson, W. R., and Gehrels, G. E., 2008, Sediment delivery to the Cordilleran foreland basin: Insights from U-Pb ages of detrital zircons in Upper Jurassic and Cretaceous strata of the Colorado Plateau: American Journal of Science, v. 308, p. 1041-1082.

Doe, M. F., Jones III, J. V., Karlstrom, K. E., Thrane, K., Frei, D., Gehrels, G., and Pecha, M., 2012, Basin formation near the end of the 1.60–1.45 Ga tectonic gap in southern Laurentia: Mesoproterozoic Hess Canyon Group of Arizona and implications for ca. 1.5 Ga supercontinent configurations: Lithosphere, v. 4, p. 77-88.

Elston, D. P., and Bressler, S. L., 1977, Paleomagnetic poles and polarity zonation from Cambrian and Devonian strata of Arizona: Earth and Planetary Science Letters, v. 36, p. 423-433.

Elston, D. P., and Grommé, C. S., 1994, Middle Proterozoic magnetostratigraphic polar path and polarity zonation from Grand Canyon, Northern Arizona, US Geological Survey, Menlo Park (ms.).

Elston, D. P., and Young, R. A., 1991, Cretaceous-Eocene (Laramide) landscape development and Oligocene-Pliocene drainage reorganization of transition zone and Colorado Plateau, Arizona: Journal of Geophysical Research: Solid Earth, v. 96, p. 12389-12406.

Evans, D. A., Veselovsky, R. V., Petrov, P. Y., Shatsillo, A. V., and Pavlov, V. E., 2016, Paleomagnetism of Mesoproterozoic margins of the Anabar Shield: A hypothesized billion-year partnership of Siberia and northern Laurentia: Precambrian Research, v. 281, p. 639-655.

Fisher, N. I., Lewis, T., Embleton, B. J. J., 1987, Statistical analysis of spherical data: Cambridge University Press, 329 p.

Fitzgerald, P. G., Fryxell, J. E., and Wernicke, B. P., 1991, Miocene crustal extension and uplift in southeastern Nevada: Constraints from fission track analysis: Geology, v. 19, p. 1013-1016.

Fitzgerald, P. G. Duebendorfer, E. M., Faulds, J. E. and O'Sullivan, P., (2009), South Virgin–White Hills detachment fault system of SE Nevada and NWArizona: Applying apatite fission track thermochronology to constrain the tectonic evolution of a major continental detachment fault: Tectonics, v. 28, doi:10.1029/2007TC002194.

Flowers, R. M., and Farley, K. A., 2012, Apatite $^{4}He/^{3}He$ and (U-Th)/He evidence for an ancient Grand Canyon: Science, v. 338, p. 1616-1619.

Flowers, R. M., and Farley, K. A., 2013, Response to comments on "Apatite $^{4}He/^{3}He$ and (U-Th)/He evidence for an ancient Grand Canyon": Science, v. 340, p. 143-143.

Flowers, R. M., Wernicke, B. P., and Farley, K. A., 2008, Unroofing, incision, and uplift history of the southwestern Colorado Plateau from apatite (U-Th)/He thermochronometry: Geological Society of America Bulletin, v. 120, p. 571-587.

Flowers, R. M., Farley, K. A., and Ketcham, R. A., 2015, A reporting protocol for thermochronologic modeling illustrated with data from the Grand Canyon: Earth and Planetary Science Letters, v. 432, p. 425-435.

Foster, D. A., Gleadow, A. J. W., Reynolds, S. J., and Fitzgerald, P. G., 1993, Denudation of metamorphic core complexes and the reconstruction of the Transition Zone, west-central

Arizona - Constraints from apatite fission-track thermochronology: Journal of Geophysical Research-Solid Earth, v. 98, no. B2, p. 2167-2185.

Fox, M., Tripathy-Lang, A., Shuster, D. L., Winn, C., Karlstrom, K., and Kelley, S., 2017, Westernmost Grand Canyon incision: testing thermochronometric resolution: Earth and Planetary Science Letters, v. 474, p. 248-256.

Freeze, R. A., and Cherry, J. A., 1979, Groundwater: Prentice-Hall, Englewood Cliffs, N. J., 604 p.

Gehrels, G. E., and Stewart, J. H., 1998, Derital zircon U-Pb geochronology of Cambrian to Triassic miogeoclinal and eugeoclinal strata of Sonora, Mexico: Journal of Geophysical Research, v. 103, p. 2471-2487.

Gehrels, G., Valencia, V., and Pullen, A., 2006, Detrital zircon geochronology by laser-ablation multicollector ICPMS at the Arizona LaserChron Center: The Paleontological Society Papers, v. 12, p. 67-76.

Gehrels, G. E., Valencia, V. A., and Ruiz, J., 2008, Enhanced precision, accuracy, efficiency, and spatial resolution of U-Pb ages by laser ablation–multicollector–inductively-coupled plasma–mass spectrometry: Geochemistry, Geophysics, Geosystems, v. 9, no. 3.

Gehrels, G. E., Blakey, R., Karlstrom, K. E., Timmons, J. M., Dickinson, B., and Pecha, M., 2011, Detrital zircon U-Pb geochronology of Paleozoic strata in the Grand Canyon, Arizona: Lithosphere, v. 3, p. 183-200.

Gehrels, G., and Pecha, M., 2014, Detrital zircon U-Pb geochronology and Hf isotope geochemistry of Paleozoic and Triassic passive margin strata of western North America: Geosphere, v. 10, p. 49-65.

Gillett, S. L., and Van Alstine, D. R., 1979, Paleomagnetism of Lower and Middle Cambrian sedimentary rocks from the Desert Range, Nevada: Journal of Geophysical Research: Solid Earth, v. 84, p. 4475-4489.

Harlan, S. S., 1993, Paleomagnetism of Middle Proterozoic diabase sheets from central Arizona: Canadian Journal of Earth Sciences, v. 30, p. 1415-1426.

Hereford, R., 1977, Deposition of the Tapeats Sandstone (Cambrian) in central Arizona: Geological Society of America Bulletin, v. 88, p. 199-211.

Hill, C. A., and Polyak, V. J., 2014, Karst piracy: A mechanism for integrating the Colorado River across the Kaibab uplift, Grand Canyon, Arizona, USA: Geosphere, v. 10, p. 627–640, doi:10.1130/GES00940.1.

Hill, C. A., Polyak, V. J., and Asmerom, Y., 2016, Constraints on a Late Cretaceous uplift, denudation, and incision of the Grand Canyon region, southwestern Colorado Plateau, USA, from U-Pb dating of lacustrine limestone: Tectonics, v. 35, p. 896-906.

Hillhouse, J. W., 2010, Clockwise rotation and implications for northward drift of the western Transverse Ranges from paleomagnetism of the Piuma Member, Sespe Formation, near Malibu, California: Geochemistry, Geophysics, Geosystems, v. 11, no. 7.

Hodych, J. P., and Buchan, K. L., 1994, Early Silurian palaeolatitude of the Springdale Group redbeds of central Newfoundland: a palaeomagnetic determination with a remanence anisotropy test for inclination error: Geophysical Journal International, v. 117, p. 640-652.

Hoffman, M., Stockli, D. F., Kelley, S. A., Pederson, J., and Lee, J., 2011, Mio-Pliocene erosional exhumation of the central Colorado Plateau, eastern Utah—New insights from apatite (U-Th)/He thermochronometry, in Beard, L.S., et al., eds., CRevolution 2 - Origin and Evolution

of the Colorado River System, workshop abstracts: U.S. Geological Survey Open-File Report 2011–1210, p. 132-136.

House, M. A., Wernicke, B. P., and Farley, K. A., 1998, Dating topography of the Sierra Nevada, California, using apatite (U–Th)/He ages: Nature, v. 396, p. 66.

Howard, J. L., 1989, Conglomerate clast populations of the upper Paleogene Sespe Formation, southern California, in Colburn, I. P. et al., eds., Conglomerates in Basin Analysis: a Symposium Dedicated to A. O. Woodford: Pacific Section, Society of Economic Paleontologists and Mineralogists, Bakersfield, p. 269-280.

Howard, J. L., 1996, Paleocene to Holocene paleodeltas of ancestral Colorado River offset by the San Andreas fault system, southern California: Geology, v. 24, p. 783-786.

Howard, J. L., 2000, Provenance of quartzite clasts in the Eocene–Oligocene Sespe Formation: Paleogeographic implications for southern California and the ancestral Colorado River: Geological Society of America Bulletin, v. 112, p. 1635-1649.

Howard, J. L., 2005, The quartzite problem revisited: Journal of Geology, v. 113, no. 6, p. 707-713.

Howard, J. L., 2006, Provenance of metavolcanic clasts in the upper Paleogene Sespe Formation near Los Angeles, and its bearing on the origin of the Colorado River in Southern California, in Girty, G. H. and Cooper, J. D. eds. Stratigraphy, sedimentology, and geochemistry to unravel the geologic history of the southwestern Cordillera, Society of Economic Paleontologists and Mineralogists, Pacific Section, Book 101, p. 179-192.

Huntington, K. W., Wernicke, B. P., and Eiler, J., 2010, Influence of climate change and uplift on Colorado Plateau paleotemperatures from carbonate clumped isotope thermometry, Tectonics, v. 29, TC3005, doi:10.1029/2009TC002449.

Ingersoll, R. V., Grove, M., Jacobson, C. E., Kimbrough, D. L., and Hoyt, J. F., 2013, Detrital zircons indicate no drainage link between southern California rivers and the Colorado Plateau from mid-Cretaceous through Pliocene: Geology, v. 41, p. 311–314.

Ingersoll, R. V., Spafford, C. D., Jacobson, C. E., Grove, M., Howard, J. L., Hourigan, J., and Pedrick, J., 2018, Provenance, paleogeography and paleotectonic implications of the mid-Cenozoic Sespe Formation, coastal southern California, USA, in Ingersoll, R.V., Lawton, T. F., and Graham, S. A., eds., Tectonics, sedimentary basins, and provenance: A celebration of the career of William R. Dickinson: Geological Society of America Special Paper 540, p. 441-462.

Izaguirre-Pompa, A. and Iriondo, A., 2007, Mesoproterozoic (~1.2 Ga) quartzite and intruding anorthosite (~1.08 Ga) from Sierra Prieta, NW Sonora: Mexican additions to the Precambrian history of SW Laurentia, in Ores and Orogenesis, Program with Abstracts, Arizona Geological Society, Tucson, Arizona, p. 147-148.

Jacobson, C. E., Grove, M., Pedrick, J. N., Barth, A. P., Marsaglia, K. M., Gehrels, G. E., and Nourse, J. A., 2011, Late Cretaceous–early Cenozoic tectonic evolution of the southern California margin inferred from provenance of trench and forearc sediments: Geological Society of America Bulletin, v. 123, p. 485-506.

Jones, C. H., 2002, User-driven integrated software lives: “PaleoMag” Paleomagnetics analysis on the Macintosh: Computers and Geosciences, v. 28, p. 1145-1151.

Karlstrom, K. E., and Timmons J. M., 2012, Many unconformities make one 'Great Unconformity': Geological Society of America, *Special Paper* 489, p73-79. DOI: 10.1130/2012.2489(04).

Karlstrom, K. E., Crow, R., Crossey, L. J., Coblentz, D., and Van Wijk, J. W., 2008, Model for tectonically driven incision of the younger than 6 Ma Grand Canyon: Geology, v. 36, p. 835-838.

Karlstrom, K. E., Lee, J., Kelley, S., Crow, R., Crossey, L., Young, D., Beard, L. S., Ricketts, J., Fox, M., and Shuster, D., 2014, Formation of the Grand Canyon 5 to 6 million years ago through integration of older palaeocanyons: Nature Geoscience , v. 7, p. 239–244, doi:10.1038/ngeo2065.

Karlstrom, K. E., Crossey, L. J., Embid, E., Crow, R., Heizler, M., Hereford, R., Beard, L. S., Ricketts, J.W., Cather, S., and Kelley, S., 2017, Cenozoic incision history of the Little Colorado River: Its role in carving Grand Canyon and onset of rapid incision in the past ca. 2 Ma in the Colorado River System: Geosphere, v. 13, no. 1, p. 49–81, doi:10.1130 /GES01304.1.

Kelly, T. S., Lander, E. B., Whistler, D. P., Roeder, M. A., and Reynolds, R. E., 1991, Preliminary report on a paleontologic investigation of the lower and middle members, Sespe Formation, Simi Valley Landfill, Ventura County, California: PaleoBios , v. 13, p. 1-13.

Kelly, T. S., and Whistler, D. P., 1994, Additional Uintan and Duchesnean (middle and late Eocene) mammals from the Sespe Formation, Simi Valley, California: Natural History Museum of Los Angeles County, Contributions to Science, v. 439, p. 1-29.

Kies, R. P., and Abbott, P. L., 1983, Rhyolite clast populations and tectonics in the California continental borderland: Journal of Sedimentary Research, v. 53, p. 461-475.

Kimbrough, D. L., Grove, M., Gehrels, G. E., Dorsey, R. J., Howard, K. A., Lovera, O., Aslan, A., House, P. K., and Pearthree, P. A., 2015, Detrital zircon U-Pb provenance of the Colorado River: A 5 m.y. record of incision into cover strata overlying the Colorado Plateau and adjacent regions: Geosphere, v. 11, p. 1719-1748.

Kirschvink, J. L., 1980, The least-squares line and plane and the analysis of paleomagnetic data: Royal Astronomical Society Geophysical Journal, v. 62, p. 699-718.

Kirschvink, J. L., Kopp, R. E., Raub, T. D., Baumgartner, C. T., and Holt, J. W., 2008. Rapid, precise, and high-sensitivity acquisition of paleomagnetic and rock-magnetic data: Development of a low-noise automatic sample changing system for superconducting rock magnetometers: Geochemistry, Geophysics, Geosystems, v. 9, no. 5, doi:10.1029/2007GC001856.

Lander, E. B., 2011, Stratigraphy, biostratigraphy, biochronology, geochronology, magnetostratigraphy, and plate tectonic history of the early middle Eocene to late early Miocene Sespe, Vaqueros, and lower Topanga Formations, east-central Santa Monica Mountains, Los Angeles County, southern California: Western Association of Vertebrate Paleontologists 2011 Annual Meeting Field Trip Volume and Guidebook, Altadena, CA, 65 p.

Lander, E. B., 2013, Stratigraphy, biostratigraphy, biochronology, geochronology, magnetostratigraphy, and plate tectonic history of the early middle Eocene to late early Miocene Sespe, Vaqueros, and lower Topanga Formations, east-central Santa Monica

Mountains, Los Angeles County, southern California: Society of Vertebrate Paleontology 73rd Annual Meeting Field Trip Volume and Guidebook on Arikareean and Hemingfordian Mammalian Vertebrate Paleontology of the Santa Monica Mountains National Recreation Area, Los Angeles County, Southern California, Altadena, CA.

Lechler, A. R., and Niemi, N. A., 2011, Sedimentologic and isotopic constraints on the Paleogene paleogeography and paleotopography of the southern Sierra Nevada, California: Geology, v. 39, n. 4, p. 379-382.

Lee, J. P., Stockli, D. F., Kelley, S. A., Pederson, J. L., Karlstrom, K. E., and Ehlers, T. A., 2013, New thermochronometric constraints on the Tertiary landscape evolution of the central and eastern Grand Canyon, Arizona: Geosphere, v. 9, p. 216-228.

Lucchitta, I., 2013, Comment on "Apatite $^{4}He/^{3}He$ and (U-Th)/He evidence for an ancient Grand Canyon:" Science, v. 340, no. 6129, p. 143-143.

Mahan, K. H., Guest, B., Wernicke, B. P. and Niemi, N. A., 2009, Low-temperature thermochronologic constraints on the kinematic history and spatial extent of the eastern California shear zone, Geosphere, v. 5 (6), p. 1–13; doi: 10.1130/GES00226.1.

McFadden, P. L., and Reid, A. B., 1982, Analysis of palaeomagnetic inclination data: Royal Astronomical Society Geophysical Journal, v. 69, p. 307–319.

McQuarrie, N. and Wernicke, B. P., 2005, An animated tectonic reconstruction of southwestern North America since 36 Ma: Geosphere, v. 1, no. 3, p. 1-20. doi: 10.1130/GES00016.1.

McKee, E. D., and Resser, C. E., 1945, Cambrian History of the Grand Canyon Region: Carnegie Institute Publications, v. 563, 232 p.

Meert, J. G., and Stuckey, W., 2002, Revisiting the paleomagnetism of the 1.476 Ga St. Francois Mountains igneous province, Missouri: Tectonics, v. 21, no. 2.

Minch, J. A., Howard, J. L., and Belyea, R. R., 1989, Sespe Formation conglomerates in the northern Santa Ana and Santa Monica Mountains: a field trip guide, in Colburn, I. P. et al., eds., Conglomerates in Basin Analysis: a Symposium Dedicated to A. O. Woodford: Pacific Section, Society of Economic Paleontologists and Mineralogists, Bakersfield, p. 301-312.

Minguez, D., Kodama, K. P., and Hillhouse, J. W., 2015, Paleomagnetic and cyclostratigraphic constraints on the synchroneity and duration of the Shuram carbon isotope excursion, Johnnie Formation, Death Valley Region, CA: Precambrian Research, v. 266, p. 395-408.

Molina-Garza, R. S., Acton, G. D, and Geissman, J. W., 1998, Carboniferous through Jurassic paleomagnetic data and their bearing on rotation of the Colorado Plateau: J. Geophys. Res., v. 103, p. 24,179–24,188.

Molina-Garza, R. S., and Geissman, J. W., 1999, Paleomagnetic data from the Caborca terrane, Mexico: implications for Cordilleran tectonics and the Mojave Sonora megashear hypothesis: Tectonics, v. 18, p. 293-325.

Moore, T. E., O'Sullivan, P. B., Potter, C. J., and Donelick, R. A., 2015, Provenance and detrital zircon evolution of early Brookian foreland basin deposits of the western Brooks Range, Alaska, and implications for early Brookian tectonism: Geosphere, v. 11, p. 93–122, doi:10.1130/GES01043.1.

Mulder, J. A., Karlstrom, K.E., Fletcher, K., Heizler, M.T., Timmons, J.M., Crossey, L.J., Gehrels, G.E., and Pecha, M., 2017, The syn-orogenic sedimentary record of the Grenville Orogeny in southwest Laurentia: Precambrian Research, 294, p. 33-52.

Noble, L. F., 1910, Contributions to the geology of the Grand Canyon Arizona: The geology of the Shinumo area: American Journal of Science, v. 29, no. 173, p. 369-386.

Noble, L. F., 1914, The Shinumo quadrangle, Grand Canyon district, Arizona: U.S. Geological Survey Bulletin 549, 100 p.

Pan, H., and Symons, D. T. A., 1993, The Pictou red beds' Pennsylvanian pole: Could Phanerozoic rocks in the interior United States be remagnetized?: Journal of Geophysical Research: Solid Earth, v. 98, p. 6227-6235.

Pederson, J., Mackley, R. D. and Eddleman, J. L., 2002, Colorado Plateau uplift and erosion evaluated using GIS: GSA Today, p. 4-10.

Polyak, V. J., Hill, C. A., and Asmerom, Y., 2008, Age and evolution of the Grand Canyon revealed by U-Pb dating of water table-type speleothems: Science, v. 319, p. 1377–1380, doi:10.1126/science.1151248.

Quigley, M., Karlstrom, K., Kelley, S. and Heizler, M., 2010, Timing and mechanisms of basement uplift and exhunation in the Colorado Plateau-Basin and Range Transition Zone, Virgin Mountain Anticline, Nevada-Arizona, in Umhoefer, P., Lamb, M. and Beard, L. S., eds., Miocene tectonics of the Lake Mead region, central Basin and Range:, Geological Society of America Special Paper 463, p. 311-329.

Raub, T. D., 2013, Miocene Grand Canyon with base level in Precambrian strata? Testing a Shinumo source scenario for seemingly special Sespe clasts using paleomagnetism: Geological Society of America Abstracts with Programs, 45, n. 7, 400.

Reynolds S. J., Florence, E. P. Welty, J.W., Roddy, M. S., Currier, D. A., Anderson, A. V. and Keith, S. B., 1986, Compilation of radiometric age determinations in Arizona: Arizona Bureau of Geology and Mineral Technology, Geological Survey Branch, Bulletin 197, 252 p.

Runcorn, S. K., 1964, Paleomagnetic results from Precambrian sedimentary rocks in the western United States: Geological Society of America Bulletin, v. 75, p. 687-704.

Sass, J. H., Lachenbruch, A. H., Galanis, S. P., Morgan, P., Priest, S. S., Moses, T. H. and Munroe, R. J., 1994, Thermal regime of the southern Basin and Range province 1. Heat-flow data from Arizona and the Mojave Desert of California and Nevada: Journal of Geophysical Research-Solid Earth, v. 99, p. 22093-22119.

Schoenborn, W. A., Fedo, C. M., and Farmer, G. L., 2012, Provenance of the Neoproterozoic Johnnie Formation and Stirling Quartzite, southeastern California, determined by detrital zircon geochronology and Nd isotope geochemistry: Precambrian Research, v. 206, p. 182-199.

Schoellhamer, J. E., Vedder, J. G., Yerkes, R. F., and Kinney, D. M., 1981, Geology of the Northern Santa Ana Mountains, California: U. S. Geological Survey Professional Paper 420-D, 107 p.

Sharp, R. P., 1940, Ep-Archean and Ep-Algonkian erosion surfaces, Grand Canyon, Arizona: Bulletin of the Geological Society of America, v. 51, no. 5/8, p. 1235-1269.

Spafford, C. D., 2010, Provenance implications of sandstone petrology and detrital-zircon analysis of the mid-Cenozoic Sespe Formation, coastal southern California [M.S. thesis]: Los Angeles, University of California, 117 p.

Spencer, J. E., Pecha, M. E., Gehrels, G. E., Dickinson, W. R., Domanik, K. J., and Quade, J., 2016, Paleoproterozoic orogenesis and quartz-arenite deposition in the Little Chino Valley area, Yavapai tectonic province, central Arizona, USA: Geosphere, v. 12, p. 1774-1794.

Spotila, J. A., Farley, K. A., and Sieh, K., 1998, Uplift and erosion of the San Bernardino Mountains associated with transpression along the San Andreas fault, California, as constrained by radiogenic helium thermochronometry: Tectonics, v. 17, p. 360-378.

Stewart, J. H., Gehrels, G. E., Barth, A. P., Link, P. K., Christie-Blick, N., and Wrucke, C. T., 2001, Detrital zircon provenance of Mesoproterozoic to Cambrian arenites in the western United States and northwestern Mexico: Geological Society of America Bulletin, v. 113, p. 1343-1356.

Stewart. J. H., and Roldán-Quintana, J., 1991, Upper Triassic Barranca Group; Nonmarine and shallow-marine rift-basin deposits of northwestern Mexico: Geological Society of America Special Paper 254, p. 19-36.

Stewart, J. H., 1970, Upper Precambrian and Lower Cambrian strata in the southern Great Basin, California and Nevada: U.S. Geological Survey Professional Paper 620, 206 p.

Stüwe, K., White, L., and Brown, R., 1994, The influence of eroding topography on steady-state isotherms. Application to fission track analysis: Earth and Planetary Science Letters, v. 124, p. 63-74.

Tauxe, L., Kent, D. V., 2004, A simplified statistical model for the geomagnetic field and the detection of shallow bias in paleomagnetic inclinations: Was the ancient magnetic field dipolar?, in Timescales of the Paleomagnetic Field, American Geophysical Union, Washington, D. C., Geophysical Monograph Series, v. 145, p. 101-115.

Van Alstine, D. R., and Gillett, S. L., 1979, Paleomagnetism of Upper Precambrian sedimentary rocks from the Desert Range, Nevada: Journal of Geophysical Research, v. 84, p. 4490-4500.

Wernicke, B., 2011, The California River and its role in carving Grand Canyon: Geological Society of America Bulletin, v. 123, no. 7-8, p. 1288-1316.

Wernicke, B., Raub, T. D., Grover, J. A., and Lander, B. E., 2010, Possible clasts of Shinumo Quartzite (eastern Grand Canyon) in lower Miocene conglomerates of the Sespe Formation (coastal southern California), and implications for the uplift and erosion history of the southwestern US: Geological Society of America Abstracts with Programs, 42, n. 5, p. 185.

Wernicke, B., Raub, T. D., Lander, B. E., and Grover, J. A., 2012, Testing the Arizona River hypothesis: Detrital zircon spectra from orthoquartzite clasts in the mid-Tertiary Sespe Formation of coastal southern California: Geological Society of America Abstracts with Programs, 44, n. 6, p. 80.

Wilson, C. J. L., 1973, The prograde microfabric in a deformed quartzite sequence, Mount Isa, Australia: Tectonophysics, v. 19, p. 39–81.

Winn, C., Karlstrom, K. E., Shuster, D. L., Kelley, S., and Fox, M., 2017, 6 Ma age of carving westernmost Grand Canyon: Reconciling geologic data with combined AFT, (U–Th)/He, and $^{4}He/^{3}He$ thermochronologic data: Earth and Planetary Science Letters, v. 474, p. 257-271.

Woodford, A. O., Welday, E. E., and Merriam, R., 1968, Siliceous tuff clasts in the upper Paleogene of southern California: Geological Society of America Bulletin, v. 79, p. 1461-1486.

Woodford, A. O., McCulloh, T. J., and Schoellhamer, J. E., 1972, Paleogeographic significance of metatuff boulders in middle Tertiary strata, Santa Ana Mountains, California: Geological Society of America Bulletin, v. 83, p. 3433-3436.

FIGURES

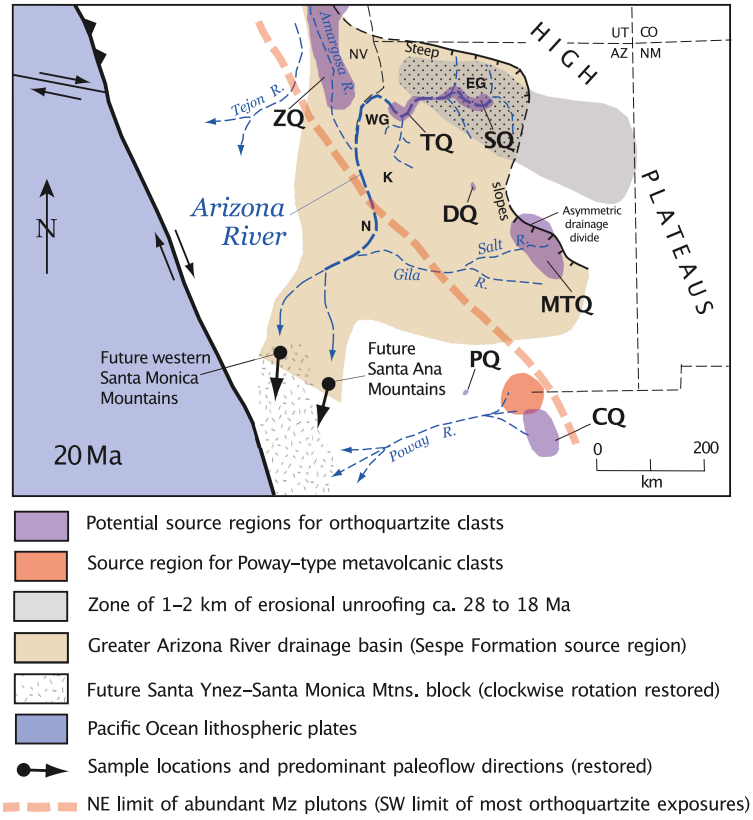

Figure 1: Geologic reconstruction of early Miocene positions of the Sespe Fm.

Geologic reconstruction, based on McQuarrie and Wernicke (2005), showing the early Miocene positions of Sespe Formation depocenters in the Santa Monica and Santa Ana Mountains with dominant paleoflow directions, and the extent of the Sespe Formation source regions, as inferred by Howard (2000, 2006) and Ingersoll et al. (2018), but including a portion of the southwestern Colorado Plateau, after Wernicke (2011). Stippled area inside zone of 28 to 18 Ma erosional unroofing delimits 30,000 km^2 area potentially contributing detritus to the Piuma Member of the Sespe Formation. The four main regions of exposed orthoquartzite (purple) include: (1) Death Valley-Mojave region, with Lower Cambrian Zabriskie Formation (ZQ) and associated Neoproterozoic orthoquartzites; (2) Grand Canyon region, with Shinumo Formation (SQ) of Mesoproterozoic age in eastern Grand Canyon (EG), and quartzitic portions of the Tapeats

Formation (TQ) of Cambrian age in western Grand Canyon (WG); (3) central Arizona highlands Paleo- to Mesoproterozoic rocks including Mazatzal, Tonto, and Hess Canyon groups (MTQ) and Del Rio Formation (DQ); (4) Neoproterozoic-Cambrian orthoquartzites (including clasts recycled in Jurassic conglomerates) in the Caborca area of Sonora, Mexico (CQ) and Mesoproterozoic quartzites at Sierra Prieta (PQ) in NW Sonora. Proposed paleorivers discussed in text shown in blue dashed lines. K, Kingman, Arizona, N, Needles, California.

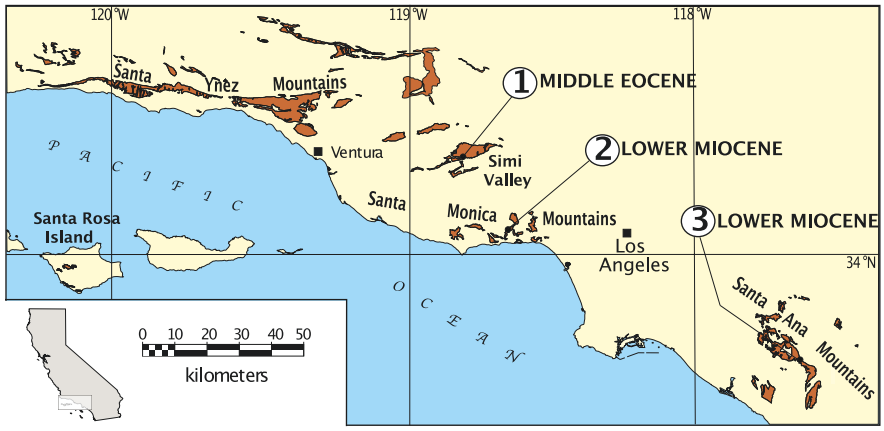

Figure 2: Map exposed early to mid-Tertiary Sespe Formation

Map showing distribution of surface exposures of early to mid-Tertiary Sespe Formation (reddish-brown shading) in the Los Angeles region (after Lander et al., 2011), and sample localities (black dots) with Sespe depositional ages, including: 1, View Lane Drive locality in Simi Valley, 2, Piuma Road and Scheuren Road localities in the Santa Monica Mountains, and 3, Red Rock Trail in Limestone Canyon Park, and Santiago Canyon Road localities in the Santa Ana Mountains (Tables 2 and 3).

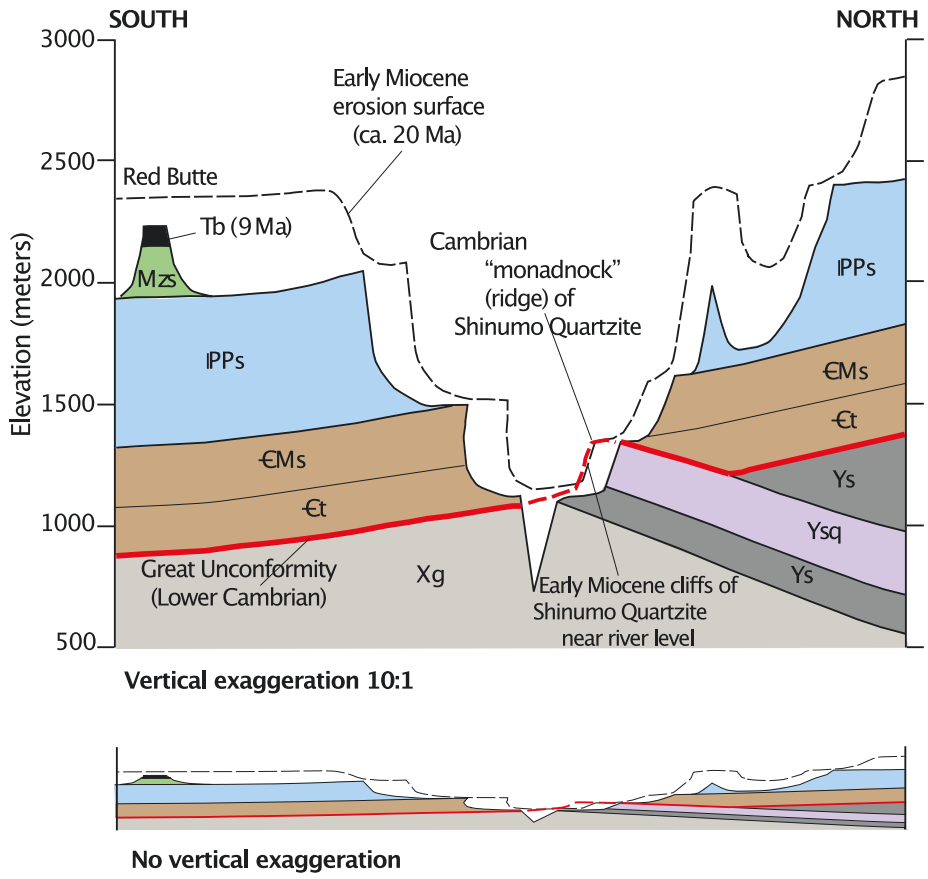

Figure 3: N-S Cross-section through Upper Granite Gorge area of eastern Grand Canyon

Generalized north-south cross-section through the Upper Granite Gorge area of eastern Grand Canyon region showing the disposition of the Shinumo Formation (Ysq) relative to a nominal early Miocene erosion surface. Xg, Paleoproterozoic gneiss, Ys, Mesoproterozoic strata, €t, Cambrian Tonto Group, €Ms, Cambrian through Mississippian strata, PPs, Pennsylvanian through Permian strata, Mzs, Mesozoic strata, and Tb, Tertiary basalt.

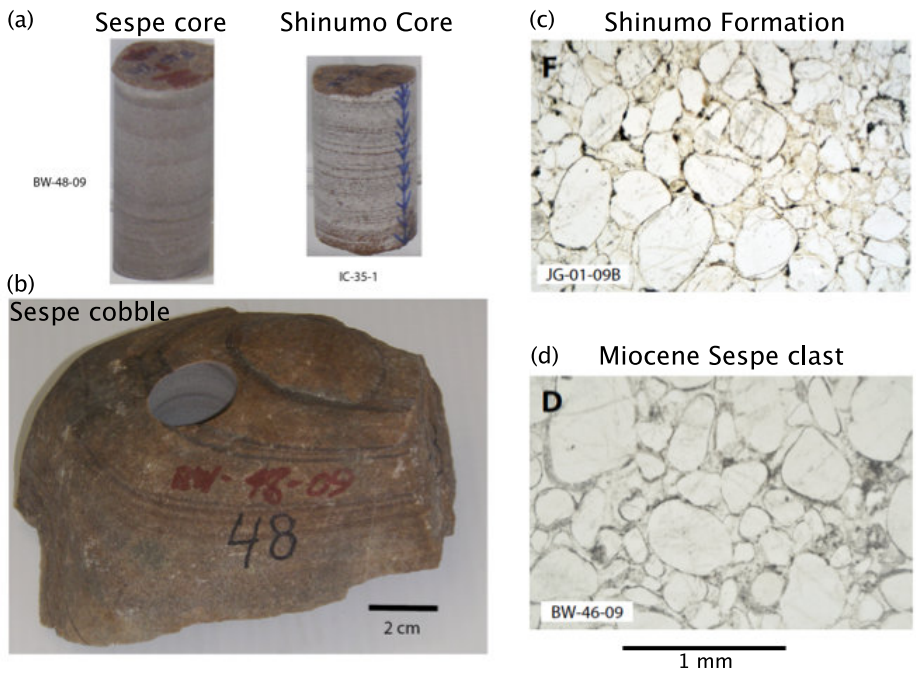

Figure 4: Photographs and photomicrographs of paleomagnetic cores of clasts

(a) Photograph of paleomagnetic cores of orthoquartzites, drilled perpendicular to bedding, from a Miocene Sespe Formation clast (left) and a bedrock sample of the Shinumo Formation (right). (b) Photograph of a Sespe Formation orthoquartzite cobble showing sedimentary lamination and drill-hole for left-hand paleomagnetic core shown in (a). (c, d) Photomicrographs of orthoquartzites from the Shinumo Formation and a clast from the Miocene Sespe Formation, respectively.

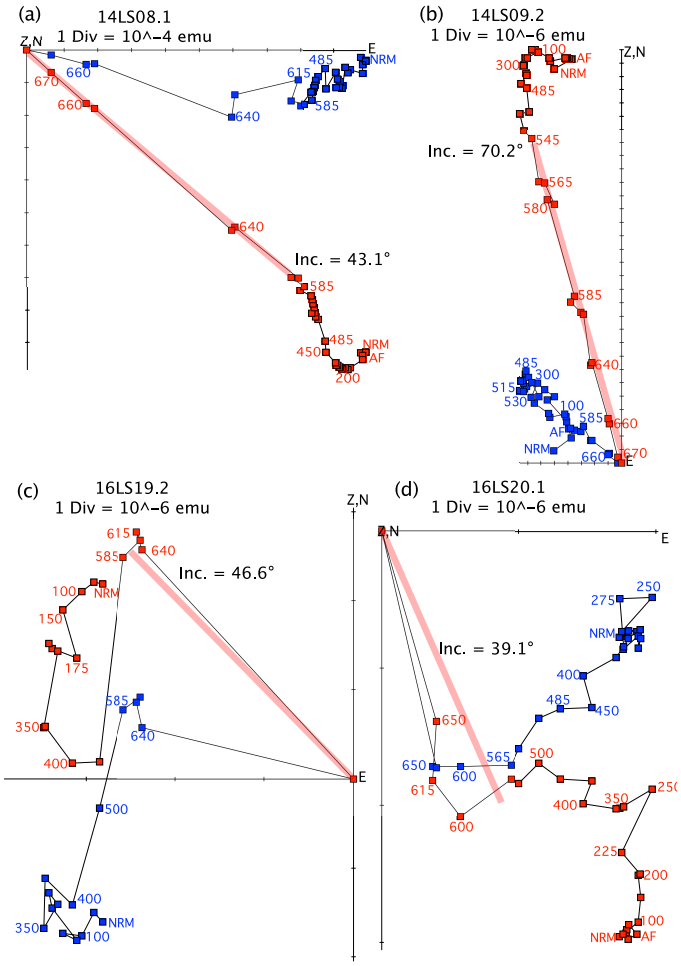

Figure 5: Zijderfeld plots of thermal demagnetizations for clasts

Zijderfeld plots showing thermal demagnetization histories of samples of orthoquartzite clasts from Miocene (a, b) and Eocene (c, d) Sespe Formation conglomerates. Detrital zircon spectra were determined for all four samples, as annotated on Figure 8.

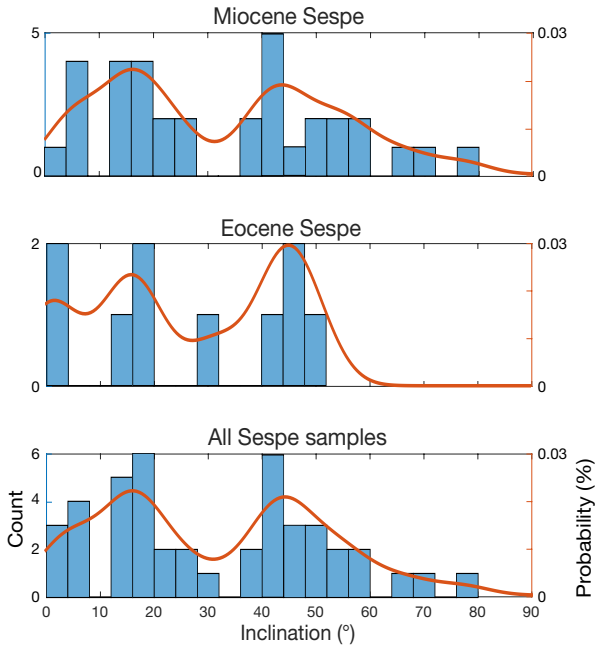

Figure 6: Histograms of paleomagnetic inclinations

Histograms and population density functions (PDFs) of paleomagnetic inclinations measured in clasts of the Miocene (a) and Eocene (b) Sespe Formation, shown as a sum in (c).

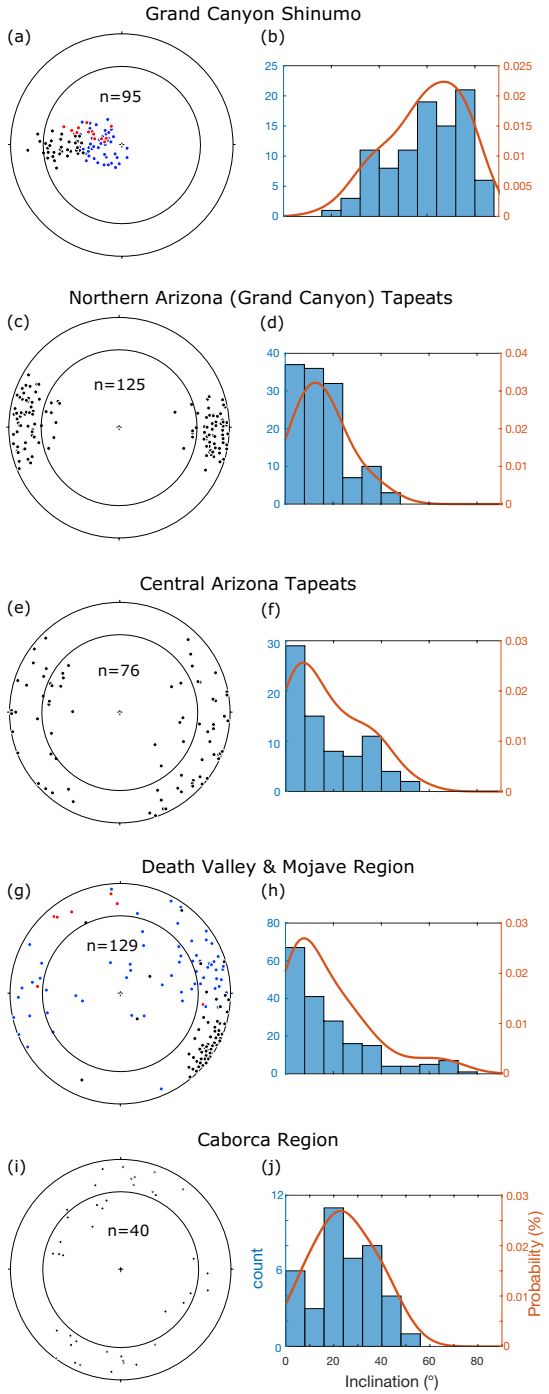

Figure 7: Inventory of published paleomagnetic data for source regions

Inventory of published orientations of CRMs for >700 individual paleomagnetic cores from known sources of orthoquartzite in southwestern North America. Stereograms of orientations of individual core samples are shown in (a), (c), (e), and (g) and respective histograms and PDFs of

paleomagnetic inclinations are shown in (b), (d), (f), and (h). (a, b) Shinumo Formation, including lower (red dots), middle (black dots), and upper (blue dots) stratigraphic levels (D. Elston and S. Gromme, written commun., 1994), eastern Grand Canyon; (c, d) Tapeats Formation, Grand Canyon (Elston and Bressler, 1977); (e, f) central Arizona highlands, including Tapeats sandstone and equivalent strata, (Elston and Bressler, 1977); (g, h) Neoproterozoic-Cambrian strata of the Death Valley-Mojave region, including the Zabriskie Formation (red, Gillett and Van Alstine, 1979), the Wood Canyon Formation (black, Gillett and Van Alstine, 1979), and the Rainstorm Member of the Johnnie Formation (blue, Van Alstine and Gillett, 1979). A 30° inclination contour is shown as a small circle on each stereogram.

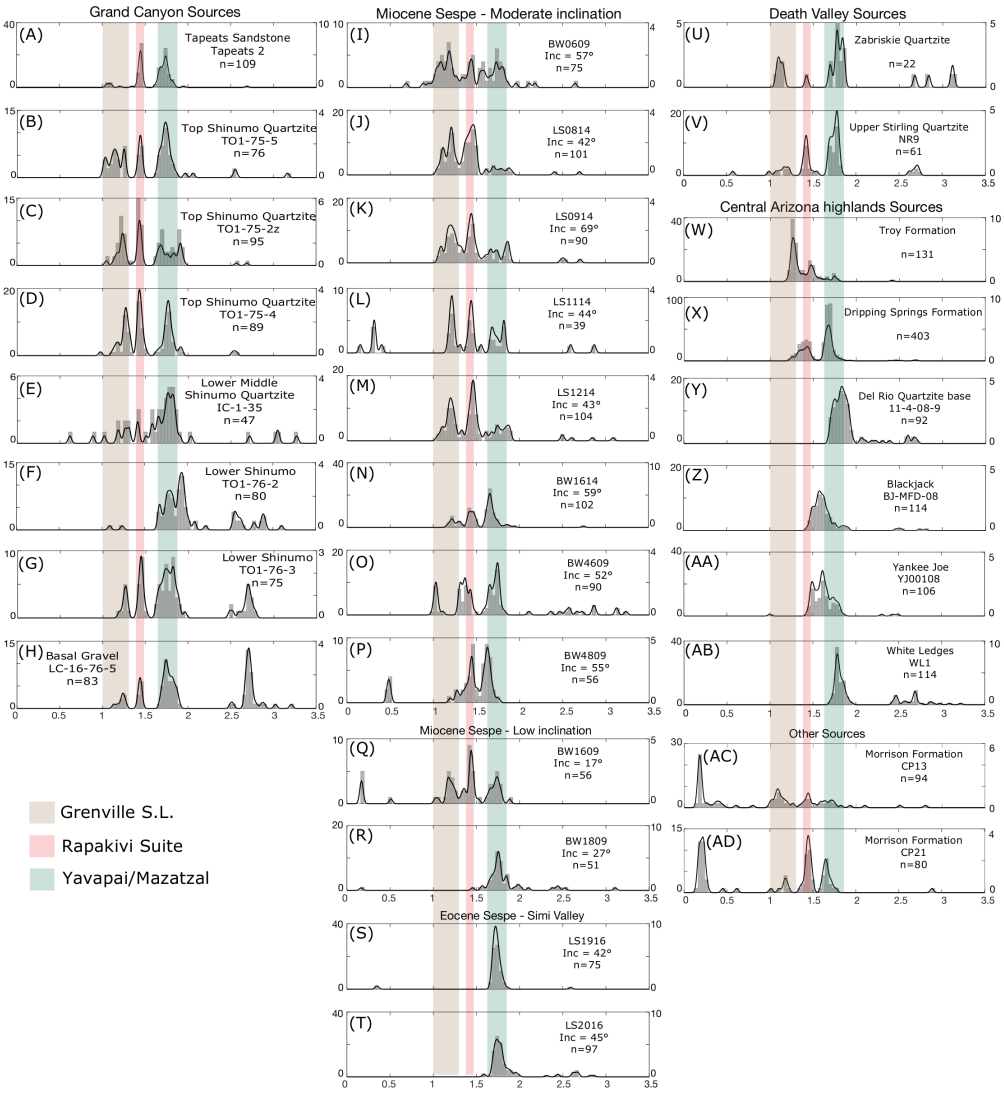

Figure 8: Detrital zircon spectra of potential sources and Sespe clasts

Detrital zircon spectra of potential sources and Sespe clasts. Potential Grand Canyon sources in the left column include the Tapeats Formation (a) and the Shinumo Formation (b-h). The center column includes Miocene Sespe clasts with moderate inclinations (i-p), Miocene Sespe clasts with low inclination (q, r), and Eocene Sespe clasts with moderate inclination (s, t). The right column shows Death Valley sources including the Zabriskie Quartzite (u) and Upper Stirling Quartzite (v), and central Arizona highland sources including the Troy Quartzite (3 samples) (w), the Dripping Springs Formation (3 samples) (x), the Del Rio Quartzite base (y), the Blackjack (z), Yankee Joe

(aa), and White Ledges (ab). We also include two samples of the Morrison Formation (ac) and (ad). Data sources are listed in Table 4.

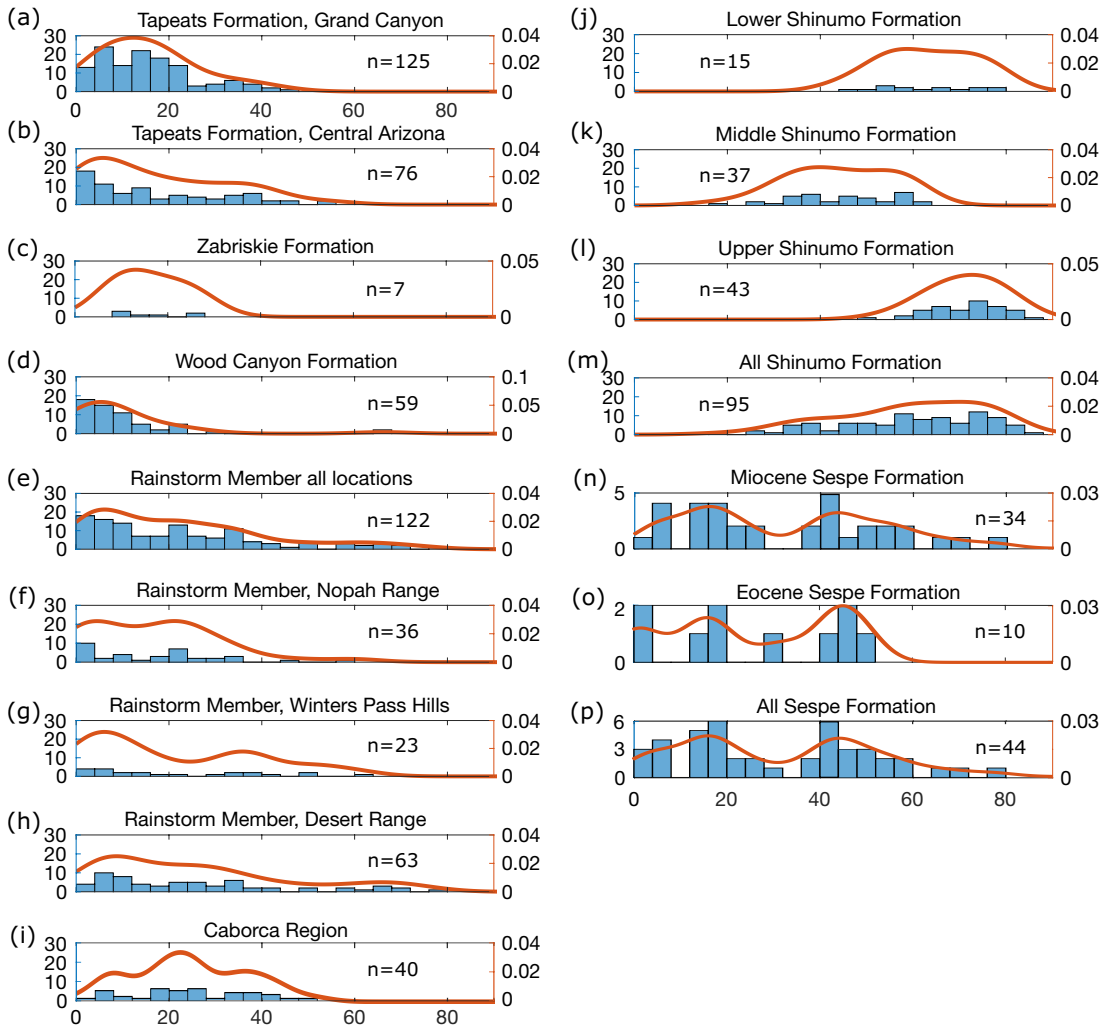

Figure 9: Histograms of paleomagnetic inclinations from potential sources and Sespe Formation

Histograms of paleomagnetic inclinations from potential sources, plotted at a uniform scale, and from clasts in the Sespe Formation, plotted at a suitably expanded scale. Potential sources from Grand Canyon include the Tapeats Formation (a) and the Shinumo Formation (j, k, l, and m). Potential sources from the central Arizona highlands include the Tapeats Formation (b). Potential Death Valley sources include the the Zabriskie Formation (c), Wood Canyon Formation (d), Rainstorm Member of the Johnnie Formation (e, f, g, and h). Potential sources from Caborca

include Ediacaran-Cambrian strata, mainly the El Arpa, Caborca, Clemente, Papalote, and Cerro Prieto formations (i). Paleomagnetic inclinations were measured in this study from the Miocene Sespe Formation (n) and the Eocene Sespe Formation (o), shown also as a sum (p). Paleomagnetic inclinations of the Rainstorm Member from the Nopah Range and Winters Pass Hills were measured after thermal demagnetization of 500-610 °C (Minguez et al., 2015), and inclinations of the Rainstorm Member from the Desert Range were demagnetized to 650 °C (Van Alstine and Gillett, 1979). Directions from the Wood Canyon (red-purple mudstones only) and Zabriskie Formations, both in the Desert Range, measured after thermal demagnetization to 640 °C (Gillett and Van Alstine, 1979 Figs 3f and 4). Paleomagnetic inclinations from the Tapeats Formation in the central Arizona highlands and in Grand Canyon were measured after thermal demagnetization at temperatures of 500-590 °C (Elston and Bressler, 1977). Inclinations from the lower Shinumo Formation were measured after demagnetization at 550 °C, from the middle Shinumo at 500-620 °C (data referred to as "Pole 4"), and from the upper Shinumo at 500-620 °C (Elston and Grommé, unpub.). Inclinations from clasts in the Miocene Sespe Formation (m) and clasts in the Eocene (n) are from this study, plotted also as a sum (o). Data sources are listed in Table 4.

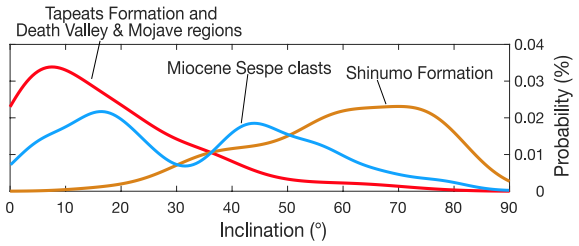

Figure 10: PDFs of inclination data from Sespe Formation and possible sources

Comparisons of probability density functions (PDFs) of paleomagnetic inclination data from Miocene Sespe orthoquartzite clasts (yellow curve), a summed population of Tapeats Formation, from both Grand Canyon and central Arizona highlands, and formations from the Death Valley-Mojave regions (blue curve), and the Shinumo Formation (red curve).

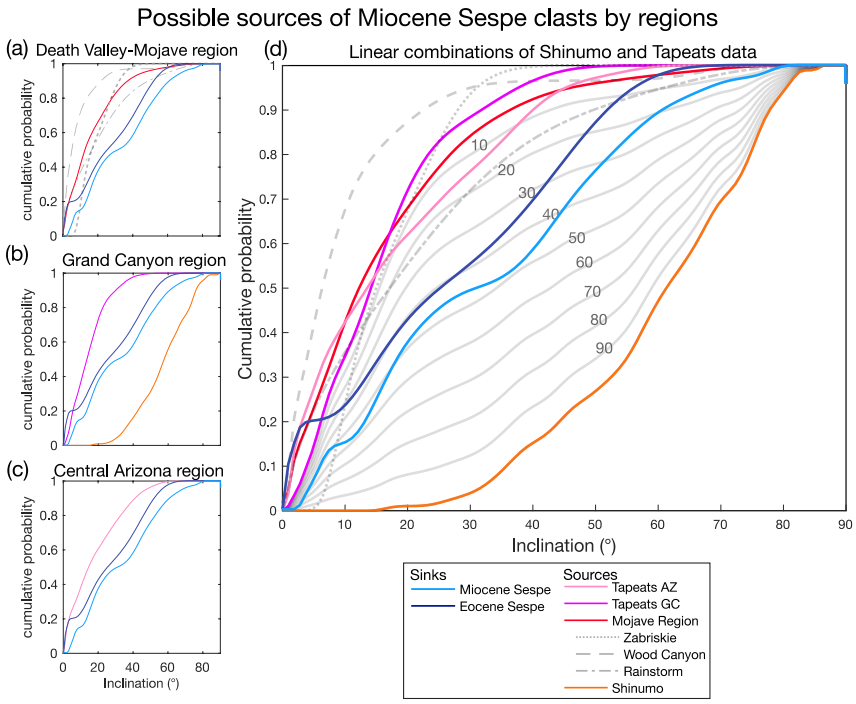

Figure 11: CDFs of inclination data from Sespe clasts and possible sources.

Comparisons of cumulative distribution functions (CDFs) of inclination data from Sespe orthoquartzite clasts (blue-hued curves) and possible sources (red-hued curves), including (a) Death Valley-Mojave region sources, (b) Grand Canyon region sources, and (c) central Arizona highlands sources. The three gray curves in (a) are summed to yield an average for the Death Valley-Mojave region (red). (d) Summary plot showing linear mixtures of Tapeats Formation from Grand Canyon and Shinumo Formations as endmembers, contoured in 10% increments (solid gray curves).

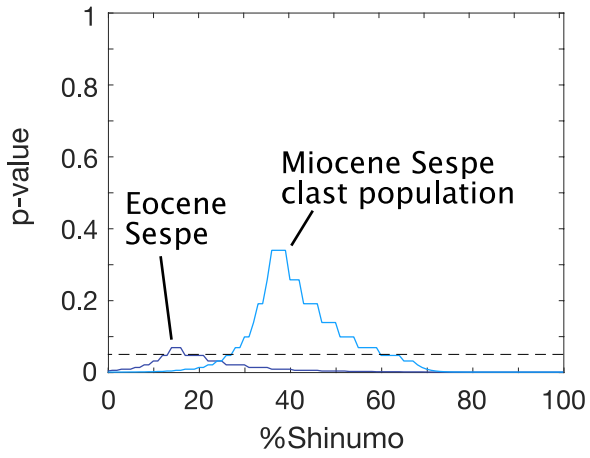

Figure 12: P-values for comparing Miocene and Eocene Sespe Fm to Grand Canyon sources

P-values for comparisons of CDFs from Figure 10, including (a) Eocene Sespe and (b) Miocene Sespe inclination populations, and mixtures of Tapeats Formation from eastern Grand Canyon (right endmembers) and Shinumo Formation (left endmembers) inclination populations.

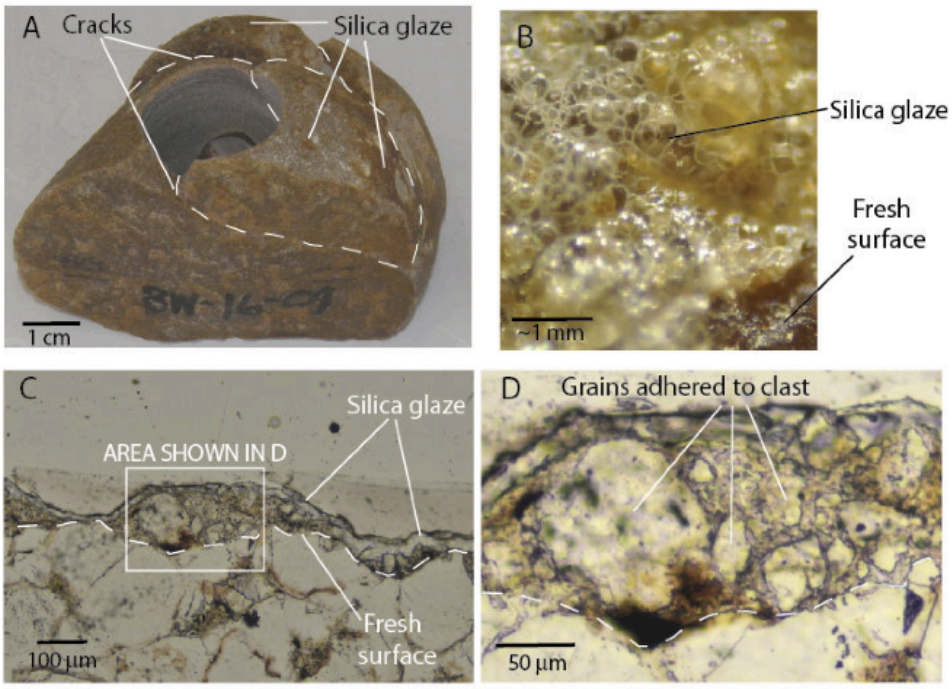

Figure 13: Silica glaze on Sespe orthoquartzite clast

Images of silica glaze on a Sespe orthoquartzite clast from roadcut on Santiago Canyon Road. (a) Photo showing light brown weathering patches of silica glaze on clast exterior, and the location of cracks within the sample that locally contain detrital material external to the clast, (b) photo showing small-scale mammillary texture of silica glaze in reflected light, (c, d) photomicrographs of thin sections cut normal to clast exterior showing silica glaze in cross-section, which includes external grains adhered to the clast, in transmitted light.

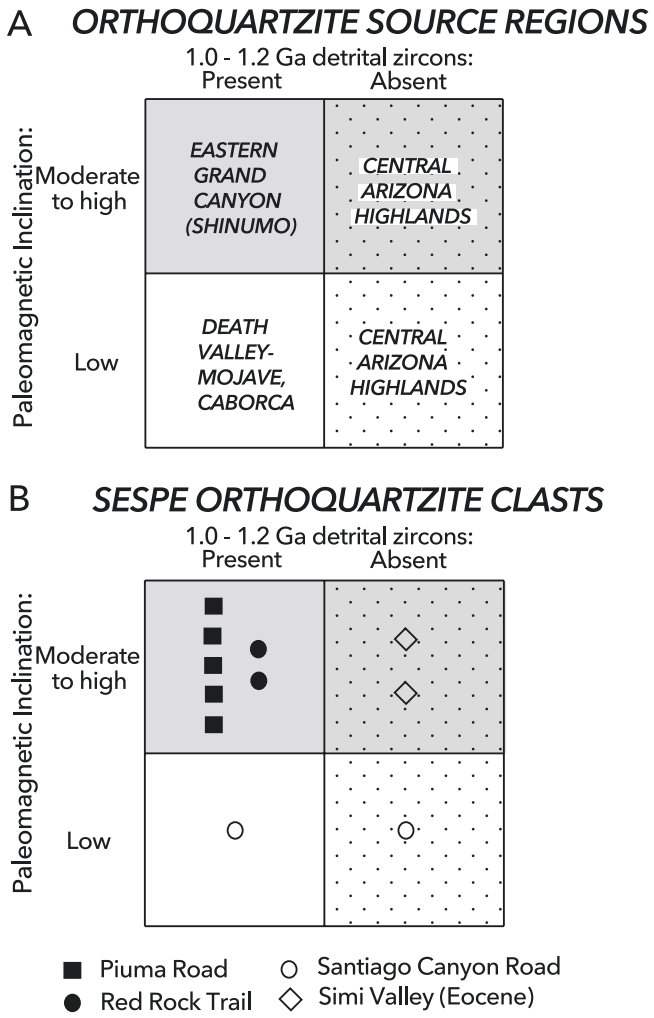

Figure 14: Summary matrix

Matrices summarizing research outcomes of paleomagnetic and detrital zircon data for (A) orthoquartzite detrital source regions and (B) pre-Mesozoic orthoquartzite clasts in which both paleomagentic inclination and detrital zircon data were obtained (n=11), keyed to sample collection locality.

TABLE 1. COLLECTED SAMPLES FROM GRAND CANYON SOURCES

Sample number	Location		Formation
	Lat (°N)	Long (°W)	
Grand Canyon, South Kaibab Trail			
IC-1-35*†§	36°05'30"N (approx)	112°05'20" W (approx)	Shinumo
Grand Canyon, Clear Creek Trail			
IC-503-35*	36°06'20"N (approx)	112°04'50" W (approx)	Tapeats
Grand Canyon, River Mile 75			
JG -01-09*	36° 03' 15.6"N	111 54' 03.37"W	Shinumo

*Petrography

†Paleomagnetic analysis

§Detrital zircon analysis

Table 1: Collected samples from Grand Canyon sources

TABLE 2. COLLECTED SAMPLES OF SESPE CLASTS FROM SOUTHERN CALIFORNI

Sample number	Location		Age
	Lat (°N)	Long (°W)	
Piuma Road, Malibu			
BW-01-09	34° 04' 13.0"N	118 39' 59.86"W	Miocene
BW-02-09	34° 04' 13.0"N	118 39' 59.86"W	Miocene
BW-03-09	34° 04' 13.0"N	118 39' 59.86"W	Miocene
BW-04-09	34° 04' 13.0"N	118 39' 59.86"W	Miocene
BW-05-09	34° 04' 13.0"N	118 39' 59.86"W	Miocene
BW-06-09*†§	34° 04' 13.0"N	118 39' 59.86"W	Miocene
BW-07-09	34° 04' 13.0"N	118 39' 59.86"W	Miocene
BW-08-09	34° 04' 13.0"N	118 39' 59.86"W	Miocene
BW-16-14*†§	34° 4'20.25"N	118°39'29.08"W	Miocene
BW-17-14*†	34° 4'20.25"N	118°39'29.08"W	Miocene
14LS01*†	34° 4'20.25"N	118°39'29.08"W	Miocene
14LS02*†	34° 4'20.25"N	118°39'29.08"W	Miocene
14LS03*	34° 4'20.25"N	118°39'29.08"W	Miocene
14LS04*†	34° 4'20.25"N	118°39'29.08"W	Miocene
14LS05*	34° 4'20.25"N	118°39'29.08"W	Miocene
14LS06*†	34° 4'20.25"N	118°39'29.08"W	Miocene
14LS07*†	34° 4'20.25"N	118°39'29.08"W	Miocene
14LS08*†§	34° 4'20.25"N	118°39'29.08"W	Miocene
14LS09*†§	34° 4'20.25"N	118°39'29.08"W	Miocene
14LS10*	34° 4'20.25"N	118°39'29.08"W	Miocene
14LS11*†§	34° 4'20.25"N	118°39'29.08"W	Miocene
14LS12*†§	34° 4'20.25"N	118°39'29.08"W	Miocene
14LS13*	34° 4'20.25"N	118°39'29.08"W	Miocene
14LS14*†	34° 4'20.25"N	118°39'29.08"W	Miocene
14LS15*†	34° 4'12.22"N	118°40'5.59"W	Miocene
14LS16*	34° 4'12.22"N	118°40'5.59"W	Miocene
14LS17*	34° 4'12.22"N	118°40'5.59"W	Miocene
14LS18*	34° 4'12.22"N	118°40'5.59"W	Miocene
14LS19*†	34° 4'12.22"N	118°40'5.59"W	Miocene
14LS20*†	34° 4'12.22"N	118°40'5.59"W	Miocene
Santiago Canyon Road			
BW-11-09	33° 42' 9.0"N	117 38' 31.4"W	Miocene
BW-12-09	33° 42' 9.0"N	117 38' 31.4"W	Miocene
BW-13-09	33° 42' 9.0"N	117 38' 31.4"W	Miocene
BW-14-09	33° 42' 9.0"N	117 38' 31.4"W	Miocene
BW-15-09	33° 42' 9.0"N	117 38' 31.4"W	Miocene
BW-16-09*†§	33° 42' 9.0"N	117 38' 31.4"W	Miocene
BW-17-09	33° 42' 9.0"N	117 38' 31.4"W	Miocene
BW-18-09*†§	33° 42' 9.0"N	117 38' 31.4"W	Miocene
BW-19-09	33° 42' 9.0"N	117 38' 31.4"W	Miocene
BW-20-09	33° 42' 9.0"N	117 38' 31.4"W	Miocene
BW-21-09	33° 42' 9.0"N	117 38' 31.4"W	Miocene
BW-22-09	33° 42' 9.0"N	117 38' 31.4"W	Miocene
BW-23-09	33° 42' 9.0"N	117 38' 31.4"W	Miocene
BW-24-09	33° 42' 9.0"N	117 38' 31.4"W	Miocene
Red Rock Trail, Limestone Canyon Park			
BW-46-09*†§	33° 42' 10.3"N	117 38' 56.65''W	Miocene
BW-47-09	33° 42' 10.3"N	117 38' 56.65''W	Miocene
BW-48-09*†§	33° 42' 10.3"N	117 38' 56.65''W	Miocene
BW-49-09	33° 42' 10.3"N	117 38' 56.65''W	Miocene
BW-50-09	33° 42' 10.3"N	117 38' 56.65''W	Miocene
BW-51-09	33° 42' 10.3"N	117 38' 56.65''W	Miocene
BW-52-09	33° 42' 10.3"N	117 38' 56.65''W	Miocene

BW-53-09	33° 42' 10.3"N	117 38' 56.65"W	Miocene
Schueren Road, Malibu			
15LS01†	34° 4'42.78"N	118°38'57.60"W	Miocene
15LS02†	34° 4'42.78"N	118°38'57.60"W	Miocene
15LS03†	34° 4'42.78"N	118°38'57.60"W	Miocene
15LS04	34° 4'42.78"N	118°38'57.60"W	Miocene
15LS05	34° 4'42.78"N	118°38'57.60"W	Miocene
15LS06†	34° 4'42.78"N	118°38'57.60"W	Miocene
15LS07†	34° 4'42.78"N	118°38'57.60"W	Miocene
15LS08†	34° 4'42.78"N	118°38'57.60"W	Miocene
15LS09	34° 4'42.78"N	118°38'57.60"W	Miocene
15LS10†	34° 4'42.78"N	118°38'57.60"W	Miocene
15LS11	34° 4'42.78"N	118°38'57.60"W	Miocene
15LS12†	34° 4'42.78"N	118°38'57.60"W	Miocene
15LS13†	34° 4'42.78"N	118°38'57.60"W	Miocene
15LS14†	34° 4'42.78"N	118°38'57.60"W	Miocene
15LS15†	34° 4'42.78"N	118°38'57.60"W	Miocene
15LS16†	34° 4'42.78"N	118°38'57.60"W	Miocene
15LS17	34° 4'49.18"N	118°38'49.61"W	Miocene
15LS18	34° 4'49.18"N	118°38'49.61"W	Miocene
15LS19†	34° 4'49.18"N	118°38'49.61"W	Miocene
Simi Valley, Ventura County			
16LS01†	34°17'9.97"N	118°47'35.11"W	Eocene
16LS02†	34°17'9.97"N	118°47'35.11"W	Eocene
16LS03†	34°17'9.97"N	118°47'35.11"W	Eocene
16LS04	34°17'9.97"N	118°47'35.11"W	Eocene
16LS05†	34°17'9.97"N	118°47'35.11"W	Eocene
16LS06†	34°17'9.97"N	118°47'35.11"W	Eocene
16LS07†	34°17'9.97"N	118°47'35.11"W	Eocene
16LS08†	34°17'9.97"N	118°47'35.11"W	Eocene
16LS09	34°17'9.97"N	118°47'35.11"W	Eocene
16LS10†	34°17'9.97"N	118°47'35.11"W	Eocene
16LS11	34°17'9.97"N	118°47'35.11"W	Eocene
16LS12†	34°17'9.97"N	118°47'35.11"W	Eocene
16LS13†	34°17'9.97"N	118°47'35.11"W	Eocene
16LS14†	34°17'9.97"N	118°47'35.11"W	Eocene
16LS15	34°17'9.97"N	118°47'35.11"W	Eocene
16LS16†	34°17'9.97"N	118°47'35.11"W	Eocene
16LS17	34°17'9.97"N	118°47'35.11"W	Eocene
16LS18	34°17'9.97"N	118°47'35.11"W	Eocene
16LS19†§	34°17'9.97"N	118°47'35.11"W	Eocene
16LS20†§	34°17'9.97"N	118°47'35.11"W	Eocene
16LS21†	34°17'9.97"N	118°47'35.11"W	Eocene

*Petrography

†Paleomagnetic analysis

§Detrital zircon analysis

Table 2: Collected samples from Southern California

TABLE 3. SUMMARY OF ANALYSES PERFORMED ON SESPE CLAST SAMPLES

Location	Number collected	Stratified orthoquartzites	Interpretable paleomagnetic vector	Zircon analyses
Miocene Sespe				
Santa Monica Mountains				
Piuma Road	30	17	17	6
Schueren Road	19	13	13	0
Santa Ana Mountains				
Limestone Canyon Park	8	2	2	2
Santiago Canyon Road	14	2	2	2
Eocene Sespe				
Simi Valley Landfill	21	15	10	2
Total	92	49	44	12

Table 3: Summary of analyses performed on Sespe clasts

TABLE 4. SUMMARY OF PALEOMAGNETIC RESULTS

Clast	Inclination (°)	MAD	Peak Temp. (°C)	Location	
				Lat (°N)	Long (°W)
South Kaibab Trail, Grand Canyon					
IC-1-35[†]	54.9	7.7	672	36.0917	112.0889
Bolero Lookout - Santiago Cyn Rd					
BW16-09[†]	17.1	4.2	660	33.702500	117.642056
BW18-09[†]	27	6.4	672	33.702500	117.642056
Red Rock Trail, Limestone Canyon Park					
BW46-09[†]	51.6	4.9	500	33.702861	117.649069
BW48-09[†]	55	9.8	672	33.702861	117.649069
Saddle Peak - Piuma Rd					
BW0609[†]	56.6	3.8	672	34.070278	118.666628
14LS01[*]	53.1	2.2	640-680	34.072292	118.658078
14LS02	17.6	12.7	650	34.072292	118.658078
14LS04[*]	21.2	7.6	650-660	34.072292	118.658078
14LS06	5.5	8.9	650	34.072292	118.658078
14LS07	7.0	2.2	670	34.072292	118.658078
14LS08[*†]	42.3	1.3	670-680	34.072292	118.658078
14LS09[*†]	68.7	1.7	670	34.072292	118.658078
14LS11[†]	43.6	5.3	660	34.072292	118.658078
14LS12[†]	43.4	1.7	660	34.072292	118.658078
14LS14	48.2	13.0	650	34.072292	118.658078
14LS15[*]	38.8	12.1	615-630	34.070061	118.668219
14LS17[*]	23.5	2.5	575-585	34.070061	118.668219
14LS19	13.6	9.0	555	34.070061	118.668219
14LS20	13.2	6.4	650	34.070061	118.668219
14BW16[*†]	58.5	2.2	680	34.072292	118.658078
14BW17	43.8	11.9	565	34.072292	118.658078
Saddle Peak - Schueren Rd					
15LS01[*]	17.9	7.0	650	34.078550	118.649333
15LS02[*]	4.3	2.8	615-650	34.078550	118.649333
15LS03	24.9	4.9	670	34.078550	118.649333
15LS06	77.2	7.5	600	34.078550	118.649333
15LS07	6.2	7.2	500	34.078550	118.649333
15LS08	36.6	1.6	660	34.078550	118.649333
15LS10	64.6	4.2	575	34.078550	118.649333
15LS12[*]	45.8	3.3	400-450	34.078550	118.649333
15LS13	14.4	1.3	580	34.078550	118.649333
15LS14	17.5	5.9	500	34.078550	118.649333
15LS15	40.1	7.0	515	34.078550	118.649333
15LS16	15.0	5.3	350	34.078550	118.649333
15LS19	3.2	1.8	585	34.080328	118.647114

Simi Valley					
16LS01*	12.8	1.2	670	34.286103	118.793086
16LS02	45.6	3.0	515	34.286103	118.793086
16LS06	18.7	8.0	660	34.286103	118.793086
16LS08*	50.0	0.7	640	34.286103	118.793086
16LS09	1.9	0.9	670	34.286103	118.793086
16LS12	0.4	7.1	545	34.286103	118.793086
16LS13	16.4	5.6	575	34.286103	118.793086
16LS16	31.2	4.2	650	34.286103	118.793086
16LS19*†	41.5	2.2	640	34.286103	118.793086
16LS20†	44.8	4.8	650	34.286103	118.793086

*Multiple cores

†Zircon analysis

Table 4: Summary of paleomagnetic results

TABLE 5: REFERENCES FOR PREVIOUS DETRITAL ZIRCON AND PALEOMAGNETIC DATA

Figure	Sample or Formation	Reference	
Detrital Zircon Data			
8a	Tapeats 2	Gehrels et al., 2011	
8b	Shinumo TO1-75-5	Bloch et al., 2006	
8c	Shinumo TO1-75-2z	Bloch et al., 2006	
8b	Shinumo TO1-75-4	Bloch et al., 2006	
8f	Shinumo TO1-76-2	Bloch et al., 2006	
8g	Shinumo TO1-76-3	Bloch et al., 2006	
8h	Shinumo Basal Gravel LC-16-76-5	Mulder et al., 2017	
8u	Zabriskie Quartzite	Stewart et al., 2001	
8v	Upper Stirling NR9S	Shoenborn et al., 2012	
8w	Troy Formation	Stewart et al., 2001; Mulder et al., 2017	
8x	Dripping Springs Formation	Stewart et al., 2001; Mulder et al., 2017	
8y	Del Rio Quartzite	Spencer et al., 2016	
8z	Blackjack	Doe et al., 2012	
8aa	Yankee Joe	Doe et al., 2012	
8ab	White Ledges	Doe et al., 2012	
8ac	Morrison Formation	Dickinson and Gehrels, 2008	
8ad	Morrison Formation	Dickinson and Gehrels, 2008	
Paleomagnetic data			Maximum Demagnetization Temperature (°C)
9a	Tapeats, Grand Canyon	Elston and Bressler, 1977	500-590
9b	Tapeats, central Arizona	Elston and Bressler, 1977	undetermined
9c	Zabriskie Formation	Gillett and Van Alstine, 1979	640
9d	Wood Canyon Fm (red-purple mudstones only)	Gillett and Van Alstine, 1979 (Fig 3f and 4)	640
9e	Rainstorm, all locations	Minguez et al., 2015 and Van Alstine and Gillett, 1979	500-610
9f	Rainstorm, Nopah Range	Minguez et al., 2015	500-610
9g	Rainstorm, Winters Pass Hills	Minguez et al., 2015	500-610
9h	Rainstorm, Desert Range	Van Alstine and Gillett, 1979	650
9i	Neoproterozoic - Cambrian, Caborca Region	Molina-Garza and Geissman, 1999	355-660 (avg. 530)
9j	Lower Shinumo	Elston and Grommé, 1994	550
9k	Middle Shinumo (Pole 4)	Elston and Grommé, 1994	500-620
9l	Upper Shinumo	Elston and Grommé, 1994	650
9m	All above Shinumo	Elston and Grommé, 1994	see above

Table 5: References for previous paleomagnetic and detrital zircon data

TABLE 6: SUMMARY OF RESULTS FOR SAMPLES WITH PALEOMAGNETIC AND DETRITAL ZIRCON DATA

Sample and location	Paleomagnetic Inclination (°)	Grenville DZ Peak?	Interpreted source region
Miocene Sespe – moderate & high inclination			
Piuma Road			
LS1114	44	Yes	Morrison Formation
BW0609	57	Yes	Grand Canyon (Shinumo)
LS0814	42	Yes	Grand Canyon (Shinumo)
LS0914	69	Yes	Grand Canyon (Shinumo)
LS1214	43	Yes	Grand Canyon (Shinumo)
BW1614	59	Yes	Grand Canyon (Shinumo)
Red Rock Trail, Limestone Canyon Park			
BW4609*	52	Yes	Grand Canyon (Shinumo)
BW4809	55	Yes	Grand Canyon (Shinumo)
Miocene Sespe – low inclination			
Santiago Canyon Road			
BW1609	17	Yes	Death Valley
BW1809	27	No	Central Arizona highlands
Eocene Sespe – moderate inclination			
Simi Valley			
LS1916	42	No	Central Arizona highlands
LS2016	45	No	Central Arizona highlands

* Characteristic magnetization is carried by magnetite, which has not been observed in the extant database for Shinumo

Table 6: Summary of results for samples with paleomagnetic and detrital zircon data

SUPPLEMENTAL FIGURES


14LS08
14LS08


15LS16


16LS09
FINE


16LS07

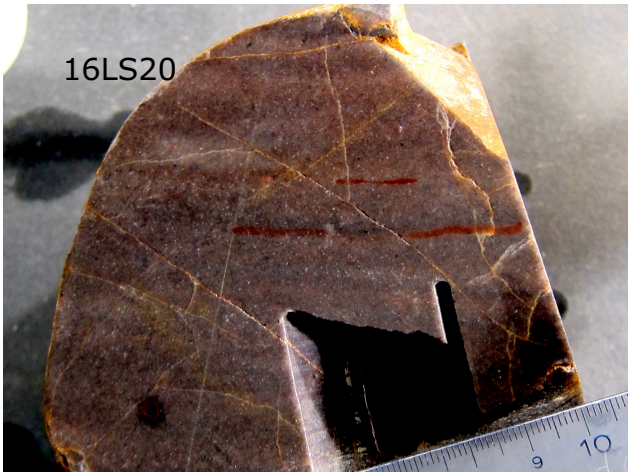
16LS20
9
10


14LS09


BW1614

Figure S1: Photographs of seven representative clasts showing stratification.

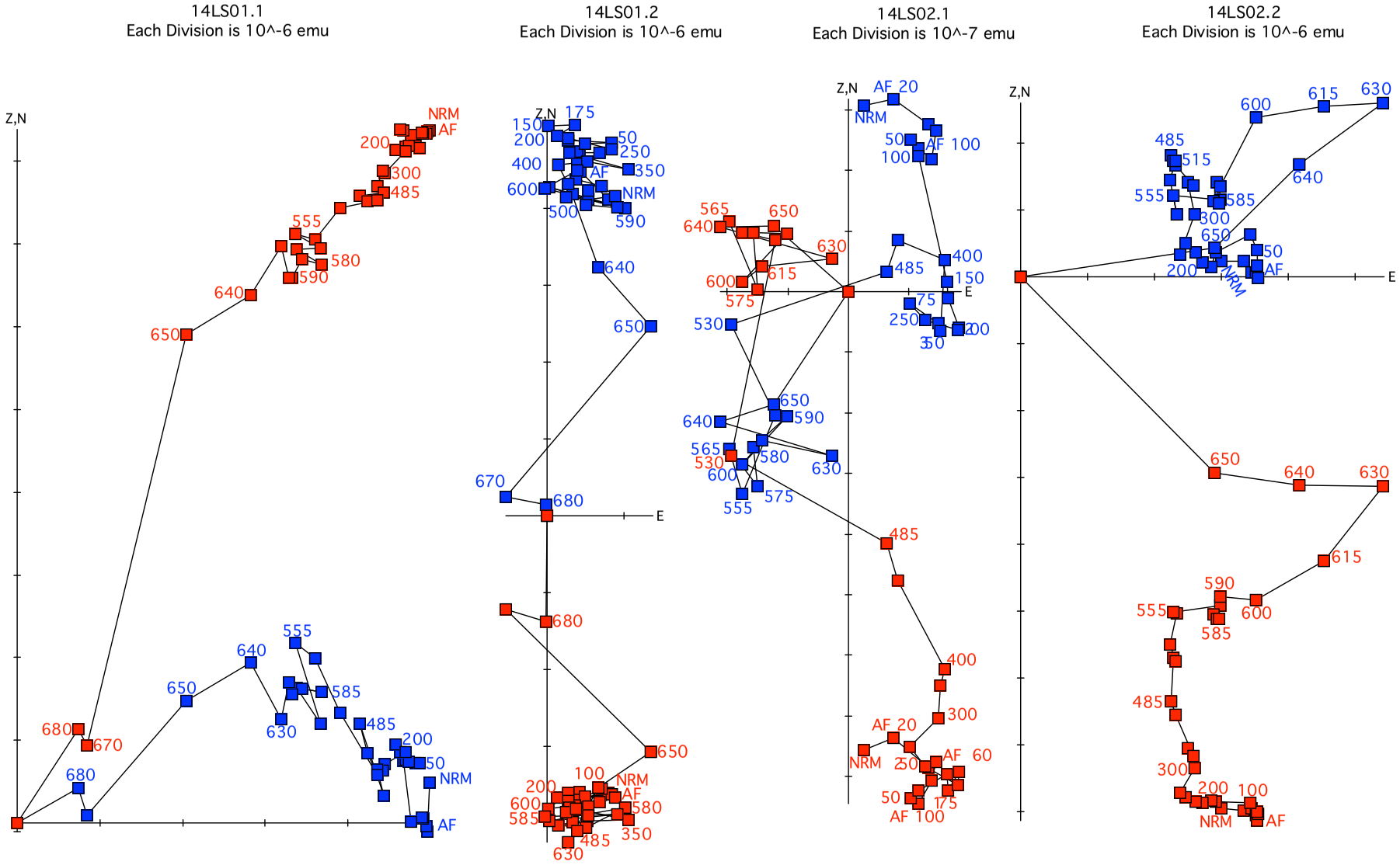
14LS01.1
Each Division is 10^-6 emu
Z,N
NRM
AF
200
300
485
555
580
590
640
650
555
640
650
585
485
200
50
NRM
AF
630
680
670
680
14LS01.2
Each Division is 10^-6 emu
Z,N
175
150
200
50
250
400
AF
350
600
NRM
500
590
640
650
670
680
E
680
650
100
NRM
200
AF
600
580
585
485
350
630
14LS02.1
Each Division is 10^-7 emu
Z,N
AF 20
NRM
50
AF 100
100
565
650
640
630
485
400
600
615
150
575
E
75
530
250
650
640
590
565
580
630
530
600
575
555
485
400
300
AF 20
NRM
AF 60
50
175
AF 100
14LS02.2
Each Division is 10^-6 emu
Z,N
600
615
630
485
515
640
555
585
300
650
50
200
NRM
AF
E
650
640
630
615
590
555
600
585
485
300
200
100
NRM
AF

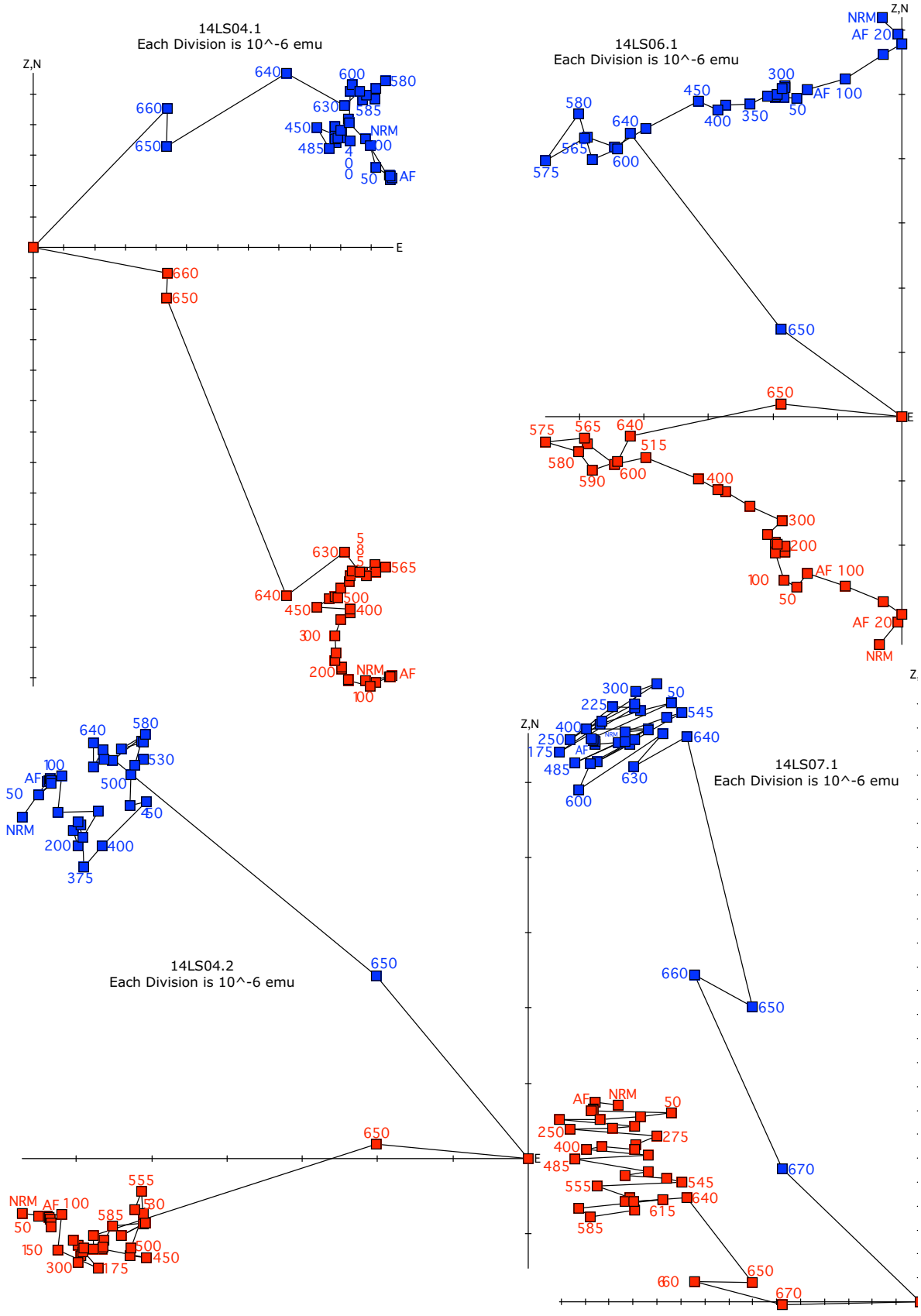
14LS04.1
Each Division is 10^-6 emu
Z,N
E
640
600
580
660
630
585
650
450
NRM
485
AF
660
650
630
565
640
450
400
300
200
NRM
AF
14LS06.1
Each Division is 10^-6 emu
Z,N
NRM
AF 20
300
450
AF 100
580
400
350
50
640
565
600
575
650
650
575
565
640
515
580
600
590
400
300
200
AF 100
100
50
AF 20
NRM
14LS04.2
Each Division is 10^-6 emu
640
580
530
100
AF
500
50
450
NRM
200
400
375
650
650
555
NRM
AF
100
530
585
50
500
150
450
300
175
14LS07.1
Each Division is 10^-6 emu
Z,N
300
50
225
545
400
250
640
175
AF
485
630
600
660
650
AF
NRM
50
250
275
400
485
670
555
545
640
615
585
650
660
670

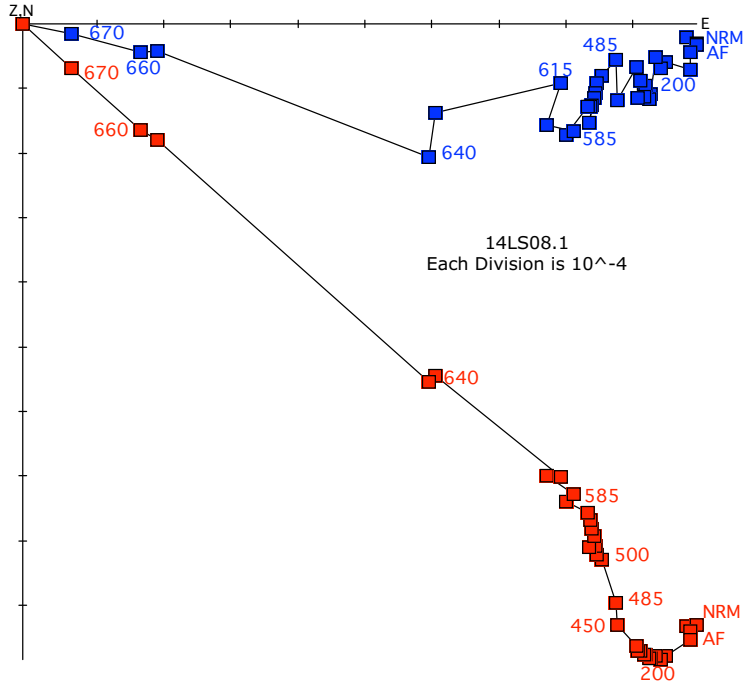

14LS08.1
Each Division is 10^-4

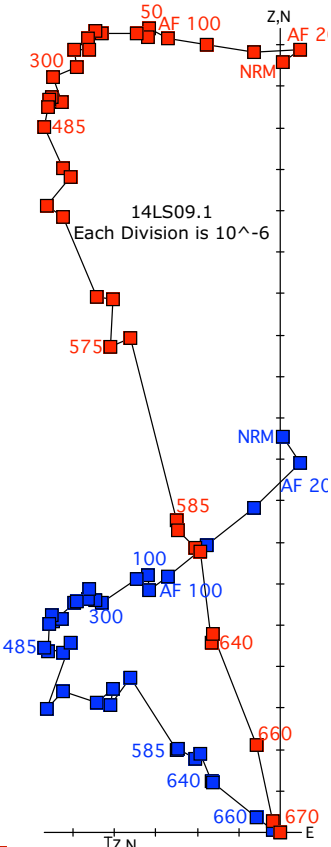

14LS09.1
Each Division is 10^-6

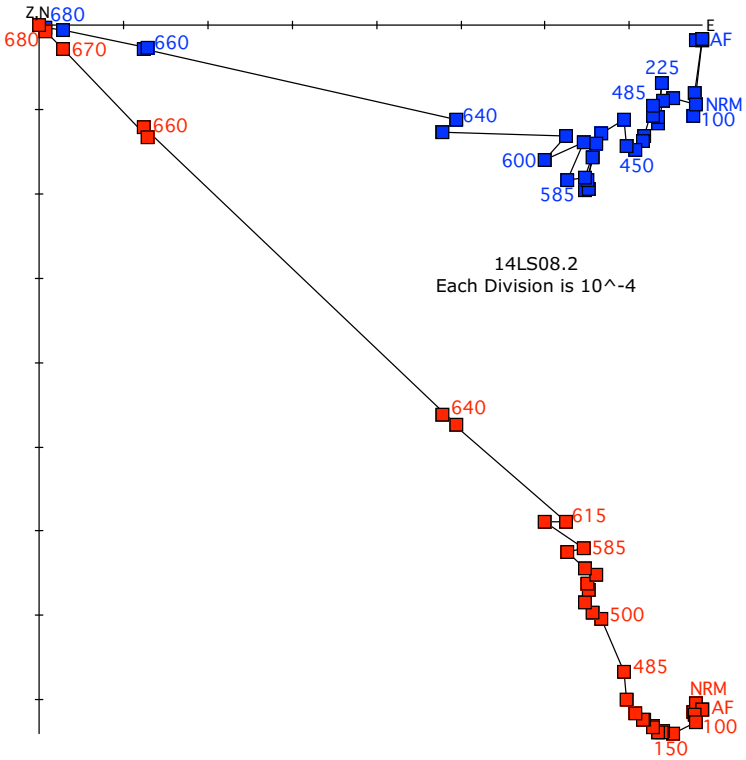

14LS08.2
Each Division is 10^-4

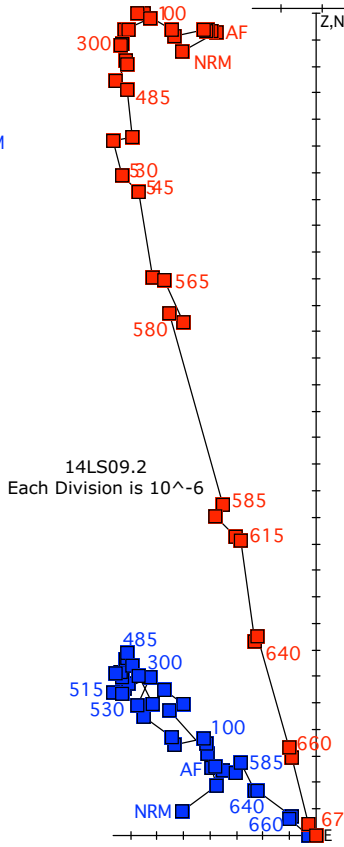

14LS09.2
Each Division is 10^-6

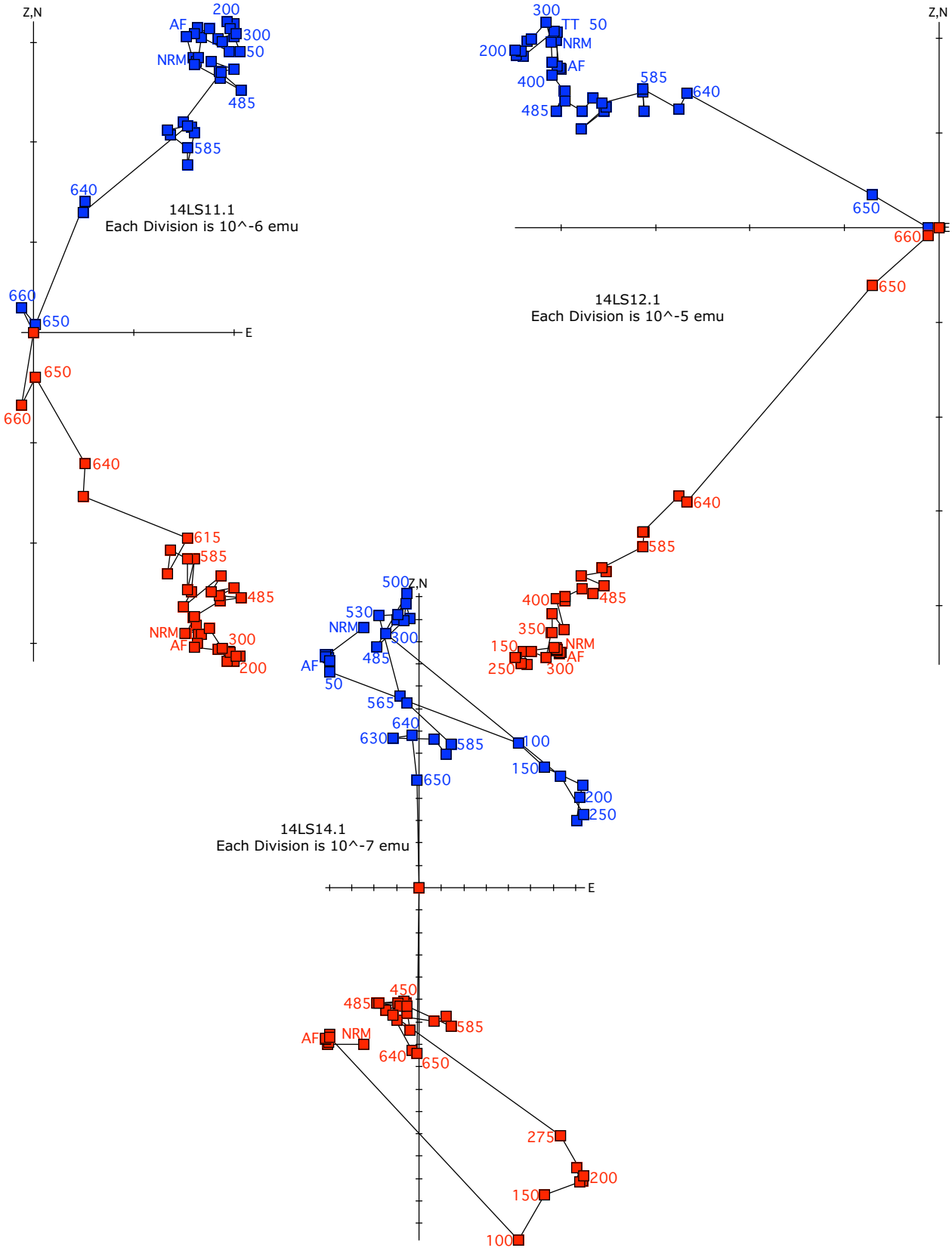
Z,N
200
AF
300
50
NRM
485
585
640
14LS11.1
Each Division is 10^-6 emu
660
650
E
650
660
640
615
585
485
NRM
AF
300
200
300
TT 50
NRM
200
AF
400
585
640
485
650
Z,N
660
E
650
14LS12.1
Each Division is 10^-5 emu
640
585
400
485
350
150
NRM
AF
250
300
500
Z,N
530
NRM
300
485
AF
50
565
640
630
585
650
100
150
200
250
14LS14.1
Each Division is 10^-7 emu
E
450
485
585
AF
NRM
640
650
275
200
150
100

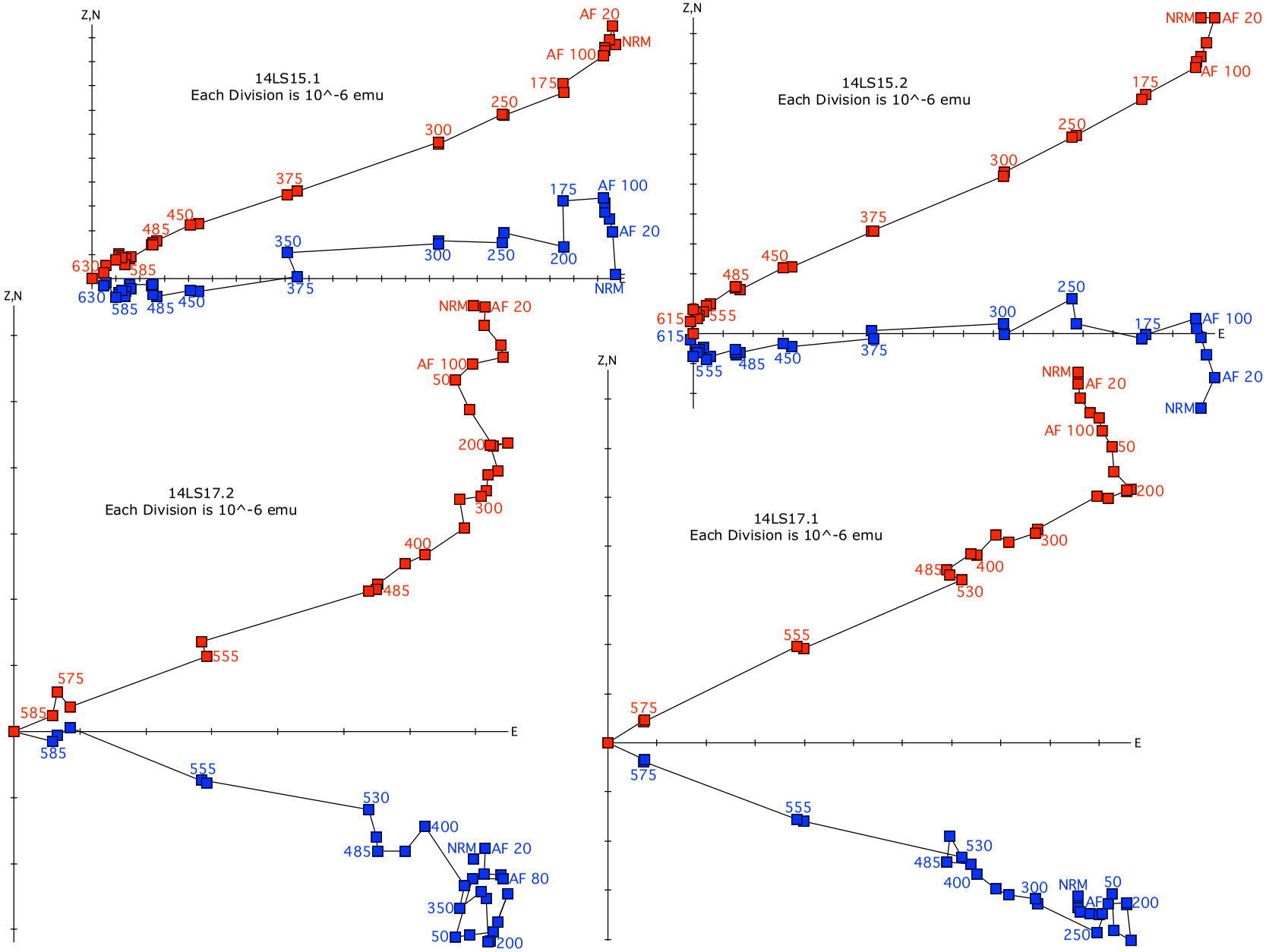
14LS15.1
Each Division is 10^-6 emu
Z,N
AF 20
NRM
AF 100
175
250
300
375
450
485
630
585
350
200
14LS15.2
Each Division is 10^-6 emu
615
555
14LS17.2
Each Division is 10^-6 emu
AF 80
50
400
530
575
E
14LS17.1
Each Division is 10^-6 emu

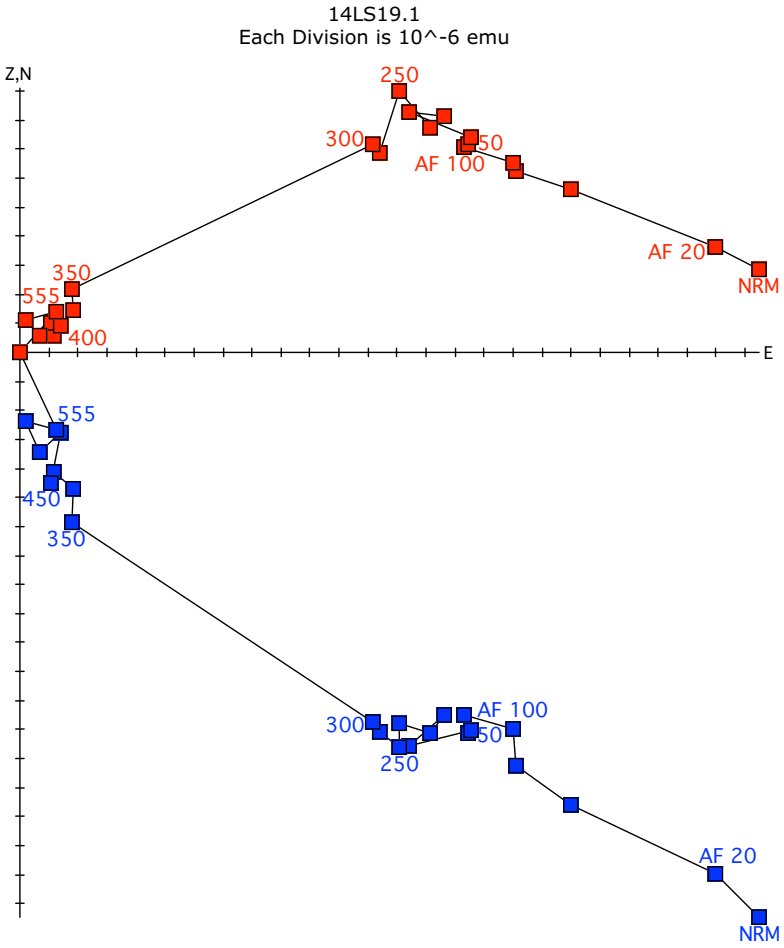
14LS19.1
Each Division is 10^-6 emu
Z,N
E
250
300
50
AF 100
AF 20
NRM
350
555
400
555
450
350
300
AF 100
50
250
AF 20
NRM

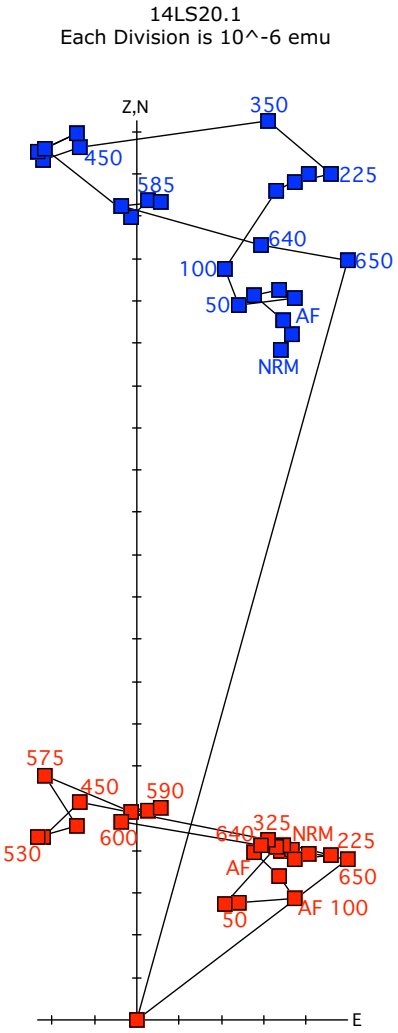
14LS20.1
Each Division is 10^-6 emu
Z,N
E
350
450
225
585
640
650
100
50
AF
NRM
575
450
590
530
600
640
325
NRM
225
AF
650
50
AF 100

15LS01.1
Each Division is 10^-6

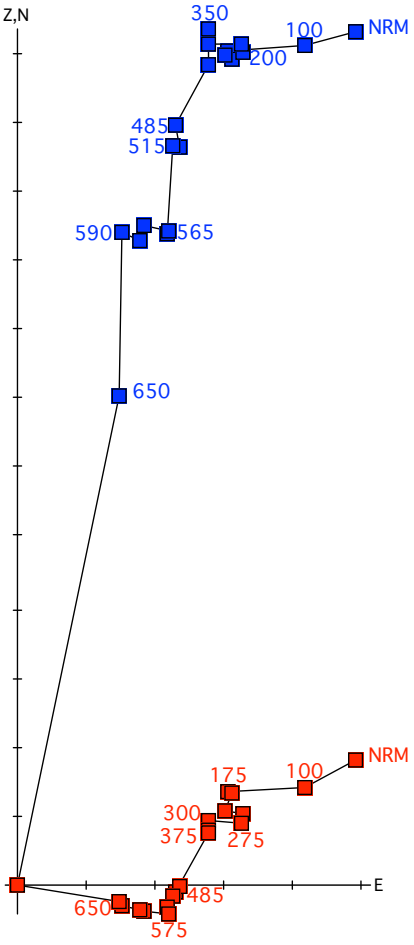

15LS01.2
Each Division is 10^-6

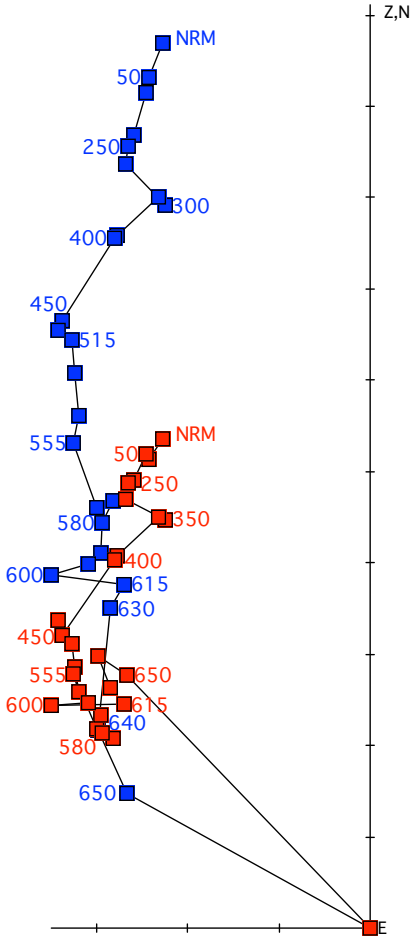

15LS02.1
Each Division is 10^-6

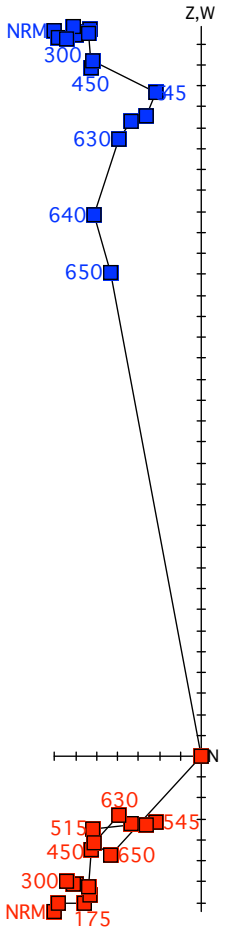

15LS02.2
Each Division is 10^-6

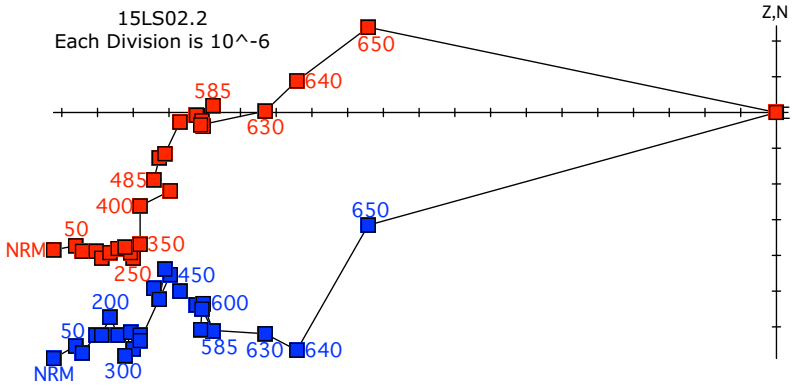

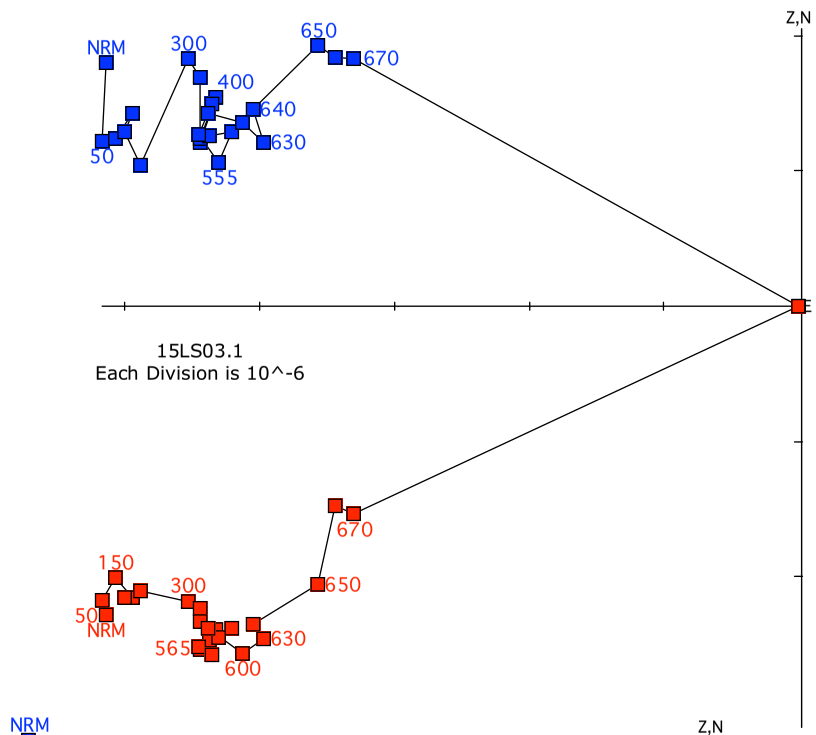
Z,N
NRM
300
650
670
400
640
630
50
555
15LS03.1
Each Division is 10^-6
670
150
300
650
50
NRM
630
565
600

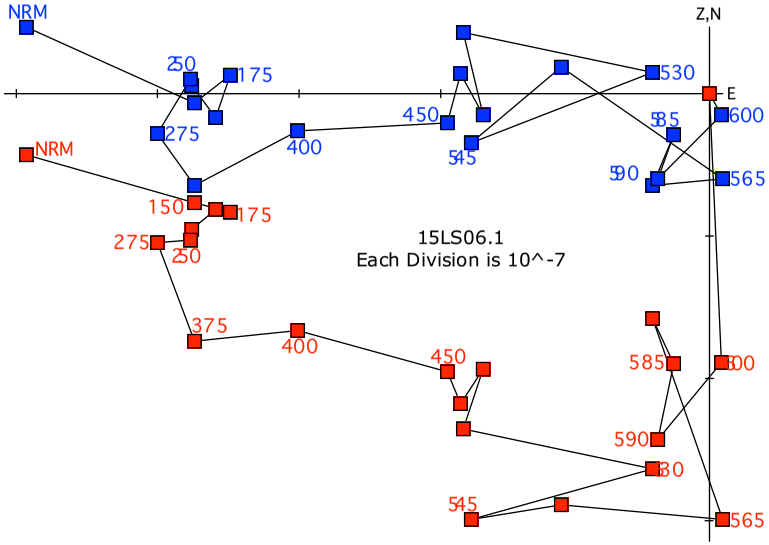
NRM
Z,N
250
175
530
E
450
600
275
400
585
NRM
545
590
565
150
175
275
250
15LS06.1
Each Division is 10^-7
375
400
450
585
600
590
580
545
565

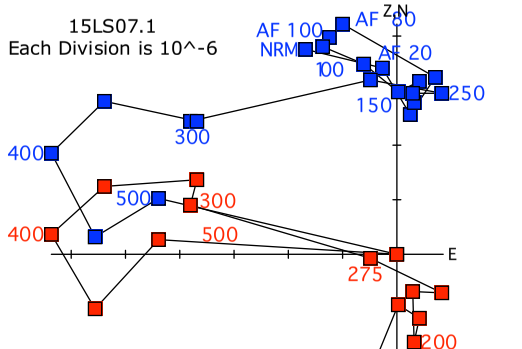
15LS07.1
Each Division is 10^-6
Z,N
AF 100
AF 80
NRM
AF 20
100
250
150
300
400
500
300
400
500
E
275
200
AF 100
50

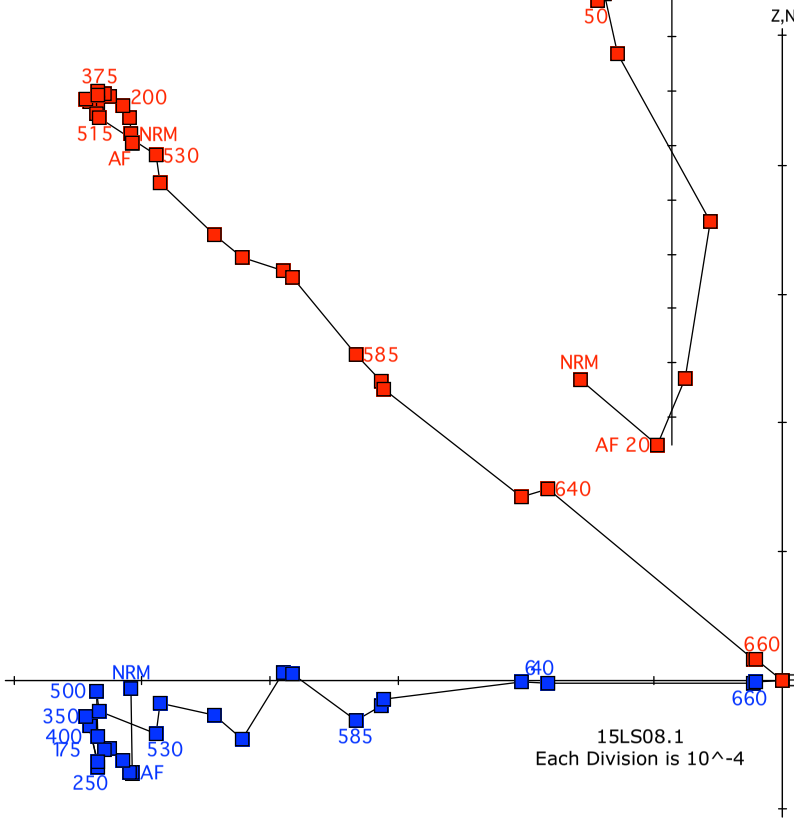
Z,N
375
200
515
NRM
AF
530
585
NRM
AF 20
640
660
NRM
640
500
660
350
400
585
175
530
250
AF
15LS08.1
Each Division is 10^-4

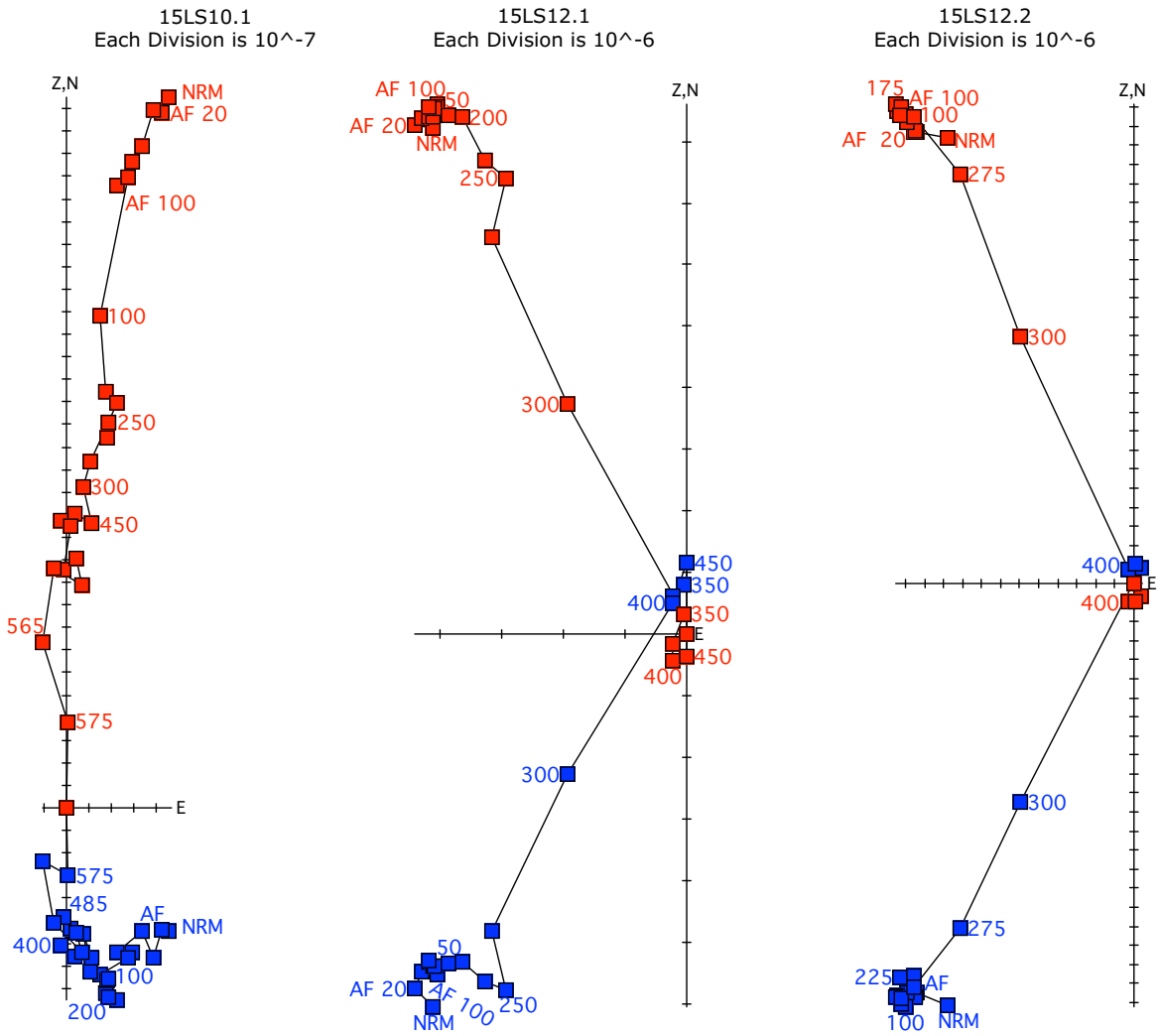

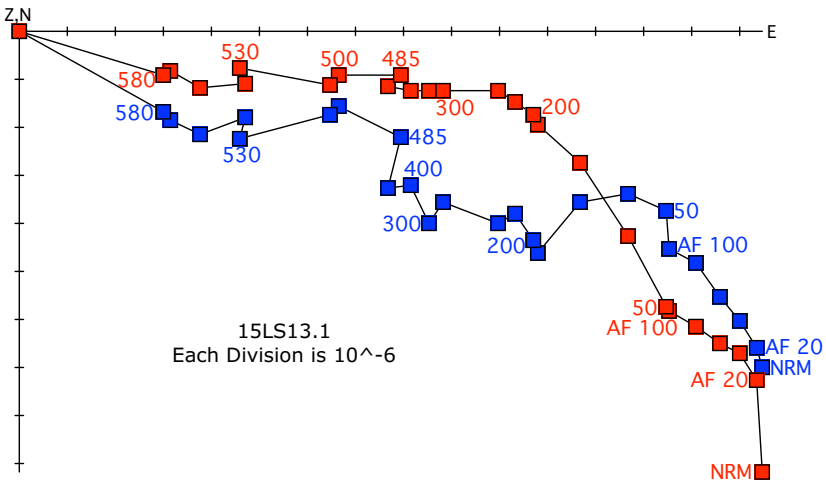

15LS13.1
Each Division is 10^-6

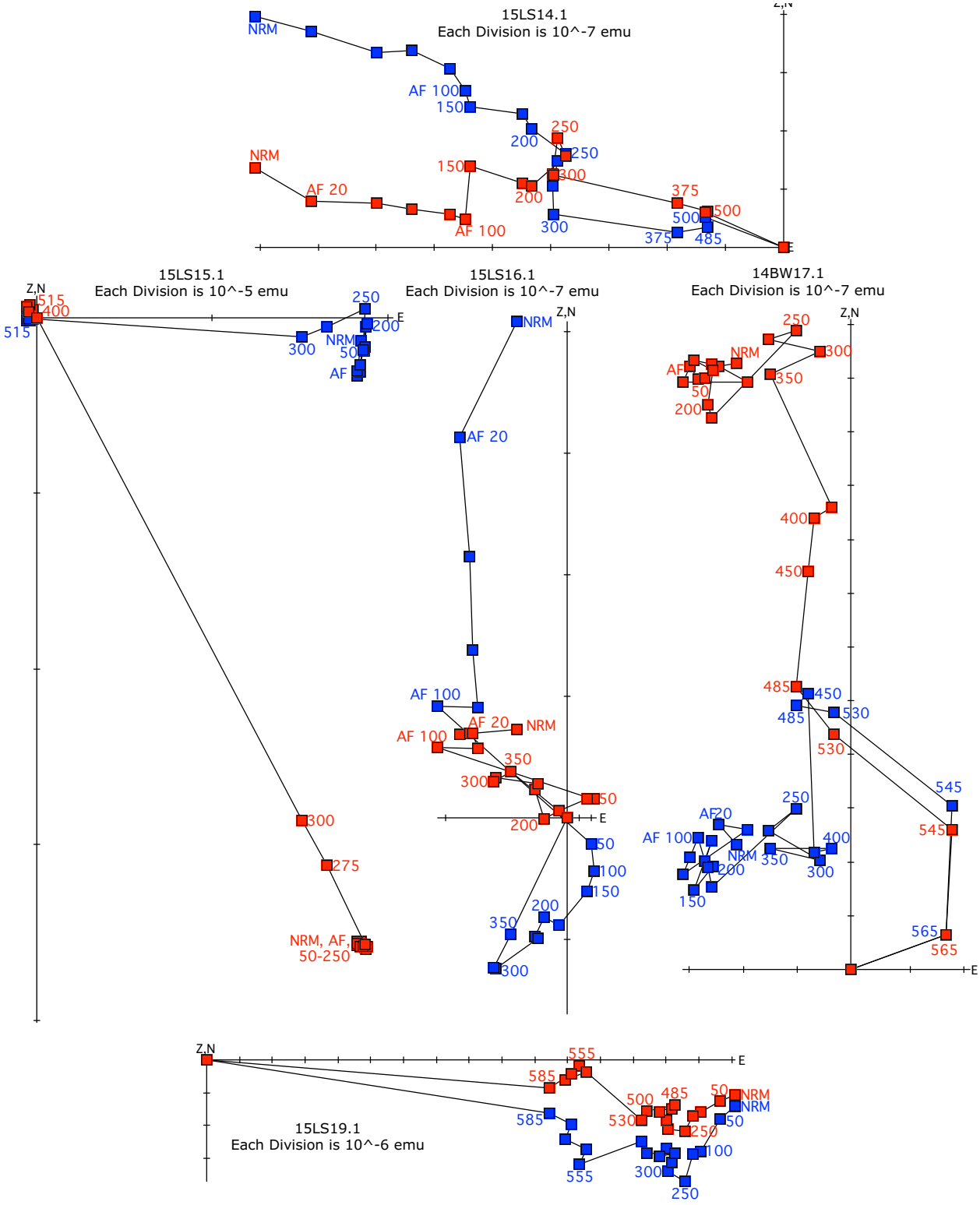
15LS14.1
Each Division is 10^-7 emu
NRM
AF 100
150
200
250
NRM
AF 20
150
AF 100
200
250
300
300
375
500
500
375
485
15LS15.1
Each Division is 10^-5 emu
Z,N
515
400
515
250
200
300
NRM
50
AF
300
275
NRM, AF,
50-250
15LS16.1
Each Division is 10^-7 emu
Z,N
NRM
AF 20
AF 100
AF 20
NRM
AF 100
350
300
50
200
50
100
150
200
350
300
14BW17.1
Each Division is 10^-7 emu
Z,N
250
NRM
300
AF
350
50
200
400
450
485
450
485
530
530
545
250
AF20
AF 100
400
NRM
350
200
300
150
545
565
565
15LS19.1
Each Division is 10^-6 emu
Z,N
555
585
585
500
485
50
NRM
NRM
530
50
250
100
555
300
250

14BW16.1
Each Division is 10^-4 emu

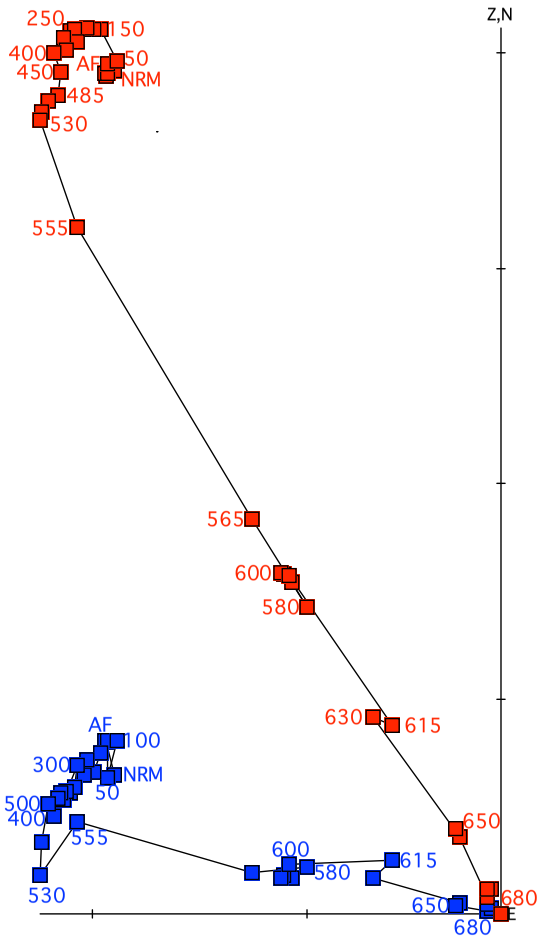

14BW16.2
Each Division is 10^-4 emu

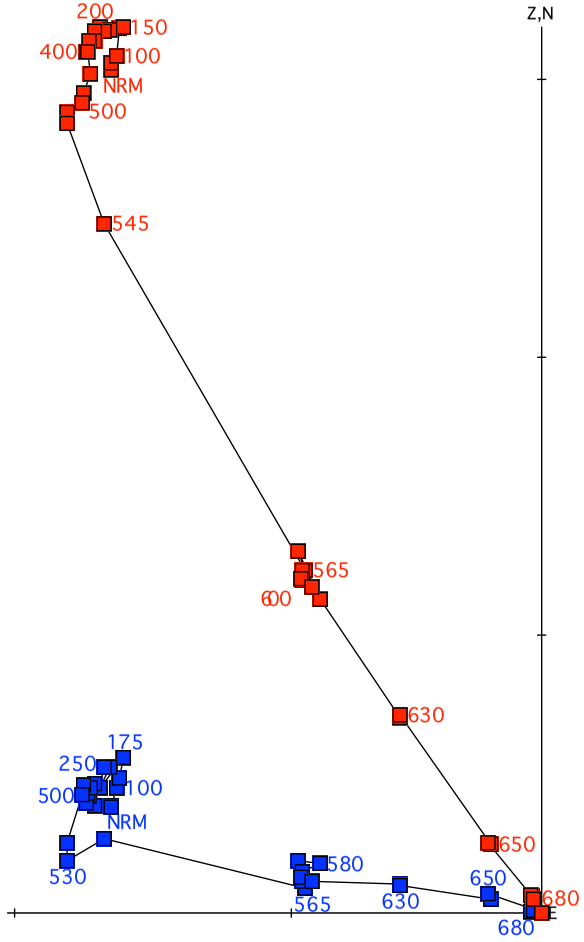

14BW16.3
Each Division is 10^-4 emu

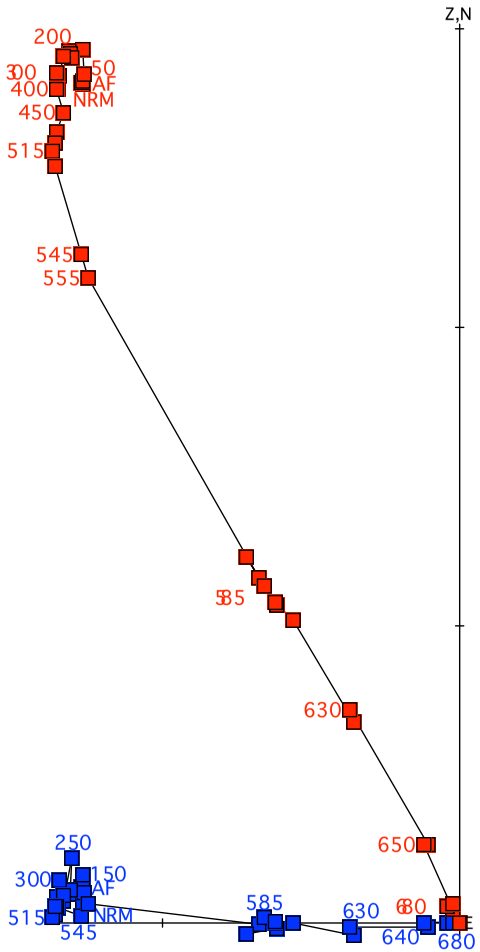

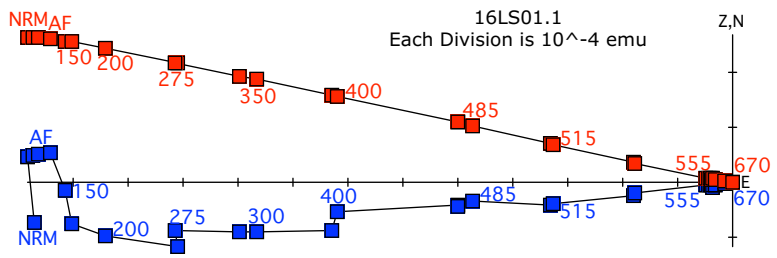
16LS01.1
Each Division is 10^-4 emu
Z,N
E
NRM
AF
150
200
275
350
400
485
515
555
670
AF
150
200
275
300
400
485
515
555
670
NRM

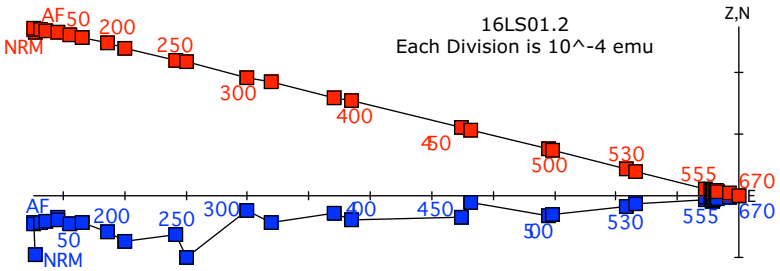
16LS01.2
Each Division is 10^-4 emu
Z,N
E
AF
50
200
250
300
400
450
500
530
555
670
NRM
AF
50
200
250
300
400
450
500
530
555
670
NRM

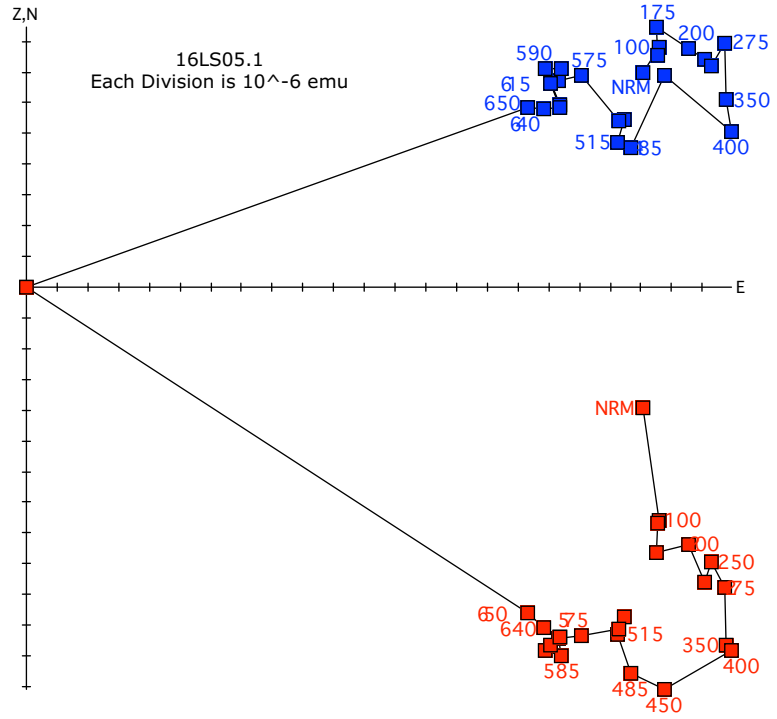
16LS05.1
Each Division is 10^-6 emu
Z,N
E
175
200
275
590
575
100
615
650
NRM
350
640
515
485
400
NRM
100
200
250
275
650
640
575
515
350
585
485
400
450

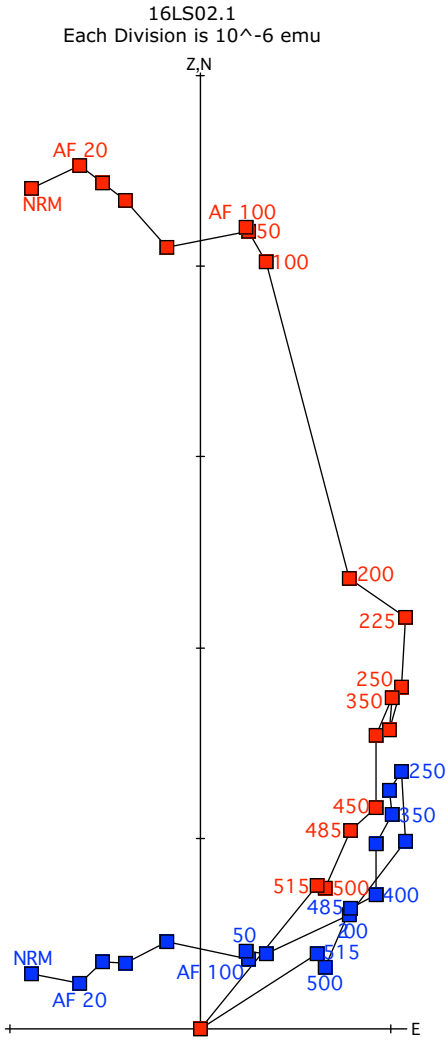
16LS02.1
Each Division is 10^-6 emu
Z,N
E
AF 20
NRM
AF 100
150
100
200
225
250
350
250
450
350
485
515
500
400
485
200
50
515
500
NRM
AF 100
AF 20

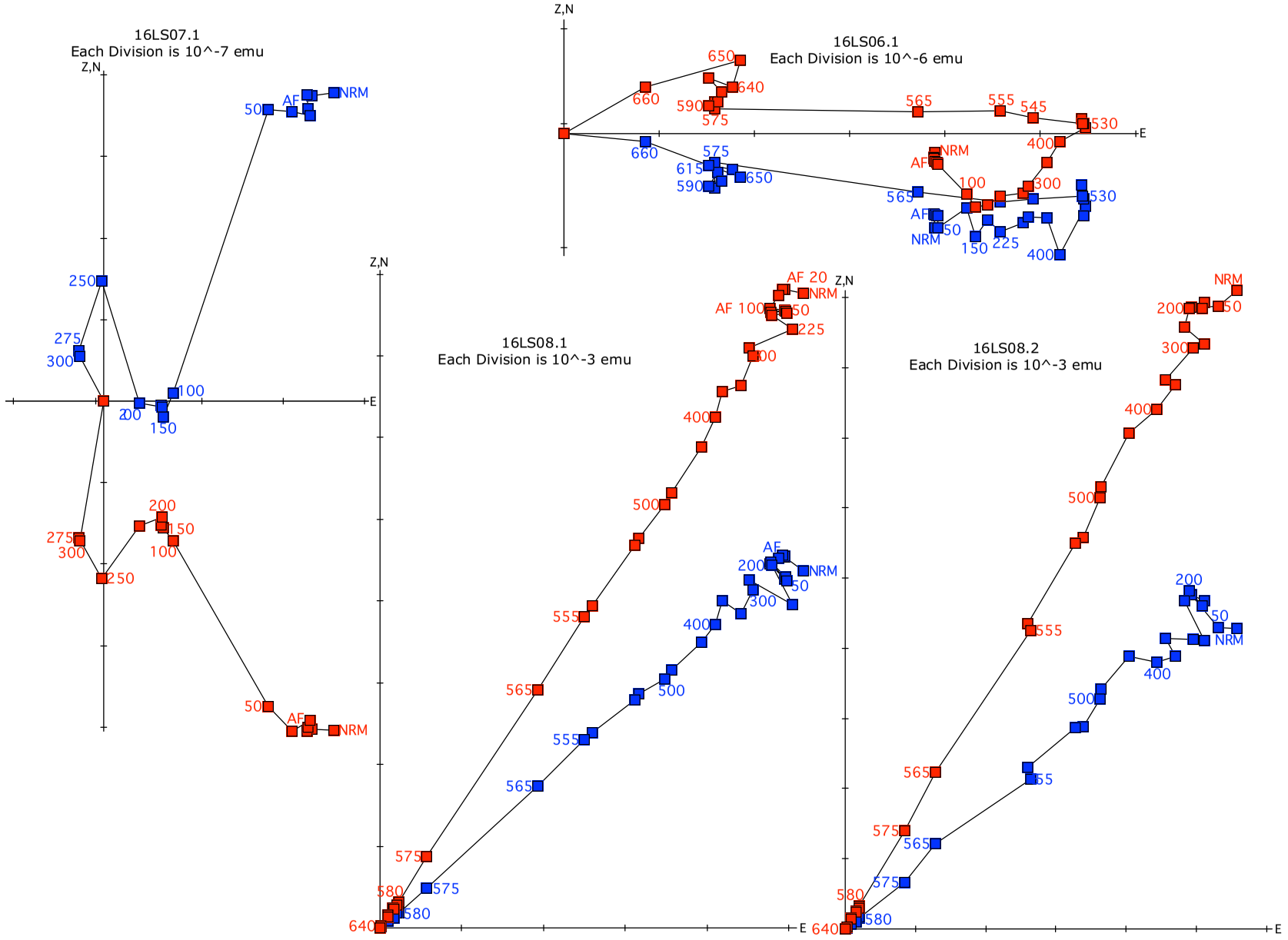
16LS07.1
Each Division is 10^-7 emu
Z,N
E
NRM
AF
50
250
275
300
100
200
150
16LS06.1
Each Division is 10^-6 emu
650
640
660
590
575
565
555
545
530
615
400
300
225
16LS08.1
Each Division is 10^-3 emu
AF 20
AF 100
NRM
50
225
400
500
555
565
575
580
640
16LS08.2
Each Division is 10^-3 emu
NRM
200
50
300
400
500
555
565
575
580
640

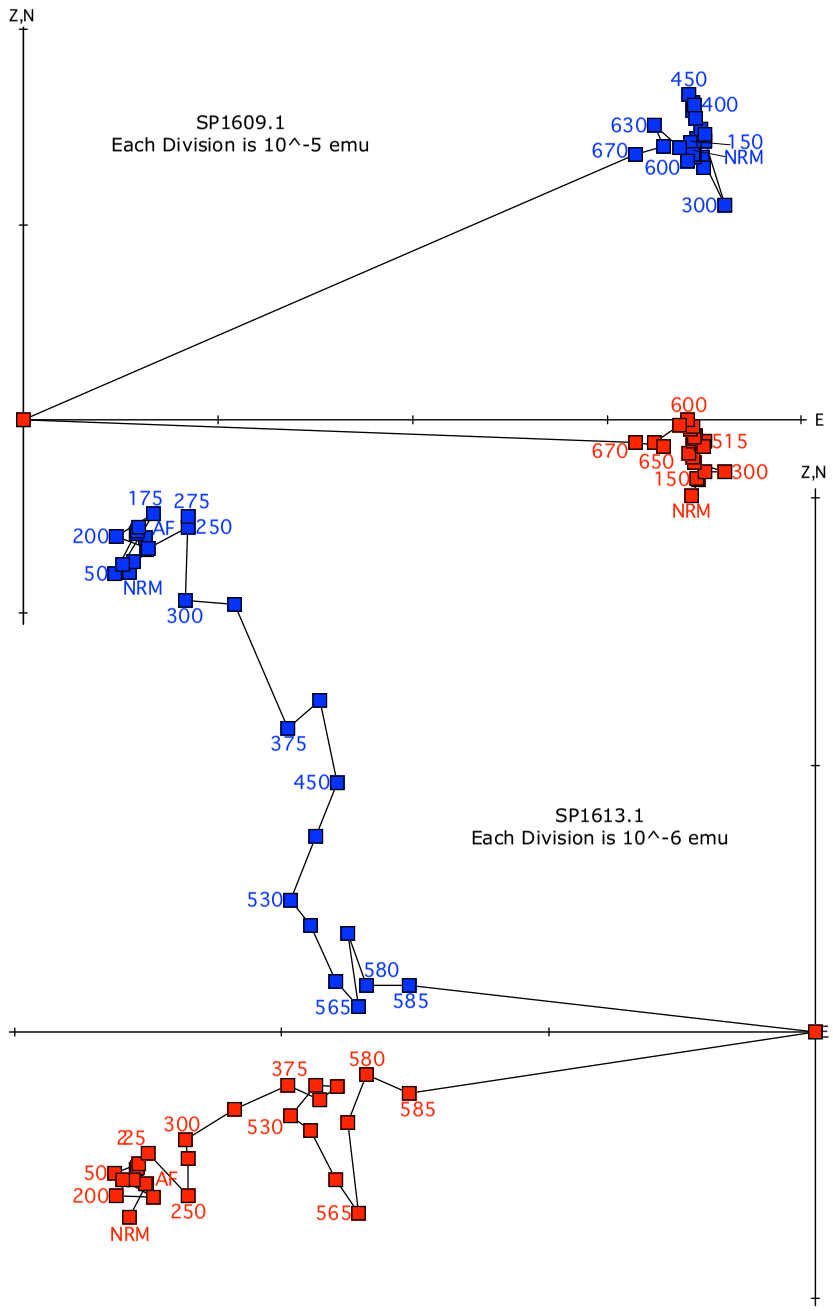
Z,N
SP1609.1
Each Division is 10^-5 emu
450
400
630
150
670
600
NRM
300
600
E
670
515
650
150
300
NRM
Z,N
175
275
AF
250
200
50
NRM
300
375
450
530
580
565
585
225
300
375
580
530
585
50
AF
200
250
NRM
565

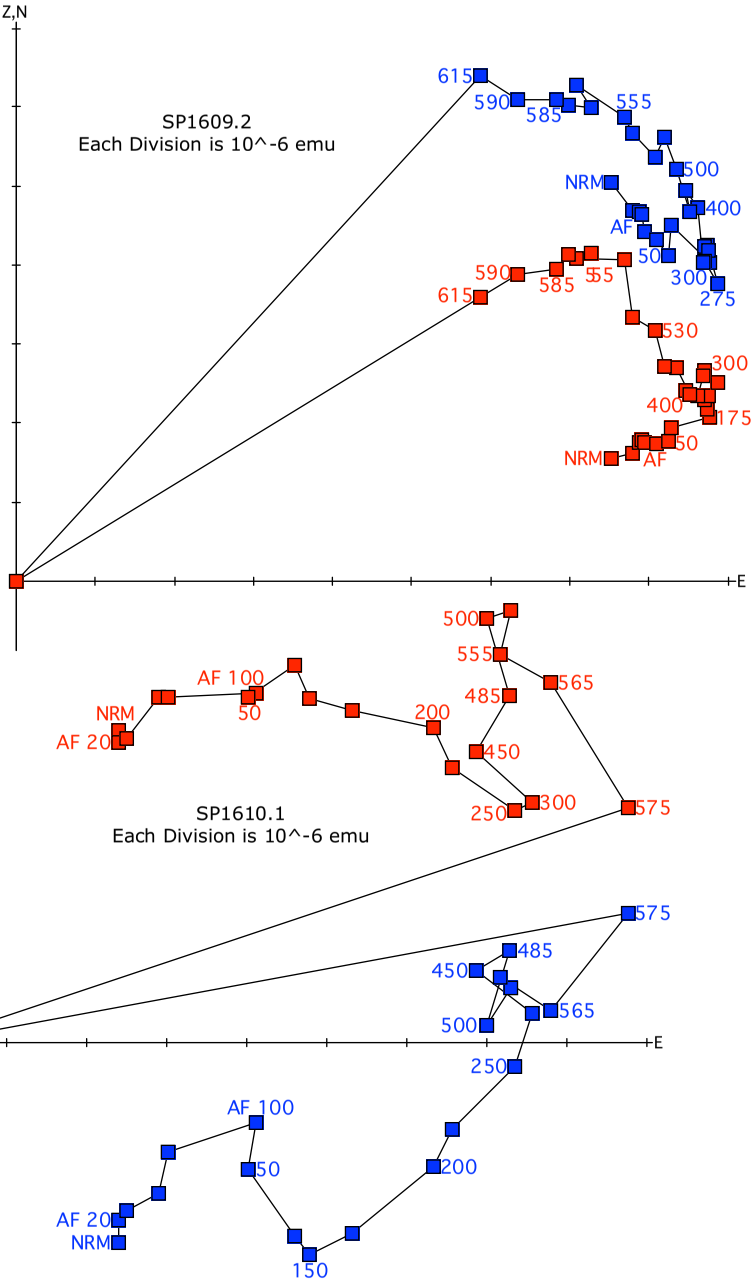
Z,N
SP1609.2
Each Division is 10^-6 emu
615
590
585
555
500
NRM
400
AF
50
300
275
590
585
555
615
530
300
400
175
NRM
AF
50
Z,N
SP1610.1
Each Division is 10^-6 emu
500
555
AF 100
565
NRM
485
50
200
AF 20
450
250
300
575
575
485
450
565
500
250
AF 100
50
200
AF 20
NRM
150

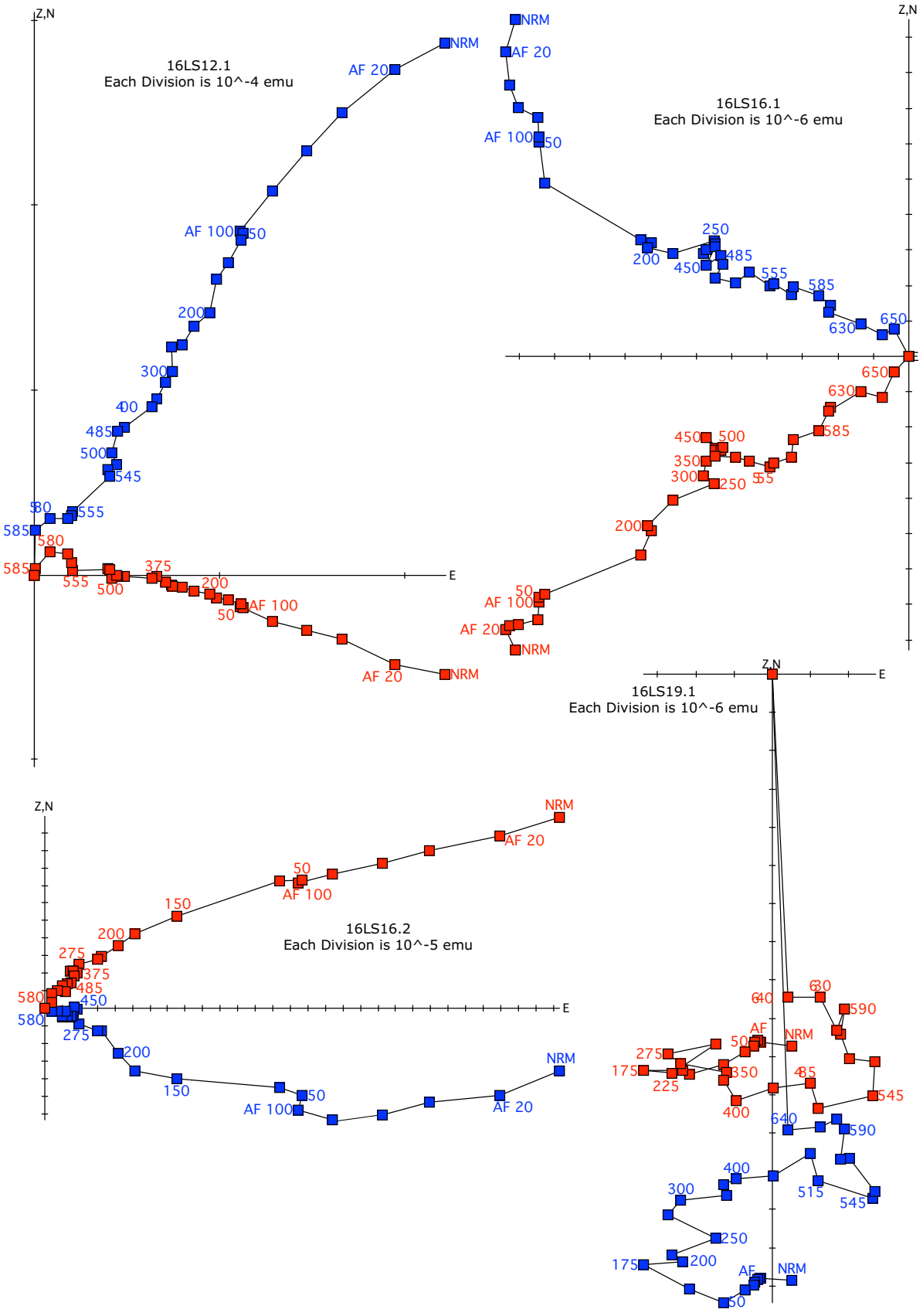
16LS12.1
Each Division is 10^-4 emu
Z,N
E
NRM
AF 20
AF 100
50
200
300
400
485
500
545
555
580
585
375
16LS16.1
Each Division is 10^-6 emu
250
450
555
585
630
650
16LS16.2
Each Division is 10^-5 emu
150
275
16LS19.1
Each Division is 10^-6 emu
590
640
515

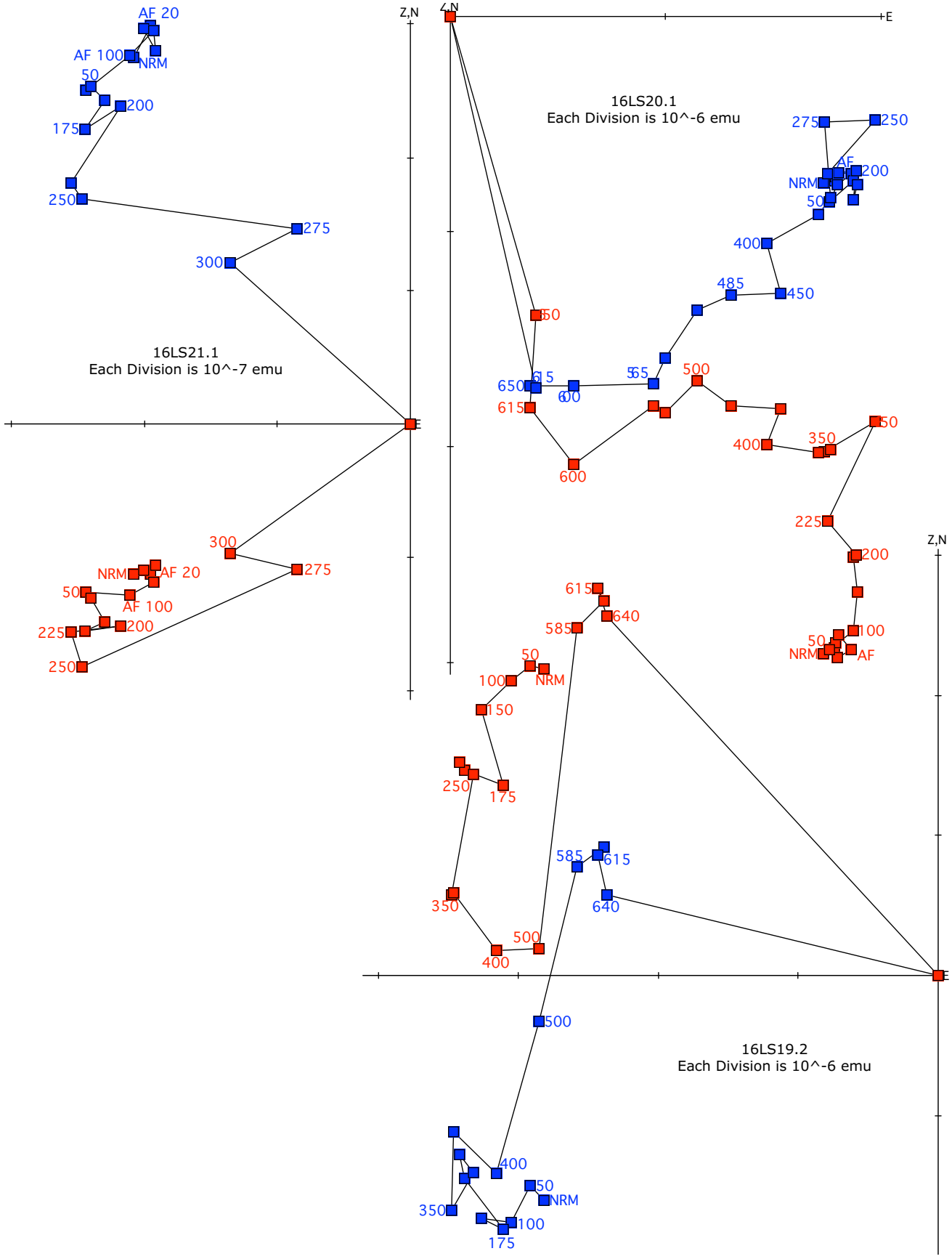
16LS21.1
Each Division is 10^-7 emu
Z,N
E
AF 20
AF 100
NRM
50
200
175
250
275
300
16LS20.1
Each Division is 10^-6 emu
650
615
600
565
500
485
450
400
350
275
250
225
200
100
NRM
AF
16LS19.2
Each Division is 10^-6 emu
640
585
615
500
400
350
250
175
150
100
50
NRM

Figure S2: Zijderveld demagnetization plots for all paleomagnetic data

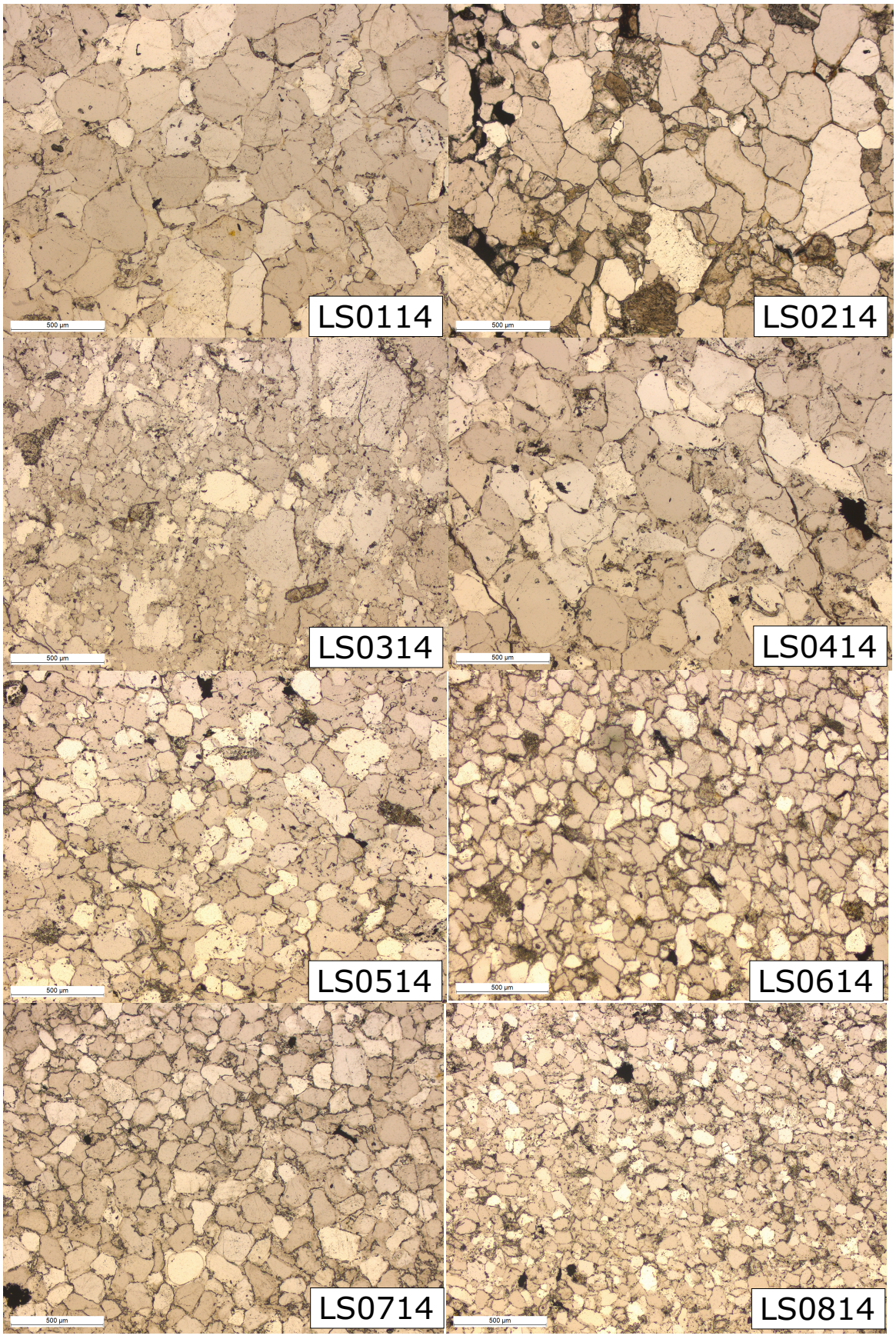
LS0114
LS0214
LS0314
LS0414
LS0514
LS0614
LS0714
LS0814

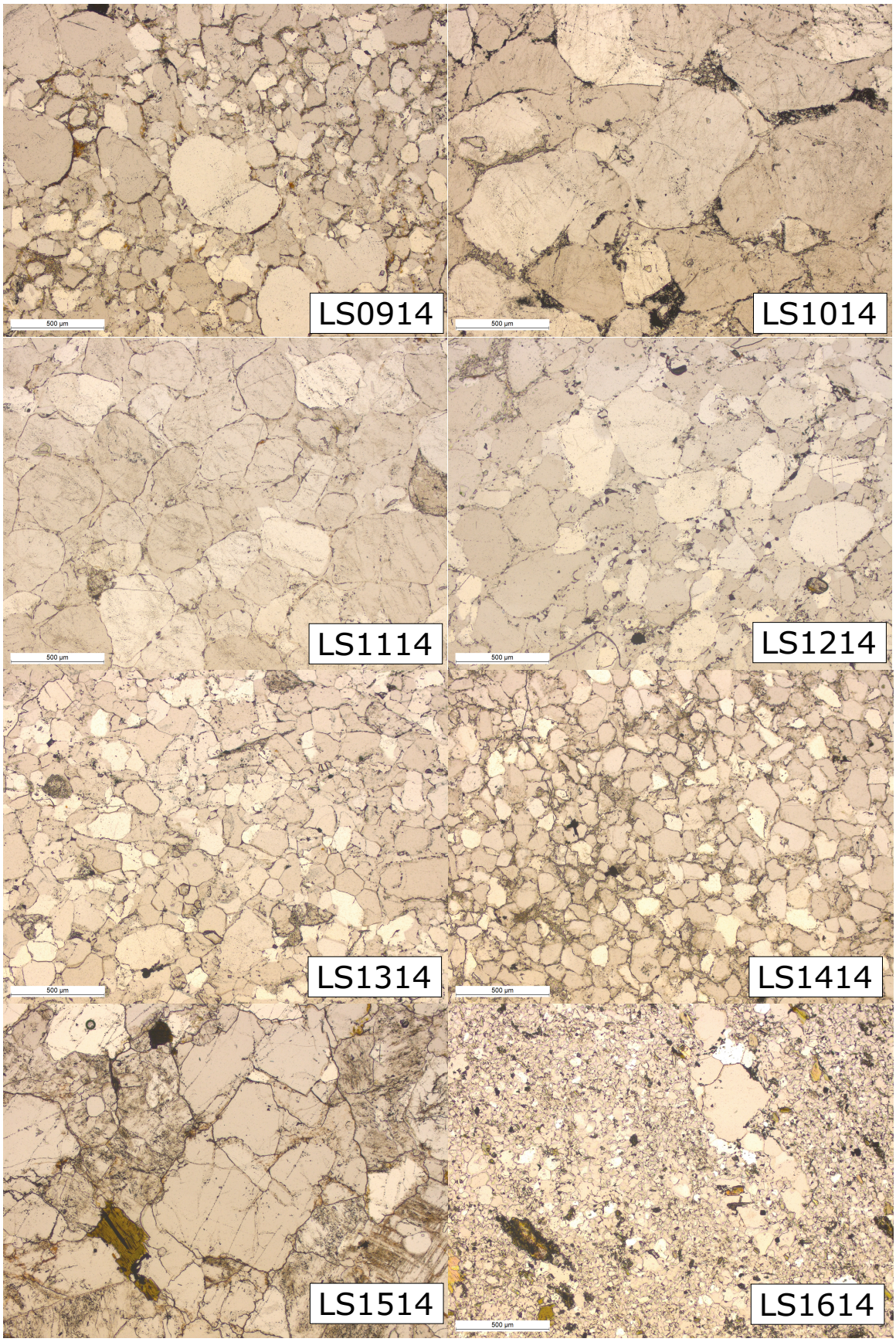
LS0914
LS1014
LS1114
LS1214
LS1314
LS1414
LS1514
LS1614
500 µm

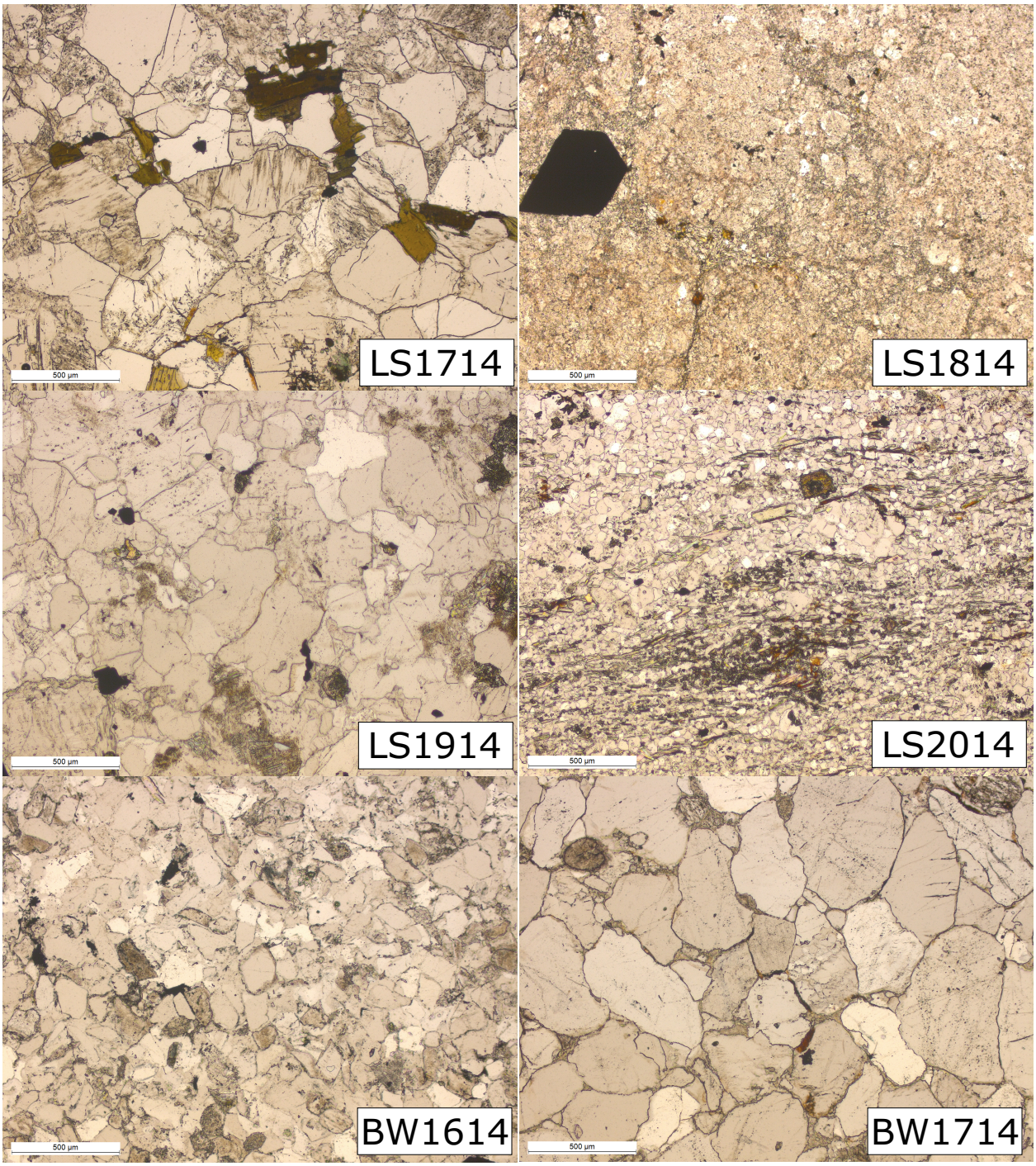

Figure S3. Photomicrographs of selected samples

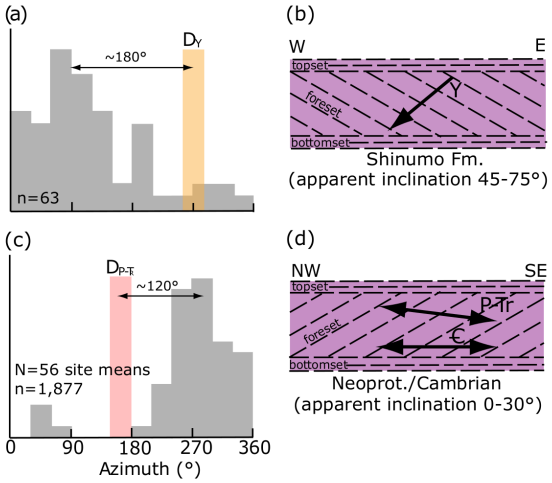

Figure S4: Relationship between paleomagnetic vectors and foreset dip directions

Orientation histograms (grey shading) and schematic cross-sections showing relationship between paleomagnetic vectors and foreset dip directions in Shinumo Formation (a) and (b), and Neoproterozoic-Cambrian formations (c) and (d). DY, mean declination of Mesoproterozoic Shinumo Formation; DP-Tr, mean declination of Permian/Triassic strata. Foreset orientation data in (a) from Appendix I in Daneker (1975) and in (c) from Table 2 in Stewart (1970).

SUPPLEMENTAL TEXT

Primary Structure

Orthoquartzites in the southwestern United States are substantially compacted after deposition, commonly cross-stratified, and locally contain paleoliquefaction structures. These features, to the extent that they are sampled by our clast populations, could potentially affect the distinction between clasts derived from low-inclination Neoproterozoic-Cambrian strata and moderate- to high-inclination Shinumo clasts. In the case of compaction (Tauxe and Kent, 2004), we note that the degree of this effect is probably fairly uniform over the sample population, and therefore would not be expected to blur the distinction between low and high-inclination populations. In the case of cross-stratification, if foreset bedding systematically dips in the opposite direction of the paleomagnetic plunge, it would produce a population of clasts with "apparent inclination" that is skewed to steeper angles, because the magnetic plunge and foreset dip would be roughly additive (Figure S4).

Alternatively, if foreset bedding tended to dip in the same direction as paleomagnetic plunge, then the clast population would be skewed to shallower inclinations.

We can evaluate this issue because there are abundant data available on dip directions of foreset laminations for nearly every major orthoquartzite body in the southwestern US. Data from both the Shinumo Formation and Neoproterozoic-Cambrian strata from the Death Valley-Mojave region show preferred orientations in dip of foreset stratification relative to topset and bottomset bedding. Based on 63 measurements in the upper, non-feldspathic part of the Shinumo Formation (Figure S4a), there is a strong tendency for foreset laminations to dip eastward (Figure S4a). There is approximately a 180° difference between the mode in foreset dip directions at 90° azimuth and the mean direction of paleomagnetic plunge at 270° (Figure 7a). These observations suggest that the component of Sespe clasts derived from foresets will skew the population from moderate to steeper apparent inclination, in direct proportion to the amount of foreset dip (Figure S4b). Assuming a mean foreset dip of 15° and paleomagnetic inclination of 45°, this population would yield an apparent mean inclination of 60°.

Neoproterozoic-Cambrian strata distributed throughout the Death Valley-Mojave region (Table 2 in Stewart, 1970), and Cambrian strata in the Grand Canyon and central Arizona regions (Figure 9 in McKee and Resser, 1945; Table 1 in Hereford, 1977) show a strong tendency for foreset laminations to dip westward. Based on 1,877 measurements from the Johnnie, Stirling, Wood Canyon, and Zabriskie formations, the dip directions of foresets show a well-defined peak at an azimuth of 270°, with orientations scattering broadly between 180° and 360° (Figure S4c). As noted earlier, the expected magnetization directions in these strata are either Ediacaran-Cambrian or Permian-Triassic in age, with inclinations of 0° to 30° (Figure 7g). Ediacaran-Cambrian magnetizations generally plunge shallowly to the east or west, and Permian-Triassic magnetizations are expected to plunge gently SE (e.g., Molina-Garza et al., 1998; Figure S4c). Given these observations, the population of clasts derived

from foresets with Neoproterozoic-Cambrian magnetization would be expected to record inclinations either steeper or shallower than true inclination by the amount of foreset dip, dispersing the population to somewhat higher and lower values. In the population of clasts derived from foresets with Permian-Triassic magnetizations, the situation is somewhat more complex because of the SE magnetic declination. For the case of foresets dipping due west 30° recording a Permian magnetization oriented with D=150°, I=15° (near the upper end of Permian inclinations for southwestern North America), the apparent inclination would be 28°, only 13° steeper than the true inclination.

Thus, to the extent that the Sespe orthoquartzite clast population samples foreset laminations in these formations, the overall effect of the foreset population would be to steepen the inclination distributions by adding a component of clasts with inclinations that range from 10° to 30° steeper than the remainder of the population, with the exception of Neoproterozoic-Cambrian magnetizations, which would be either shallower or steeper by a similar amount. Even if every clast in the Sespe population were derived from steeply dipping foresets optimally oriented to maximize the apparent inclination, the steepening would be expected to affect both the Neoproterozoic-Cambrian and Shinumo populations by a similar, relatively modest amount, thus preserving the difference in inclination. In general, however, the volume fraction of orthoquartzite sources that are moderately to steeply cross-stratified is low in most formations, and is therefore not likely to have a major effect on the distributions of inclinations. Nonetheless, the tendency for rather shallow eastward inclination in data from the Death Valley-Mojave region may be a reflection of this effect (compare Figure 7g and Figure S4d).

Convoluted bedding associated with paleoliquefaction represents at most 10% of the volume of the upper part of the Shinumo Formation in sections where it is most commonly exposed (Daneker, 1975). These convoluted strata are generally not developed in densely cemented orthoquartzite. Thus,

although some of these samples may affect the clast population in the Sespe, there is little chance that they would form a statistically significant fraction of the clast population.

References Cited

Daneker, T. M., 1975, Sedimentology of the Precambrian Shinumo Sandstone, Grand Canyon, Arizona: M.S. thesis, Northern Arizona University, 195 p.

Hereford, R., 1977, Deposition of the Tapeats Sandstone (Cambrian) in central Arizona: Geological Society of America Bulletin, v. 88, p. 199-211.

McKee, E. D., and Resser, C. E., 1945, Cambrian History of the Grand Canyon Region: Washington, D. C., Carnegie Institute Publications, v. 563, 232 p.

Molina-Garza, R. S., Acton, G. D, and Geissman, J. W., 1998, Carboniferous through Jurassic paleomagnetic data and their bearing on rotation of the Colorado Plateau: J. Geophys. Res., v. 103, p. 24,179–24,188.

Stewart, J. H., 1970, Upper Precambrian and Lower Cambrian strata in the southern Great Basin, California and Nevada: U.S. Geological Survey Professional Paper 620, 206 p.

Tauxe, L., Kent, D. V., 2004, A simplified statistical model for the geomagnetic field and the detection of shallow bias in paleomagnetic inclinations: Was the ancient magnetic field dipolar?, in Timescales of the Paleomagnetic Field, American Geophysical Union, Washington, D. C., Geophysical Monograph Series, v. 145, p. 101-115.